ABSTRACT

HEIDARPOURROUSHAN, MAEDEH. Dynamics of DNA Looping in Nanochannels. (Under supervision of Dr. Robert Riehn).

This thesis is devoted to the study of protein-DNA interactions and especially how proteins can mediate DNA loop formation in nanochannels. In the last decade, a large number of studies have been performed, wherein DNA molecules were confined to the channels with cross-section around the persistence length of DNA molecule. Such nanochannels provide a good model system for studying of the physics of confined DNA. The results of this thesis increase our understanding of how different DNA-binding proteins can change the DNA configuration.

In the first study, we have investigated the kinetic evolution of DNA loops (48500 bp) induced by the T4 ligase enzyme inside a nanofabricated channel system with a channel cross-section of 100 x 100 nm^2, and a few hundred micron channel length. We found that addition of the ligase profoundly alters the behavior of DNA. In particular, ligase acts to stabilize hairpin geometries in which the extended forward and backward arms of the hairpin scan past each other. From the linear density of DNA inside the channel, we deduce that the effective excluded volume vanishes upon addition of T4 ligase and ATP. We furthermore observed the influence of proteins on the dynamics of DNA loops in real time, and found that different protein binding modes lead to unique signatures in the configuration dynamics.

In the second study, we extensively probed the interactions of dyes and the enzyme co-factor ATP with DNA under nanoconfinement. We find negligible effects if DNA is visualized using groove-binding dyes such as DAPI. However, if an intercalating dye (YOYO-1) is used, we find a significant shortening of the DNA in the presence of ATP that we attribute to an

interaction of dye and ATP (as well as AMP and CTP). We did not record a noticeable effect due to Mg^{+2}.

In the third study, we present a sensitive assay for enzyme activity coupled to ATP hydrolysis that is based solely on an induced motion of DNA molecules when confined to nanochannels.

Dynamics of DNA Looping in Nanochannels

by
Maedeh Heidarpourroushan

A dissertation submitted to the Graduate Faculty of
North Carolina State University
In partial fulfillment of the
requirements for the Degree of
Doctor of Philosophy

Physics

Raleigh, North Carolina
2015

APPROVED BY:

Dr. Shuang Fang Lim	Dr. Hong Wang
Dr. Glenn M. Walker	Dr. Robert Riehn Chair of Advisory Committee

DEDICATION

To my Husband:

Dr. Mohammad Ali Rezaei

And to my parents and parents in law.

BIOGRAPHY

Maedeh Heidarpourroushan was born in Tehran, Iran. She received her B.Sc. in Physics (Solid State Physics) from University of Mazandaran, Mazandaran, Iran in 2008 and M.Sc. degrees in Physics (Gravitation & Astronomy) from University of Tehran, Tehran, Iran in 2011. In fall 2011, she joined the Physics department of Washington State University to pursue her Ph.D and transferred to Physics department of North Carolina State University, Raleigh, in spring 2012 to pursue her Ph.D. degree. Her main research interest is in the area of biophysics: Micro and Nano fluidics, BioMEMS.

ACKNOWLEDGMENTS

To my husband, who is the sunshine of my life and source of my passion for the pursuit of happiness.

I would like to express my deepest gratitude to my Ph.D. adviser and mentor, Dr. Robert Riehn for all his guidance and support. During my research, I have benefited tremendously from his knowledge, creative thinking and professional insight. I feel blessed to have such a great scholar with such a warm character as my mentor.

I'd like to thank Dr. Shuang Fang Lim, my co-advisor, for her encouragement and support as a good teacher.

I also would like to extend my gratitude to Dr. Hong Wang and Dr. Glenn M. Walker for serving on my committee and their feedback and support.

Thanks to our postdocs: Dr. Gideon Livshits and Dr. Janina Wirth and my colleagues Mr. Zubair Azad and Mr. Kory Green for all the enlightening discussion and friendship through all my study and life at NCSU.

.

TABLE OF CONTENTS

LIST OF TABLES

LIST OF FIGURES

1. Introduction

1. Introduction of DNA

DNA plays an important role in all living organisms. DNA is responsible for storage of genetic information. Understanding the behavior DNA and process of using the genetic information, which is translates sequences of amino acids into proteins, is central to biology. Although sequencing technology of DNA is becoming mature, reading out the genetic information directly from long single DNA molecules have not been achieved [1]. DNA is a heteropolymetric molecule consisting of four nucleotides, adenine (A), thymine (T), guanine (G), and cytosine (C). The chemical structure of single stranded DNA and the complementary base pairs are shown in Figure 1.1. The standard picture of double stranded DNA as revealed by x-ray crystallography is shown in Figure 1.2.

Quantitative and qualitative analysis of DNA sequences provide information essential to a variety of field such as disease diagnostic medical therapeutics, gene expiration profiling, environmental analysis, and drug discovery. Routine laboratory methods require a larger amount of samples than is available for many analyses; for example, early disease diagnosis. In order to detect low-abundance nucleic acid target, conventional methods predominantly rely on the use of sequence amplification techniques such as PCR to raise the quantity of DNA to detectable level. However the amplification process is expensive and time-consuming and

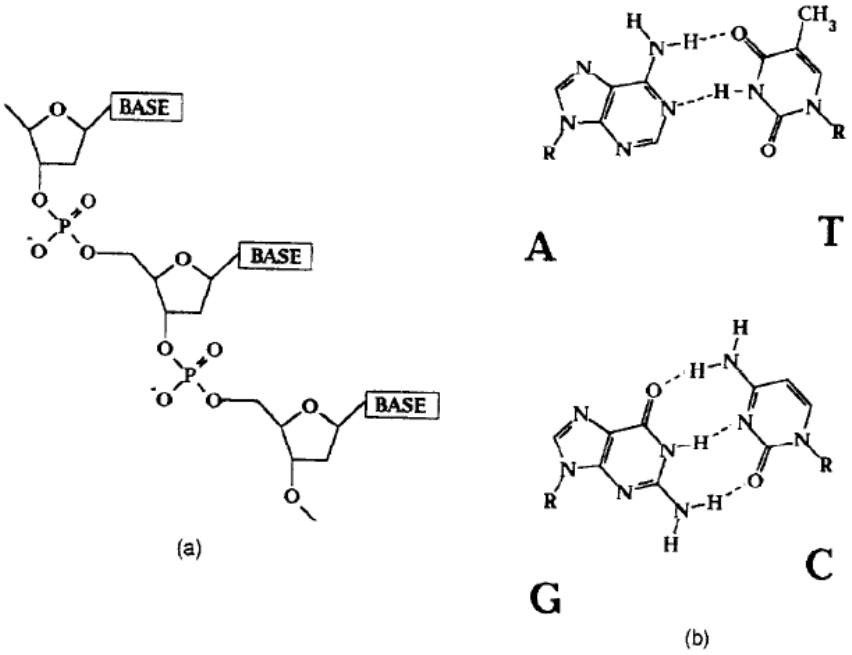

Figure 1.1: (a) DNA single strand and (b) the Watson-Crick complementary base pairs[138]**.**

tends to be complicated by false-positive and negative results due to contamination. For these reasons, single molecule detection (SMD) is receiving increased attention in an effort to enhance the sensitivity of nucleic acid detection and validate currently available techniques by means of its PCR-like sensitivity and potential to achieve high accuracy quantification of low abundant targets [2]. In the last two decades a variety of optical SMD techniques which measure single molecules either in solution or on solid surfaces have been developed [3], [4], [5], and [6].

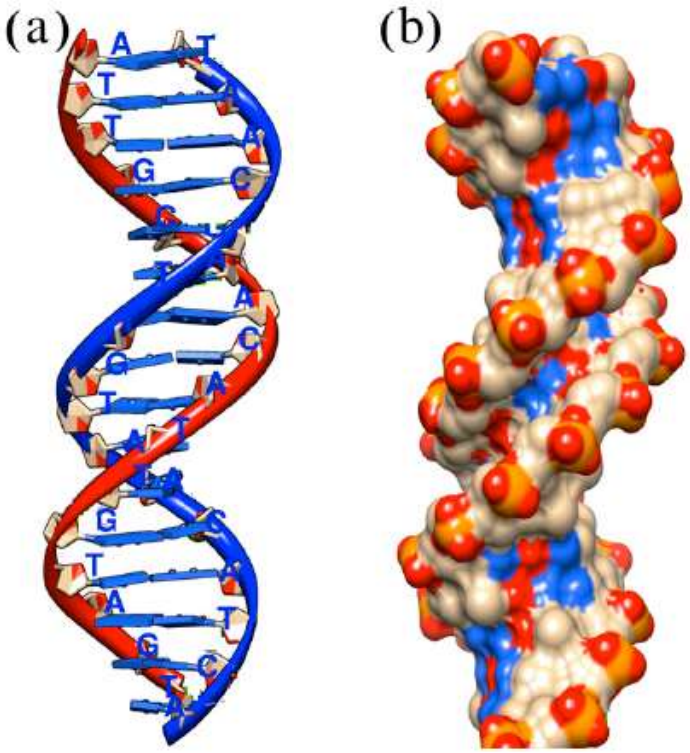

Figure 1.2: (a) Structure of the DNA double helix. A base pairs with T (two hydrogen bonds) and G with C (three hydrogen bonds). (b) A hydrophobic map of the same sequence, with a heat map from red (highly polar) to blue (highly hydrophilic) [2]**.**

At first it appears as if reading the base pair sequence of DNA would reveal the entire information that is stored within it. However this is wrong, because the DNA molecule in a cell is not a straight piece of two twisted together of single-stranded polymers but rather exists in a highly compacted three-dimensional structure. DNA is in particular twisted and folded by proteins call histones into chromatin complex [1]. Many early studies into the physical and chemical studies of DNA were performed in bulk and obtain average of a measured quantity. In contrast, single molecule experiment obtain the distribution of the measured quantity and are sensitive to rare events and small subpopulations. Important techniques for studying single molecules in biophysics are

1. Atomic Force Microscopy (AFM), which observes mechanically manipulated single molecule.

2. Laser Traps (optical and magnetic tweezers), which observed direct mechanically manipulated single molecule.

3. Single Molecule Fluorescence

In our lab, we are exploring how DNA molecules behave in volumes comparable to the persistence length of the molecules. The device design is based on nanofabricated channels, into which DNA molecules are introduced. A fluorescent microscope is used to observe motion of DNA either under at equilibrium or under applied stress.

DNA molecules stretch out in nanochannels, due to self-avoidance interactions and nanochannels create a linear image of genome along the channel for analysis [8], [9]. This method is one of the most promising method for genomic mapping, DNA dynamics, protein-DNA, and DNA-DNA interactions.

The physics of how DNA stretches when confined in a nanochannel is still an active area of research. I will outline the basic concepts of the stretching process in the following section.

2. Theory of Polymer Dynamic

In 1920, Staudinger proposed the macromolecular hypothesis: "polymers are molecules made of covalently bonded elementary units, called monomer" [10]. For example DNA is a

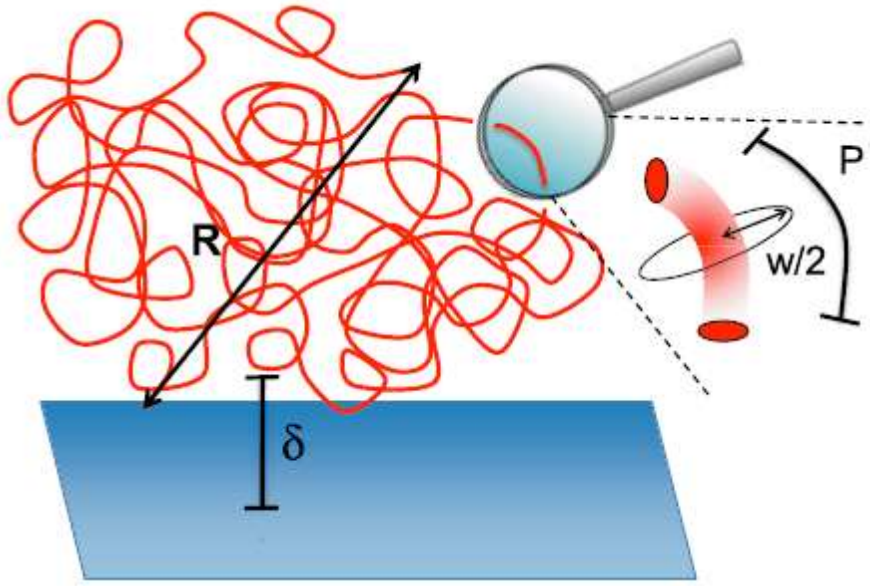

Figure 1.3: defining the end to end length (R), persistence length (p), effective width (w), and wall-DNA depletion width (δ) [1].

heteropolymer consisting of four different types of monomers (nucleotides). Each polymer is defined based on some key physical parameters, those important parameters are:

- Contour length (L)
- Persistence length (p)
- Effective width (w)

Those key parameters for DNA are illustrate in Figure 1.3. Because my main focus research is on DNA molecule, I will explain all of those key physical parameters in the contents of DNA.

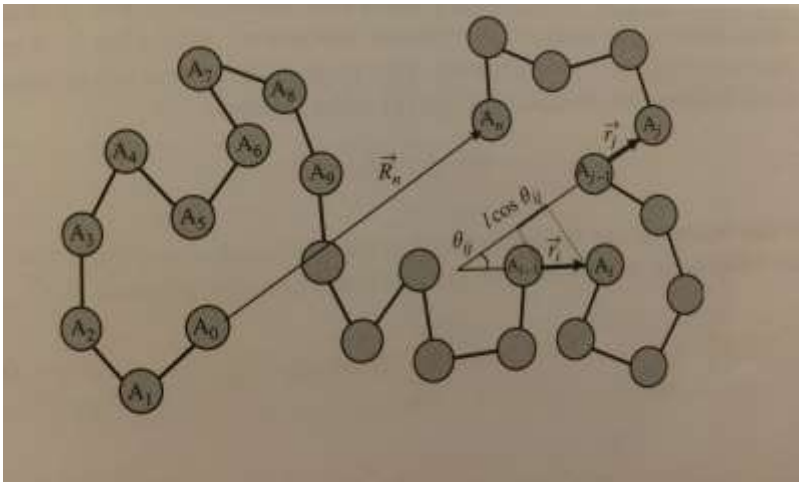

Figure 1.4: configuration of a polymer and end-to-end length of polymer is shown by $\vec{R}_n$. When the polymer totally stretches out the end to end length is equal the contour length[8]**.**

2.1 Contour Length of DNA

The contour length of a polymer (in our case DNA) (L) is the length of polymer, when the polymer stretched end-to-end as if it were a piece string with no thermal fluctuations. The contour length is simply the number of monomers N (for DNA is the number of base pairs), multiplied by the average length of monomer (for DNA the length of base pair is 0.34 nm). For a polymer the end-to-end vector is sum of all N bond vector in the chain (Figure 1.4):

$$\vec{R}_N = \sum_{i=1}^{N} \vec{r}_i \qquad (1.1)$$

The maximum of end-to-end vector is the contour length. For example the contour length of λ-DNA (dsDNA), which has 48.5 kbp, with the length of base pair 0.34 nm, the contour length is 16.5μm.

2.2 Persistence Length

The persistence length is a basic mechanical property quantifying the stiffness of a polymer. Formally, the persistence length of a polymer is defined as the distance in contour over which the DNA molecule 'forgets' its orientation [12], [13], or the length over which correlations in the direction of the tangent are lost. If one starts at one end of a dsDNA molecule (L = 0) in solution and constructs a unit length tangent vector *f(s)*, the persistence length *P* determines the scale "*s*" over which the tangent–tangent correlation function along the molecule contour length decays [13].

$$\left\langle \vec{f}(0).\vec{f}(s)\right\rangle = \exp\left(-\frac{s}{P}\right) \tag{1.2}$$

The persistence length of DNA can be obtained from single-molecule elasticity studies [11], in which DNA is stretched by optical or magnetic tweezer and directly the force-extension curve measured. Based on classic theory, the force-extension behavior of a semiflexible molecule then can be used to fit the force-extension curve and obtain an estimate of *P* and L [2]. DsDNA is not a rigid polymer, otherwise it was difficult to put two meters of DNA into a cell which is 10μm in diameter. Because of this limited rigidity, thermal fluctuations will randomize the configuration of the polymer in space. The persistence length of DNA is shown in Figure 1.3.

For buffers with ionic strength greater than around 10mM and at *T* = 300 K, the persistence length of dsDNA is close to 50 nm [1]. Of course, the persistence length *P*

ultimately is determined by the molecular architecture of the atoms, the absolute temperature *T*, and the dimension of space.

2.3 Effective Width of DNA

The effective width gives the effective interaction range of two genetically distant DNA segments as they approach each other (Figure 1.3). The quantity is often estimated as being the intrinsic chain width plus approximately twice the Debye length [1]. The effective width can be calculated via a theoretical model for the excluded volume between two charged cylinders of diameter ω_0 and length l analogous to the classic expression for neutral cylinders, but taking into account the true electrostatic rod–rod interaction. Onsager was the first to do so [14] and the calculation was later refined by Stigter and Fixman [15], [16]. The main idea is (1) to calculate an effective rod–rod interaction potential using Poisson–Boltzmann theory then (2) use this interaction to evaluate the rod–rod excluded volume by evaluating the virial integral over the rod positions and orientations [17]. The virial integral for two particles interacting via the potential $U(r_1, r_2)$ is given by,

$$\chi \approx \int \left[1 - \exp\left(- \frac{U(r_1 - r_2)}{K_B T} \right] \mathrm{d}\vec{r}_1 \, \mathrm{d}\vec{r}_2 \qquad (1.3)$$

Stigter worked out this integral using an interaction potential obtained from solving the linearized Poisson–Boltzmann equation for a charged rod and matching the solution to the full non-linearized theory at the Stern layer [15], [18], and [16]. He calculated the effective width, based on calculating the rod excluded volume as

$$\omega = \lambda_D \left[0.7704 + \log\left(\frac{\nu^2}{2\varepsilon\varepsilon_0 k_B T \kappa} \right) \right] \qquad (1.4)$$

Where "ν" is an effective DNA line charge. The DNA linear charge density is $\approx -6e$ per nm. Stigter discussed in detail in [18],[7]. Equation (1.4) suggests that ω is indeed proportional to λ_D (Debye length), but with a pre-factor that depends on the DNA charge and increases the estimate of ω. Experiment and theory together suggest that the effective width depends strongly on the ionic strength, ranging from around 5 nm at 100mM salt to as high as 20 nm at 5mM.

3. Ideal Chain Model

Polymer is described as a number of monomers and how those monomers are connected together to form a long chain of polymer. Based on this we have several models of ideal chain polymer. Each model makes different assumptions about the value of torsion "φ_i" and bond angles "θ_i" (Figure 1.5), however an ideal model ignores interactions between monomers separated by large distance along the chain. The chemical structure of polymer determines the population of torsion and bond angles. In this section I will describe some common ideal chain models following Michael Rubinstein and Ralph H. Colby [8].

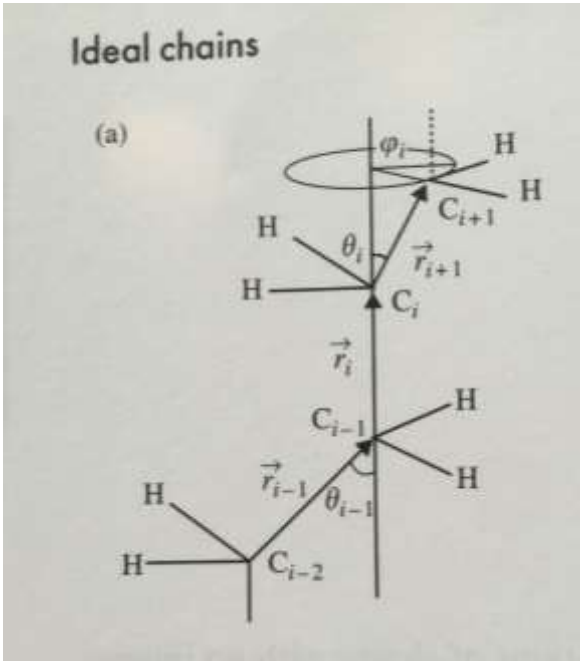

Figure 1.5: An Ideal chain model, torsion angel φ_i and bond angle θ_i [8]**.**

3.1 Freely Jointed Chain Model (FJC)

The freely jointed chain (FJC) model is one of the simplest models of an ideal polymer. In the FJC model, it is assumed that the bond length (length of monomer, l) is constant and there is no correlations between the directions of different bond vectors. In other word, the bond angle and torsion angle are free. The mean-square end-to-end distance of any polymer is;

$$< R^2 > = < \vec{R}_n . \vec{R}_n > = \sum_{i=1}^{N} \sum_{j=1}^{N} < \vec{r}_i . \vec{r}_j > \qquad (1.5)$$

If all bond vectors have the same length $l = |\vec{r}_i|$, the above equation can be rewritten based on the angle θ_{ij}, which is the angle between bond vector $\vec{r}_i$ and $\vec{r}_j$ as shown in Figure 1.4.

$$< R^2 >= \sum_{i=1}^{N} \sum_{j=1}^{N} < \vec{r}_i . \vec{r}_j >= l^2 \sum_{i-1}^{n} \sum_{j=1}^{n} \left\langle \cos\theta_{ij} \right\rangle \tag{1.6}$$

In the FJC model, $\left\langle \cos\theta_{ij} \right\rangle = 0$ for $i \neq j$. The only non-zero terms is $\cos\theta_{ij} = 1$ for i = j . As a result the mean-square end-to-end distance of freely jointed chain is:

$$\left\langle R^2 \right\rangle = Nl^2, \tag{1.7}$$

where l is the length of monomer and N is number of monomers.

3.2 Freely Rotating Chain Model (FRC)

The FRC model ignores the differences between the probabilities of different torsion angles and assumes all torsion angles $-\pi \leq \varphi_i \leq \pi$ to be equally probable. This model also assumes that all bond length and bond angles are fixed (constant) and all torsion angle are equally likely and independent of each other. The mean-square end-to-end distance according to the Equation (1.6) will be:

$$\begin{aligned} < R^2 > &= \sum_{\mathrm{i=1}}^{\mathrm{N}} \left(\sum_{\mathrm{j=1}}^{\mathrm{i\text{-}1}} \left\langle \vec{r}_i . \vec{r}_j \right\rangle + \left\langle \vec{r}_i^{\,2} \right\rangle + N \sum_{j=i+1} \left\langle \vec{r}_i . \vec{r}_j \right\rangle \right) \\ &= \sum_{\mathrm{i=1}}^{\mathrm{n}} \left\langle \vec{r}_i^{\,2} \right\rangle + l^2 \sum_{i=1}^{n} \left(\sum_{j=1}^{i-1} (\cos\theta)^{i-j} + \sum_{j=i+1}^{n} (\cos\theta)^{j-i} \right), \end{aligned} \tag{1.8}$$

we can rewrite the $(\cos\theta)^{|j-i|}$ term as:

$$(\cos\theta)^{|j-i|} = \exp[|j-i| \ln(\cos\theta)] - \exp\left[-\frac{|j-i|}{s_p} \right], \tag{1.9}$$

where s_p is defined as the number of main-chain bonds in a persistence segment:

$$s_p = -\frac{1}{\ln(\cos\theta)}. \tag{1.10}$$

The persistence length is the length of this persistence segment:

$$P = s_p l. \tag{1.11}$$

After simplification the mean-square end-to-end displacement for FRC model is:

$$< R^2 > = Nl^2 \frac{1+\cos\theta}{1-\cos\theta}. \tag{1.12}$$

3.3 Worm like Chain Model

The worm-like chain model can be described as a special case of the FRC chain model for very small values of the bond angle. This is a good model for stiff polymers, such as double-stranded DNA for which the flexibility is due to fluctuations of the contour of the chain from a straight line rather than to torsion bond. For small value of the bond angle ($\theta << 1$) we have,

$$\cos\theta \cong 1 - \frac{\theta^2}{2}\ . \tag{1.13}$$

The persistent length in this model [Equation (1.10), (1.11), and (1.13)] is;

$$P = s_p l = l\left(-\frac{1}{\ln(\cos\theta)}\right) \cong l\frac{2}{\theta^2}. \tag{1.14}$$

The Kuhn length $l = \frac{< R^2 >}{R_{\max}}$ is twice of persistence length. For example the persistence length of a double-helical DNA is $P \approx 50nm$ therefore the Kuhn length is $l \cong 100\,nm$. The

mean-square end-to-end distance of the worm-like chain can be evaluated using the Equation (1.9) [8].

$$< R^2 >= l^2 \sum_{i=1}^{N} \sum_{j=1}^{N} < \cos\theta_{ij} >= l^2 \sum_{i=1}^{N} \sum_{j=1}^{N} \exp\left(-\frac{|j-i|}{P} l \right),$$
$$< R^2 >= 2PNl - 2P^2 \left(1 - \exp\left(-\frac{Nl}{P} \right) \right). \tag{1.15}$$

4. Free Energy of an Ideal Chain

"Every possible conformation of an ideal chain can be mapped onto a random walk. A particle, which is making random steps defines as random walk. If the length of each step is constant and the direction of each step is independent to the previous steps, the trajectory of the random walk is one conformation of a freely joint chain. Hence, random walk statistics and ideal chain statistics are similar" [8]. The entropy *S (N, R)* is the product of the Boltzmann constant *K* and logarithm of number of states Ω *(N, R):*

$$S(N, \vec{R}) = K \ln \Omega(N, \vec{R}), \tag{1.16}$$

The probability distribution function is the fraction of all conformations that have an end-to-end vector $\vec{R}$ between $\vec{R}$ and $\vec{R} + d\vec{R}$:

$$P_{3d}(N, \vec{R}) = \frac{\Omega(N, \vec{R})}{\int \Omega(N, \vec{R})\, dR} \tag{1.17}$$

The one-dimensional probability distribution function for components of a random walk along each of those three axes can be obtain by mean-square displacements due to the central limit theorem:

$$P_{3d}(N,\vec{R}_x) = \frac{1}{\sqrt{2\pi < R_x^2 >}} Exp\left(-\frac{R_x^2}{2 < R_x^2 >}\right) = \sqrt{\frac{3}{2\pi N l^2}} Exp\left(-\frac{3R_x^2}{2Nl^2}\right), \tag{1.18}$$

where l is the length of monomer. The probability function for the end-to-end vector $\vec{R}$ of an ideal linear chain of *N* monomers is the product of the three independent distribution functions:

$$P_{3d}(N,\vec{R}) = \left(\frac{3}{2\pi N l^2}\right)^{3/2} \exp\left(-\frac{3\vec{R}^2}{2Nl^2}\right). \tag{1.19}$$

The entropy of an ideal chain with *N* monomers and end-to-end vector $\vec{R}$ is thus related to the probability distribution function:

$$S(N,\vec{R}) = -\frac{3}{2}K\frac{\vec{R}^2}{Nl^2} + \frac{3}{2}k\ln\left(\frac{3}{2\pi N l^2}\right) + K\ln\left[\int \Omega(N,\vec{R})d\vec{R}\right] \tag{1.20}$$

The last two terms of Equation (1.20) depend only on the number of monomers *N*, but not on the end-to-end vector length and can be denoted by $S(N,0)$:

$$S(N,\vec{R}) = -\frac{3}{2}K\frac{\vec{R}^2}{Nl^2} + S(N,0). \tag{1.21}$$

The Helmholtz free energy of the chain F is the energy U minus the product of absolute temperature T and entropy S:

$$F(N,\vec{R}) = U(N,\vec{R}) - TS(N,\vec{R}). \tag{1.22}$$

The energy of an ideal chain $U(N,\vec{R})$ is independent of $\vec{R}$, since the monomers of the ideal chain have no interaction energy. The free energy can be written as

$$F(N,\vec{R}) = \frac{3}{2}KT\frac{\vec{R}^2}{Nl^2} + F(N,0). \tag{1.23}$$

According to Equation (1.22), the largest number of chain conformations corresponds to $\vec{R} = 0$. The number of conformations decreases with increasing $\left|\vec{R}\right|$, leading to the decreases of polymer entropy and increase of its free energy. The free energy of an ideal chain $F(N,\vec{R})$ increases quadratically with the magnitude of the end-to-end vector length. This implies that the entropic elasticity of an ideal chain satisfies Hooke's law. To separate the chain ends by a distance R_x in the *x* direction, requires force f_x:

$$f_x = \frac{\partial F(N,\vec{R})}{\partial R_x} = \frac{3KT}{Nl^2}R_x. \tag{1.24}$$

The force to hold chain ends separated by a general vector $\vec{R}$ is linear in $\vec{R}$, like a simple elastic spring:

$$\vec{f} = \frac{3KT}{Nl^2}\vec{R}. \tag{1.25}$$

The coefficient of proportionality $\frac{3KT}{Nl^2}$ is the entropic spring constant of an ideal chain. It is easier to stretch polymers with larger number of monomer *N*, larger monomer size l, and at lower temperature *T*. The fact that the spring constant is proportional to temperature is a signature of entropic elasticity.

5. Real Chain

We studied the conformation of an ideal chain that ignores the interaction between monomers separated by many bonds along the chain. In this section, we study the effect of these interactions on polymer conformations.

The conformations of a real chain in a solvent are determined by the balance of the effective repulsion energy between monomers that tends to swell the chain and the entropy loss due to such deformation. One of the most successful simple models that captures the essence of this balance is the Flory theory, which makes a rough estimates of both the energetic and the entropic contributions to the free energy [8].

"Consider a polymer with N monomers, swollen to the size $R > R_0 = bN^{1/2}$. Flory theory assumes that monomers are uniformly distributed within the volume R^3 with no correlations between them. The probability of a second monomer being within the excluded volume "v" of a given monomer is the product of excluded volume "v" and the number density of monomers in the pervaded volume of the chain N/R^3. The energy cost of being excluded from this volume is KT per exclusion or $KTvN/R^3$ per monomer" [8]. For all N monomers in the chain, this energy is N times larger;

$$F_{\text{int}} \approx KTv\frac{N^2}{R^3} \tag{1.26}$$

The Flory estimate of the entropic contribution to the free energy of a real chain is the energy required to stretch an ideal chain to end-to-end distance

$$F_{ent} \approx KT \frac{R^2}{Nl^2}. \tag{1.27}$$

The total free energy of a real chain in the Flory approximation is the sum of the energetic interaction and the entropic contributions:

$$F = F_{\text{int}} + F_{ent} \approx KT\left(\frac{vN^2}{R^3} + \frac{R^2}{Nl^2}\right). \tag{1.28}$$

The minimum free energy of the chain gives the optimum size of the real chain in the Flory theory, $R=R_F$:

$$\begin{aligned} &\frac{\partial F}{\partial R} = 0 = KT\left(-3v\frac{N^2}{R^4{}_F} + 2\frac{R_F}{Nl^2}\right), \\ &R_F \approx v^{1/5} l^{2/5} N^{3/5}. \end{aligned} \tag{1.29}$$

The size of long real chains is much larger than that of ideal chains with the same number of monomers, as reflected in the swelling ration:

$$\frac{R_F}{lN^{1/2}} \approx \left(\frac{v}{l^3} N^{1/2}\right)^{1/5} \qquad \text{for } \frac{v}{l^3} N^{1/2} > 1 \tag{1.30}$$

"If the total interaction energy of a chain in its ideal conformation $F_{\text{int}}(R_0)$, $R_0 = lN^{1/2}$ is less than *KT*, the chain will nor swell. In this case, $N^{1/2}v/l^3 < 1$ and the chain's conformation remains nearly ideal. The prediction of the Flory theory are in good agreement with both experiments and with more sophisticated theories" [8].

Figure 1.6 illustrate the different stretching behavior of real and ideal chains if a force with magnitude of f applied at both ends of each chain. Each chain subdivided into the blob of size

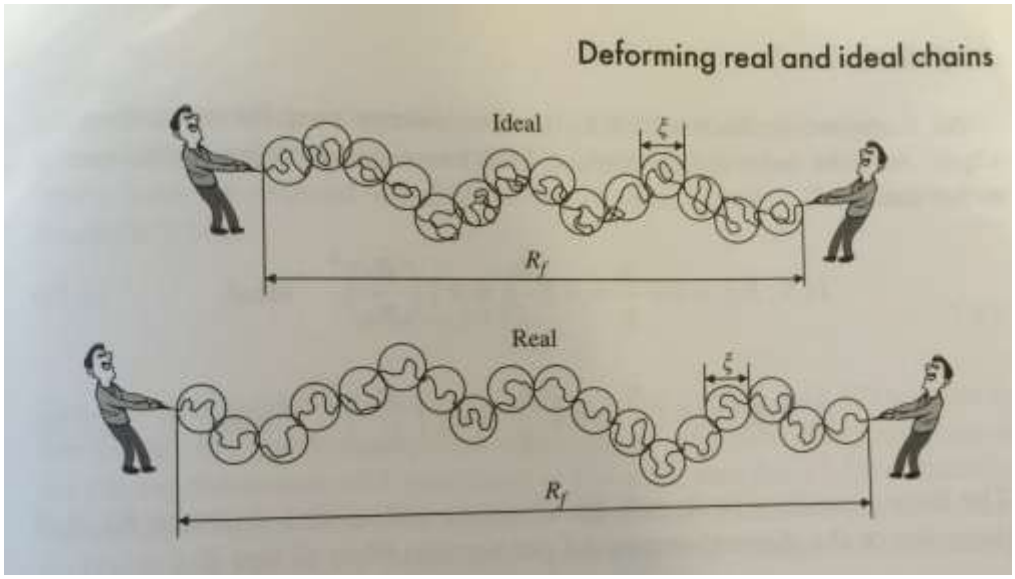

Figure 1.6: Stretching ideal and real chains of the same contour length with the same force f [8].

ξ containing g monomers each, such that on length scales smaller these tension blobs the chain statistics are unperturbed are given by Equations (1.7) and (1.29) [8].

$$\xi \approx g^{1/2} l \qquad \text{(Ideal)}, \tag{1.31}$$

$$\xi \approx g^{3/5} l \qquad \text{(Real)}, \tag{1.32}$$

Since each chain is a stretched array of tension blobs, their end-to-end distance R_f is an extended state is the product of the tension blob size ξ and the number of these blobs N/g per chain [8]:

$$R_f \approx \xi \frac{N}{g} \approx \frac{Nl^2}{\xi} \approx \frac{R_0^2}{\xi} \qquad \text{(Ideal)}, \tag{1.33}$$

$$R_f \approx \xi \frac{N}{g} \approx \frac{Nl^{5/3}}{\xi^{2/3}} \approx \frac{R_F^{5/3}}{\xi^{2/3}} \qquad \text{(Real)}, \tag{1.34}$$

The energy cost for stretching the chains is of the order *KT* per tension blob:

$$F(N, R_f) \approx KT \frac{N}{g} \approx KT \frac{R_f}{\xi} \approx KT \left(\frac{R_f}{R_0} \right)^2 \qquad \text{(Ideal)}, \tag{1.35}$$

$$F(N, R_f) \approx KT \frac{N}{g} \approx KT \frac{R_f}{\xi} \approx KT \left(\frac{R_f}{R_0} \right)^{5/2} \qquad \text{(Real)}, \tag{1.36}$$

The force necessary to stretch the chain to end-to end distance R_f is of the order of the thermal energy *KT* per tension blob of size ξ:

$$f \approx \frac{KT}{\xi} \approx \frac{KT}{R_0^2} R_f \approx \frac{KT}{R_0} \frac{R_f}{R_0} \qquad \text{(Real)}, \tag{1.37}$$

$$f \approx \frac{KT}{\xi} \approx \frac{KT}{R_F^{5/2}} R_f^{3/2} \approx \frac{KT}{R_F} (\frac{R_f}{R_F})^{3/2} \qquad \text{(Ideal)}, \tag{1.38}$$

It is important to notice the difference between the results for ideal and real chains under torsion. Ideal chains satisfy Hook's law with the force *f* linearly proportional to elongation R_f. For real chain the dependence of force *f* on chain elongation R_f is non-linear with the exponent equal to 3/2. This nonlinear dependence of force on elongation for real chains was first derived by Pincus and tension blobs are often called Pincus blobs [8].

6. Theory of Confined Polymers

So far we discussed polymer molecules in the context of ideal and real chains. In this section, we explain what happens when DNA restricted inside a thin and narrow and very long nanochannel. In general, nanochannel confinement leads to an elongation of the polymer molecule. Depending on the cross section of the nanochannel, we may have different elongation models.

6.1 De Gennes blob theory for confined polymers

De Gennes developed the classic model of a confined self-avoiding polymer [19]. The De Gennes regime considers the case when the nanochannel has diameter (D) larger than the persistence length of the polymer. He envisioned the confined chain as being divided into a series of 'blobs' (Figure 1.7). Each 'blob' has the conformation of an unconfined self-avoiding random walk with average diameter equal to the channel width D. In this regime, the molecule will coil up locally, but will stretch along the channel mostly due to the excluded volume interactions. De Gennes argued that self-exclusion has two effects (1) the blobs repel like hard spheres due to self-exclusion, uniformly distributing the polymer contour along the channel, and (2) each blob behaves as a "Flory coil". According to his theory and based on the Flory model, the occupied length of a molecule will experience elongation in a cylinder given by the formula:

$$R_{II} \approx D\left(\frac{N}{g}\right) \approx \left(\frac{l}{D}\right)^{2/3} Nl. \qquad (1.39)$$

The free energy of confinement is of the order of *KT* per compression blob given by the formula:

$$F_{conf} \approx KT\frac{N}{g} \approx KTN\left(\frac{l}{D}\right)^{5/3}. \tag{1.40}$$

In some polymer physics text books, the radius of each blob is shown as R_b [8]. Confinement forces R_b to scale as *D* (diameter of the cylinder) and then:

$$R_F \approx D \approx R_b \cong (wp)^{1/5} L^{3/5} \tag{1.41}$$

The formula above comes from Equation (1.30) and used excluded volume $v = wp^2$. The contour stored per blob L_b can then be found by back-solving for L_b as a function of D:

$$L_b \cong \frac{D^{5/3}}{(pw)^{1/3}} \tag{1.42}$$

The extension of the chain parallel to the tube axis is then simply the number of blobs $\frac{L}{L_b}$ times the extension of each blob (D),

$$R_{deGennes} \cong \frac{L}{L_b} D \tag{1.43}$$

Using Equation (1.42) to eliminate L_b in terms of *D*, Equation (1.43) gives for end-to-end length $R_{deGennes}$ and free energy:

$$R_{deGennes} \cong L\frac{(wp)^{1/3}}{D^{2/3}}; \tag{1.44}$$

$$F_{Conf} \cong K_B T\frac{L}{L_b} \cong K_B TL\frac{(pw)^{1/3}}{D^{5/3}}. \tag{1.45}$$

6.2 Odijk Regime Theory for Confined Polymers

Now consider the case where a DNA molecule is confined inside a nanochannel with a diameter smaller than its persistence length. In this case the bending energy will rapidly increase and the confined semiflexible polymer can no longer coil. This time we are working with undulated polymer that is being reflected from wall to wall (Figure 1.7). These deflections occur on average over a spatial scale λ called the 'Odijk deflection length' [9], determining the average increment in contour between successive polymer deflections. The Odijk deflection length scales with P and D [1], [9]:

$$\lambda = \left(PD^2\right)^{1/3} \tag{1.46}$$

The extension of the polymer along the channel R_{Odijk} is the number of Odijk segments L/λ times the average projection of an Odijk segment on the channel axis. Assuming that the average deflection made by the polymer with the walls is small [10],

$$\cos(\theta) \approx 1 - \frac{1}{2}\theta^2, \qquad \theta \approx \frac{\mathrm{D}}{\lambda}; \tag{1.47}$$

$$R_{Odijk} = L\cos(\theta) = L\left[1 - A\left(\frac{D}{P}\right)^{2/3}\right], \tag{1.48}$$

A is a parameter, which dependents on geometry and which is determined numerically. According to Odijk, the free energy of confinement inside a very narrow channel is;

$$F_{conf} \approx \frac{LKT}{\lambda} \approx P^{-1/3}D^{-2/3} \qquad D << P \tag{1.49}$$

The extended de Genne regime

The two regimes in nanochannel confinement described above are only valid as limiting regimes. Recent research has identified further, intermediate regimes. One of them is extended of de Genne regime, which the critical chain size (L_{**}) can be viewed as the chain size at which the ideal and self-excluding chains are of equal extent: $\left(lL_{**}\right)^{1/2} \approx \left((lw)^{1/5}L_{**}{}^{3/5}\right)$ [1]. By considering the monomer length is equal to the persistence length ($l \approx P$), we can get:

$$L_{**} = \alpha_{**}\frac{P^3}{w^2} \tag{1.50}$$

The quantity α_{**} is a numerical pre-factor. By substituting L_{**} in Equation (1.42), we obtain the critical channel width $D_{**} \cong (lw)^{1/5}(L_b^{**})^{3/5} = \alpha_{**}^{3/5}\frac{P^2}{w}$.

As a result, there is a transition to the extended de Gennes regime characterized by elongated blobs that are at the cross-over between ideal and Flory behavior ($D = D_{**}$). At $D = 2P$, the polymer enters a "transition" regime, characterized by isolated hairpin backbends

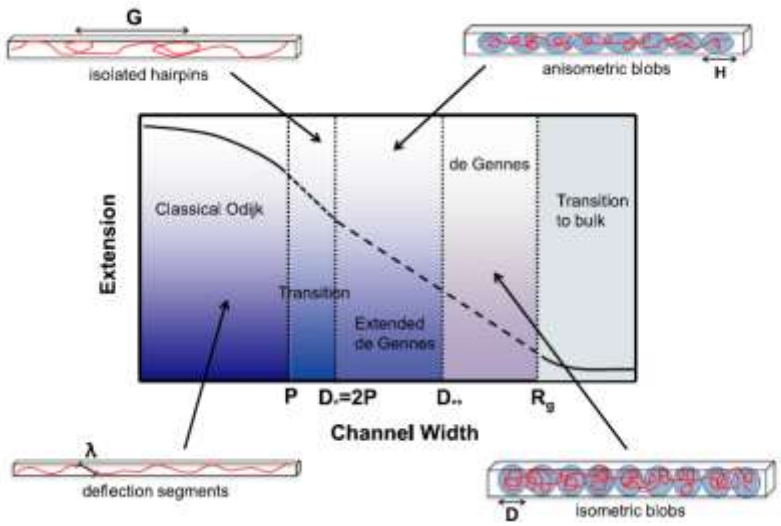

Figure 1.7: Different confinement models depending on the size of cross section of nanochannels. The de Gennes regime works for the channels, which their cross sections are bigger than persistence length of DNA, the Odijk regime works for the channels, which their cross sections are smaller than persistence length of DNA, and the transition regime occurs for channels size close to persistence length of DNA[1]**.**

with a global persistence length. For $D < P$, the hairpins are frozen out and the polymer can only store contour through a series of successive deflections with the wall, characterized by the deflection length λ (Figure 1.7) [1],[11].

In my research, I work with channels, the cross section of which was bigger than the persistence length of DNA, which means I have focused on de Gennes regime.

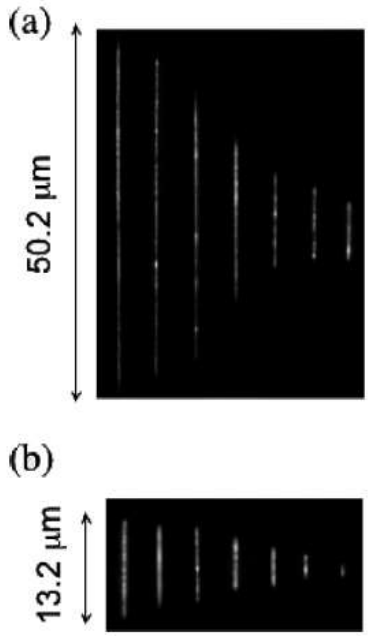

Figure 1.8: Averaged intensity of the selected T2 DNA molecules in 30×40 nm, 60×80 nm, 80×80 nm, 140×130 nm, 230×150 nm, 300×440 nm, and 440×440 nm channels (left to right). (b) Averaged intensity of selected λ-DNA molecules in the same channels.[1].

7. Ionic-Strength Dependence of Confined DNA Chain Conformation

In the prior section it was shown that the de Gennes theory predicts the DNA length inside a nanochannel . Reisner and his colleques have shown that, the stretching of the DNA molecules (λ-phage and T4 dsDNA mlecules) is clearly a function of the cross-section of nanonochannels (Figure 1.8)[10]. According to Equation (1.44), the DNA length depends on two physical constants that describe the continuum mechanics of DNA: the persistence length and the effective width. If those parameters change, the DNA length will change. Interestingly, both parameters depend on the ionic strength of the buffer in which DNA molecules are suspended.

Reisner has tested the influence of the ionic strength of the buffer and found that it plays a critical role in determining the configurational properties of DNA confined in nanochannels. In particular, he found that the end-to-end extension of DNA inside the nanochannels increases as the ionic strength is reduced [12].

The ionic strength variation affects the polymer configuration by modulating the range of electrostatic interactions between charges on the DNA phosphate backbone. Electrostatic interactions in electrolyte solution are screened over a characteristic scale known as Debye length, defined via its inverse $k^2 = \frac{2N_A e^2 I}{\varepsilon_0 \varepsilon k_B T}$ (e is the electronic charge, ε the dielectric constant of water, ε_0 the permittivity of free space, N_A Avogadro's number, k_B Boltzmann's constant, and T the temperature) [13]. It is obvious that by increasing the ionic strength, the Debye length decreases, and based on Equation (1.51) we anticipate that the effective width w decreases. Detailed calculations find a similar decrease in the persistence length of DNA with increasing ionic strength, known as the Odijk-Skolnick-Fixman theory. Empirical studies single-molecule elasticity studies close to physiological ionic strength conditions suggest that the persistence length follows the approximate relationship [14],[15],[16]

$$P = P_0 + \frac{0.0324M}{I} nm, \qquad (1.51)$$

with P_0 the high salt value of the persistence length (=50 nm).

Since both w and P decrease under increased ionic strength, we find that equations (1.4), (1.44), and (1.51) together predict that the DNA length decreases (Figure 1.9).

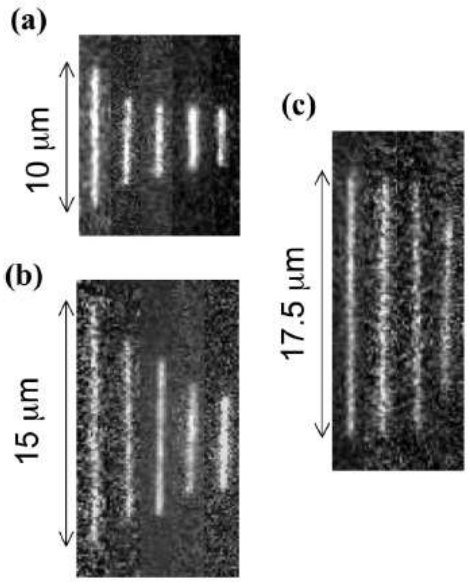

Figure 1.9: end-to-end λ-DNA molecules length measured at differing TBE dilution (left to right, 0.05×, 0.2×, 0.5×, 2×, 5× TBE) in (a) 200nm channels, (b) 100 nm channels, and (c) 50 nm channels [12]**.**

8. Introduction to Measuring Protein DNA Interaction Using Nanofluidics

DNA analysis in nanofluidic devices are a useful method to study of DNA and protein-DNA interactions at single molecule level, because DNA is free and can fluctuate along the nanochannel axis (has dynamics). For example, Streng and her colleagues have found that protein binding DNA, can alter DNA length [17]. This binding can cause confined DNA molecules length to shrink and compress. Zhang and his colleagues observed that confined DNA molecules initially elongate and eventually condense into a compact form with increasing concentration of the negatively charged proteins bovine serum albumin (BSA) and hemoglobin, because of the concomitant osmotic pressure gradient (Figure 1.10) [18] . This is

depict the fact that these proteins are not known to form a complex with DNA or to have any specific interaction with DNA.

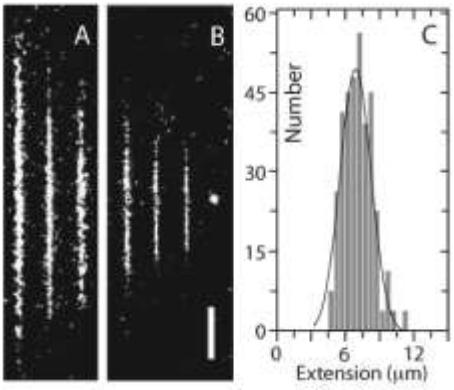

Figure 1.10: (A) Montage of fluorescence images of T4-DNA in 200 ×300 nm2 channels in 10 mM Tris/HCl (pH 8.5). From left to right, the molecule is protein-free, in 7.4 μM Hb, and in 7.4 μM BSA. (B) Asin panel A, but in 10 mM Tris/HCl with 25 mM NaCl. From left to right: protein-free, 7.4 μM Hb, 4.4 μM BSA, and 17.7 μM BSA (condensed). The scale bar denotes 2 μm. (C) Distribution in extension of a population of 330 molecules in 10 mM Tris/HCl with 25 mM NaCl. A Gaussian fit gives a mean extension of R‖ = 7 ± 2 μm [18]**.**

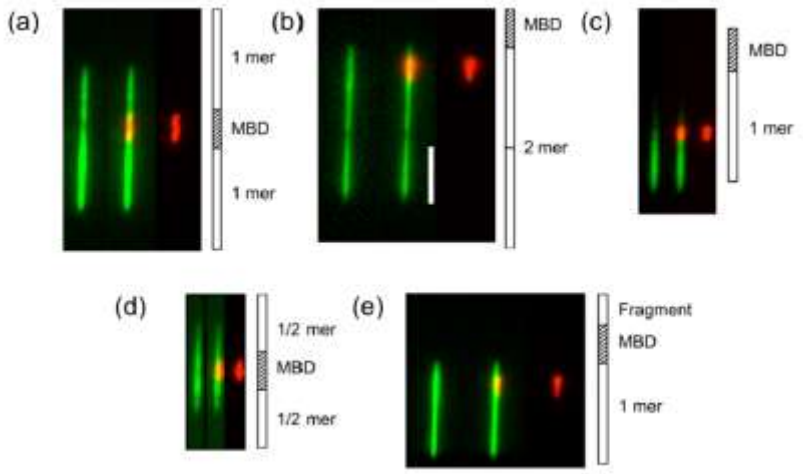

Figure 1.11: (a) Fluorescence images of concatenated methylated and non-methylated λ-DNA labeled with Alexa568MBD (red) and YOYO-1 (green), stretched out in nanochannels. Within each panel colors are split for clarity; (left) YOYO-1 only (DNA), (center) composite, (right) Alexa568 only (Alexa568-MBD). Schematic drawings in each panel illustrate the spatial position of the Alexa Fluor 568 MBD and the length of the k-DNA. The scale bar in panel (b) is 5 microns[19]**.**

The dynamics of methylated dsDNA and the direct reading of the methylation pattern on single dsDNA molecule has been studied by Lim. DNA methylation is one of the most widely studied mechanisms influencing epigenetic gene regulation and is generally thought to suppress gene expression. Figure 1.11 shows the methylation state was detected using fluorescently labeled methyl-CpG binding proteins (MBD) on DNA in nanochannels [19]. Interestingly, a compaction of DNA by MBD was again observed [19].

In this chapter we extend the study of DNA-protein interactions to the study of protein mediated DNA loops. The formation of DNA loops by proteins complexes is present in many fundamental cellular processes, including transcription, recombination and replication [20], [21], [22]. DNA loops are used to tie the ends of chromosomes and regulate the length of telomeres [23].

DNA loops can be classified according to the length of contour that is stored by the loop. Loops of a few hundred basepairs or less are short, while those many thousands of basepairs or more are long. This distinction comes from the physical processes that limit their formation. For short DNA loops, with the length comparable to the DNA persistence length (≈ 50nm), the main determination factor of looping is DNA elasticity. Thus, the bending and twisting of DNA, as well as the elastic properties of the molecules that tie the loop, play an important role. For long loops, in contrast, the limiting step is the erratic motion in the cell of the two DNA regions before they find each other. Thus, the main factor is the loss of entropy that happens when two DNA regions are tied together. In biological terms, a long length loop formation is limited by the rapidly declining probability of colocation of the anchoring sequences of the loop. Large DNA loops thus are kinetically unfavorable, and we hypothesize that proteins actively play a role in loop formation [24].

We have investigated the kinetic evolution of DNA loops (~50 kbp) induced by T4 ligase (as a model system for DNA cyclization) and T-loop forming proteins inside a nanofabricated channel system with a channel cross-section of 100 ×100 nm^2, and a few hundred microns channel length. In these nanochannels, DNA is forced in a linear configuration that makes loops that appear as folds, the size of which can be quantified easily.

2. Methods & Materials

1. Preparation of the Nanofludic Devices

In this chapter, we present and elaborate on experimental methods that are common to chapter 3-5. Many of the methods were described by Karpusenko [25], and only the major experimental steps are explained. A comprehensive treatment of the fabrication of nano-fluidic devices may be found in [26].

Experiments used mixed micro-and nano-fluidic devices made from fused silica. The technique of device fabrication is detailed in [11]. Fused silica is a convenient substrate material for nanofluidics, because it is transparent, an excellent electrical insulator, is chemically well-defined. It also has a low auto-fluorescent, and is thus suitable for fluorescence microscopy [1]. The cartoon of the device layout used in our experiments is shown in Figure 2.1.

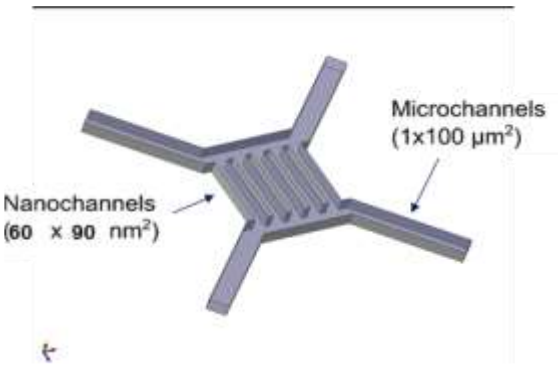

Figure 2.1: Cartoon of micro and nano-channels device. The dimension of micro and nano-channels are 1×100 μm^2 and 60×90 nm^2, respectively.

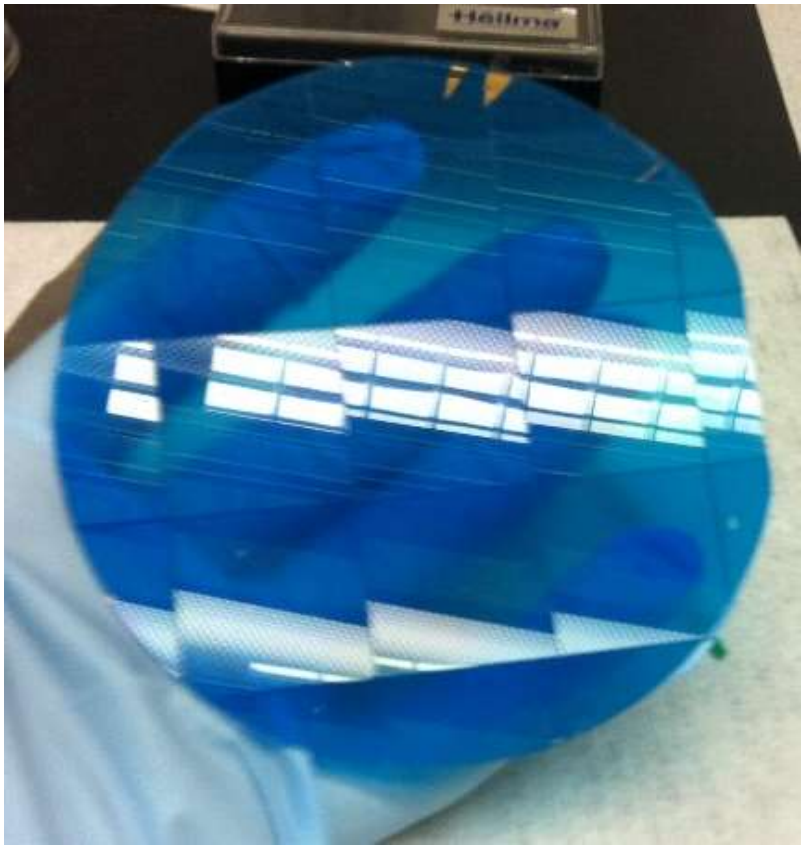

Figure 2.2: Blue film protection of chips

I received wafers after all micro-and nanofluidic features were prepared a four inch wafer is glued on the blue film to protect the nano and micro featured and diced into 9 chips 25mm×25mm (Figure 2.2). To create the access hole to the microchannels, we use a PrepStart Air Abrasion Unit (Danvill Engineering, Inc) with the abrasive blasting compound ≠14 (17.5 µm aluminum oxide from Crystal Mark, Inc). To absorb extra abrasive we use a MacroCab dust cabinet (DavillEngineering, inc). Sandblasting device is shown in Figure 2.3.

Figure 2.3: Sandblasting. Apparatus used for sandblasting through-holes in fused-silica microfluidic devices. (a) MacroCab dust cabinet used to contain the abrasive dust. (b) Output valve setting for slow sandblasting.

We drill the holes starting from the uncovered side of chip (no blue film) until the abrasive penetrates through to the other side. We ensure the access point of the microchannels is drilled directly by checking under microscope. Then we wash the chips with DI water (1 MΩ clean). Further, we remove the protective film from chips. At this point we also start processing the planar sealing substrates that are used to form a closed liquid volume by bonding to the chip. We use coverslips that are made of fused silica (170 µm thick) and have the same size as our chip [25].

We soak chips and coverslips in Microposit Remover 1165 (Rohm and Haas Electronic Materials) at 65 ˚C for one hour in the Ultrasonic Cleaner in order to remove the photoresist.

After that, we carefully rinse five times with DI water and put them in a detergent (contrex) for 1 hour. Then we rinse three times with DI water.

We keep them submerged until the RCA procedure starts. The RCA clean is a standard set of wafer cleaning steps, which needs to be performed before high temperature processing steps of silicon wafers (description is available on Wikipedia).

We used a modified RCA procedure that consists of two steps. The first step is (RCA2) performed using a 1:1:5 solution of Hydrochloric acid, 37% (J.T.Baker, Semiconductor grade), Hydrogen Peroxide, 30 % (J.T.Baker), and distilled water (18.2 MΩ clean) at 70˚C. RCA2 removes metal ions and inorganic residues with an acidic solution. Chips and coverslips on the special Teflon holder (Figure 2.4) are submerged in this solution for 15 minutes, then transferred to two DI water baths. Such treatment removes the metallic (ionic) contaminants from the surface of the chips and coverslips.

The second step (RCA1) is performed using a 1:1:5 solution of Ammonia Hydroxide, 25% (Riedel-de Han, Semiconductor grade), Hydrogen Peroxide, 30% (J.T.Baker) and distilled water (18.2 M clean) at 70˚C. RCA1 removes organic residues and introduces hydroxyl groups on the chips and coverslips surface with an alkaline solution. The same Teflon holder is transferred to this solution for 15 minutes, then placed in the two DI water baths.

To dry the activated surface, we use a flow of N_2, by drying the chip from the nanochannel side and bring back both surfaces into contact. Applying a moderate pressure with Teflon

tweezer (Figure 2.5) to ensure the air bubbles are pressed out and the two halves of the chip are bound together.

Figure 2.4: Teflon holder for holding chips and coverslips in RCA 1 & 2 baths.

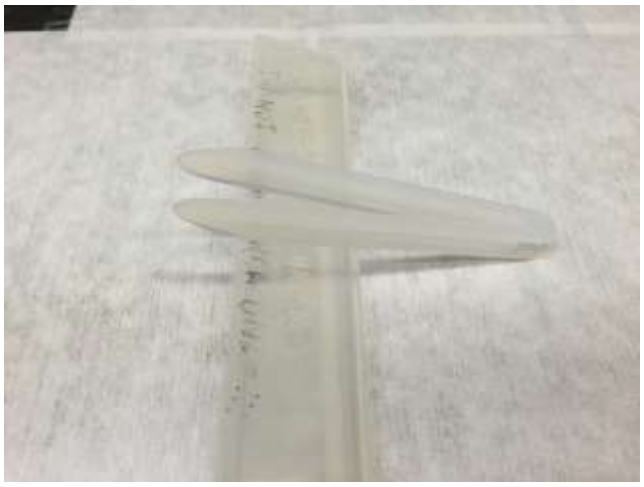

Figure 2.5: Teflon tweezer for removing air bubbles between chip and coverslip.

Figure 2.6: Bound chip.

If the pieces bind together without noticeable contamination and no air bubbles gets trapped between the two pieces (especially, on microchannels and nanochannels), we continued with the thermal step, otherwise we separate the chip and the coverslip and repeat the RCA steps again. After that we place the bound chips in the Neycraft furnace (Dentsply Prosthetics) and heat them from room temperature to 1000˚C with the rate of 450˚C/hour. When the necessary temperature is reached, chips stay heated for two hours and then they are cooled down to room temperature. A bound chip is shown in Figure 2.6.

We mount the bound device onto a plastic block, made from Poly methyl methacrylate (PMMA, commercial name Plexiglas) and metal holder, which is shown in Figure 2.7 and Figure 2.8. The mounted chip has four top screws and four side screws. From the top screws, which are connected to reservoirs, we can load our solution (Figure 2.7). From side screws we can connect our pressure pick tubing to flush and push DNA and solution to the nanochannels (Figure 2.8). Each DNA molecule is driven by hydrostatic pressure (20- 40 psi) from microchannel to nanochannel. After the DNA molecules has entered into the nanochannel, the pressure gradient is removed and the dynamics of molecule are observed.

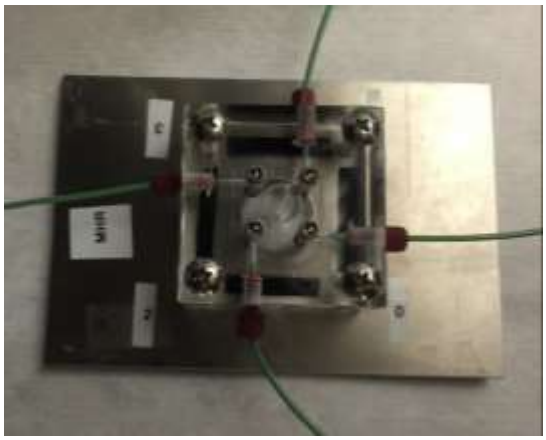

Figure 2.7: Top view of the chip holder. Small top screws are connected to reservoirs, which solution is loaded inside.

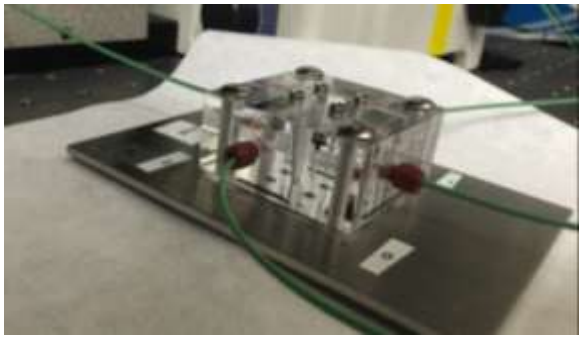

Figure 2.8: Side view of the chip holder. Chip is sandwiched between plastic block and metal plate. Tubing is connected through the ports at the side of the PMMA.

2. Fluorescence Microscopy

To image DNA and protein molecules, we use an inverted fluorescence microscope (Nikon Eclipse TE 2000-U), with an Andor iXon+EM-CCD (Electron Multiplying Charge Coupled Device) camera to monitor the emission light of our fluorescent dyes by a 50 mW laser. The key component which differentiates fluorescent microscopes from ordinary ones is the dichroic filter. The dichroic filter is thin-film filter, which used to selectively pass light of a small range of color, while reflecting other color.

The microscope objective is very important, because it allows us to get the resolution of the diffraction limit, while conserving a high brightness and low signal to noise ratio [27]. The resolution of an objective is limited by its numerical aperture (NA), which is the product of refractive index of the imaging medium "n" and sine of angular aperture "θ". The lateral resolution can be defined by Rayleigh's criterion:

$$r_{lateral} = \frac{2\lambda}{\pi NA} \tag{2.1}$$

We used an oil immersion objective with 100X magnification and numerical aperture of 1.35 (Nikon). A according to Equation (2.1), it has 262 nm lateral resolution for the emitted 535 nm light. A total Internal Reflection Fluorescence (TIRF) 100X objective was used when we wanted to observe a thin region of specimen, usually less than 200 nm, next to the coverslip. Fluorescence images were obtained by using fluorescent filters.

When it was required to observe DNA and protein signal simultaneously, we used dual imaging. In particular, a MAG Biosystems DV2 dual splitter, was used to split the emission

light from the microscope into two independent channels. The spectral channels were projected onto separate half's of the CCD simultaneously.

In our setup, we used either 50 mW class III lasers or the light source used in an Xcite 120 broadband metal halide lamp. The class III lasers (Shanghai Dream Lasers) are either blue (473nm) or green (556 nm), and are controlled through the provided gating input. In our experiment, most of the images were taken with flash length of laser (10 to 40 ms) and 50 or 90 ms acquisition time.

In single molecule fluorescence detection the molecule must contain or be labeled with an efficient fluorophore molecule. Good dyes have high absorbance and a high quantum-yield, nevertheless we typically need an intense light source, usually is laser, that can induce background fluorescence. Single molecule fluorescence has two major problems:

1. Photo bleaching: most of the fluorophore molecules have photo bleaching problem, which means after absorbing many photons in order of a few million, they chemically rearrange and stop to be fluorescent.
2. The sample is going to be study have to be very clean.

3. Biological Materials

We use λ-DNA for our experiments. λ-DNA is the genomic DNA of bacteriophage λ. The λ-DNA was linearized at the cos site by the vendor (New England Biolabs). λ- DNA has 48502 basepairs. Since DNA and protein molecules do not have native fluorescence when illuminated by visible light, we used one of fluorescent dyes to visualize DNA molecule.

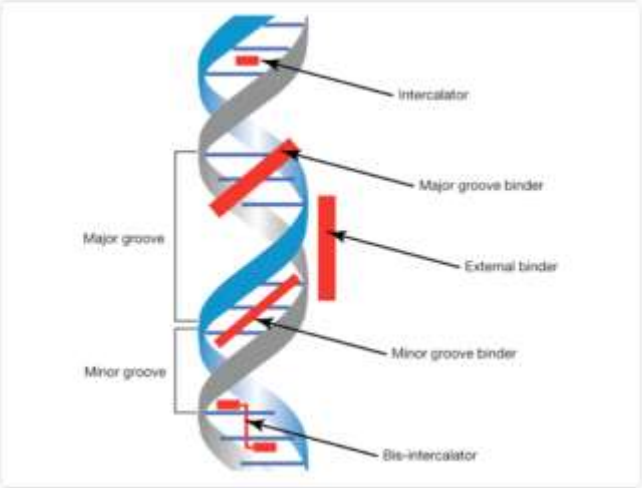

Figure 2.9: DNA with possible target sites of different fluorescent dyes [139]**.**

Fluorescent dyes such as YOYO-1 and YOYO-3 (bis-intercalator dye, Molecular Probes/ Invitrogen) are typically used for single-molecule DNA experiments. 4', 6-diamidino-2-phenylindole (DAPI, minor group binder dye), is an alternative which is compatible with a wide range of biological buffers, and does not interfere with the structural of DNA. Staining DNA with fluorescent dye can change the mechanical properties of DNA such as DNA length, DNA persistence length. The dye separates basepairs significantly, and unwind the double helix somehow [28]. A sample double stranded of DNA and possible target sites of dyes is shown in Figure 2.9.

YOYO-1(Figure 2.10) is observed by using a FITC filter set (Semrock, FITC-3540B, excitation 482/35, dichroic 506LP, and emitter 536/40).

YOYO-3 (Figure 2.11) is observed by using a dedicated filter set (Chroma, 31004, excitation 560/40, dichroic 59SLP, emitter 630/60).

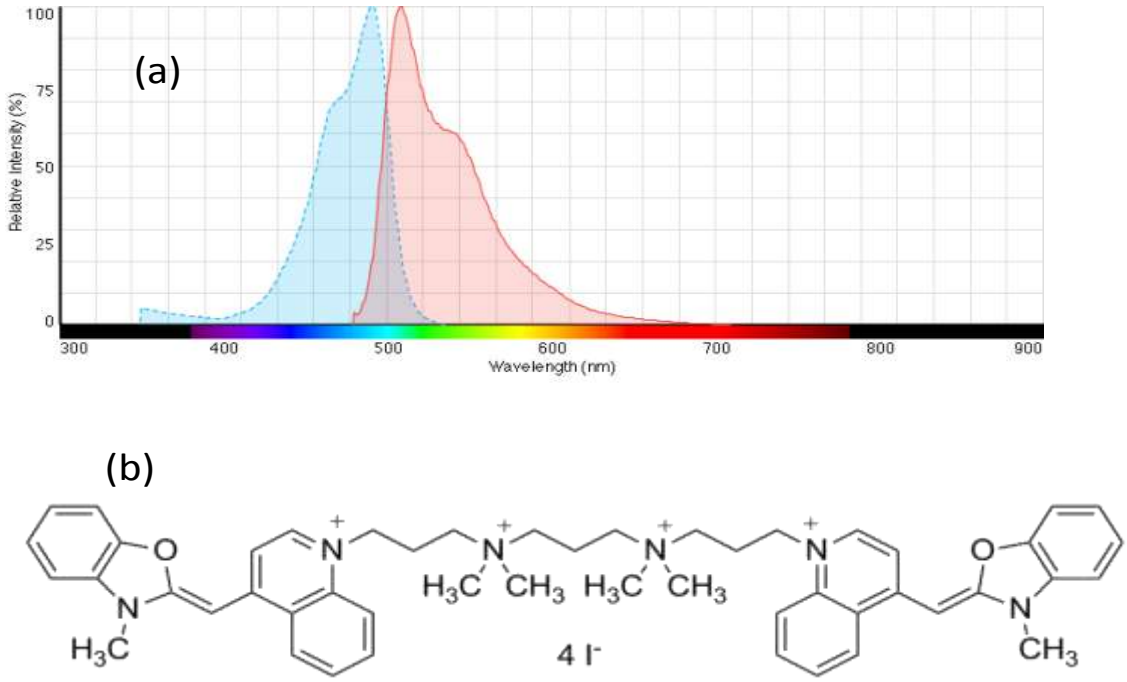

Figure 2.10: (a) Excitation (blue) and fluorescence emission (red) spectra of YOYO-1 bound to DNA. (b) Chemical structure of YOYO-1. Image provided by Thermo Fisher Scientific.

DAPI (Figure 2.12) is observed with a dedicated filter (Chroma, 49000, excitation 350/50X, dichroic 400 LP, emitter 460/50).

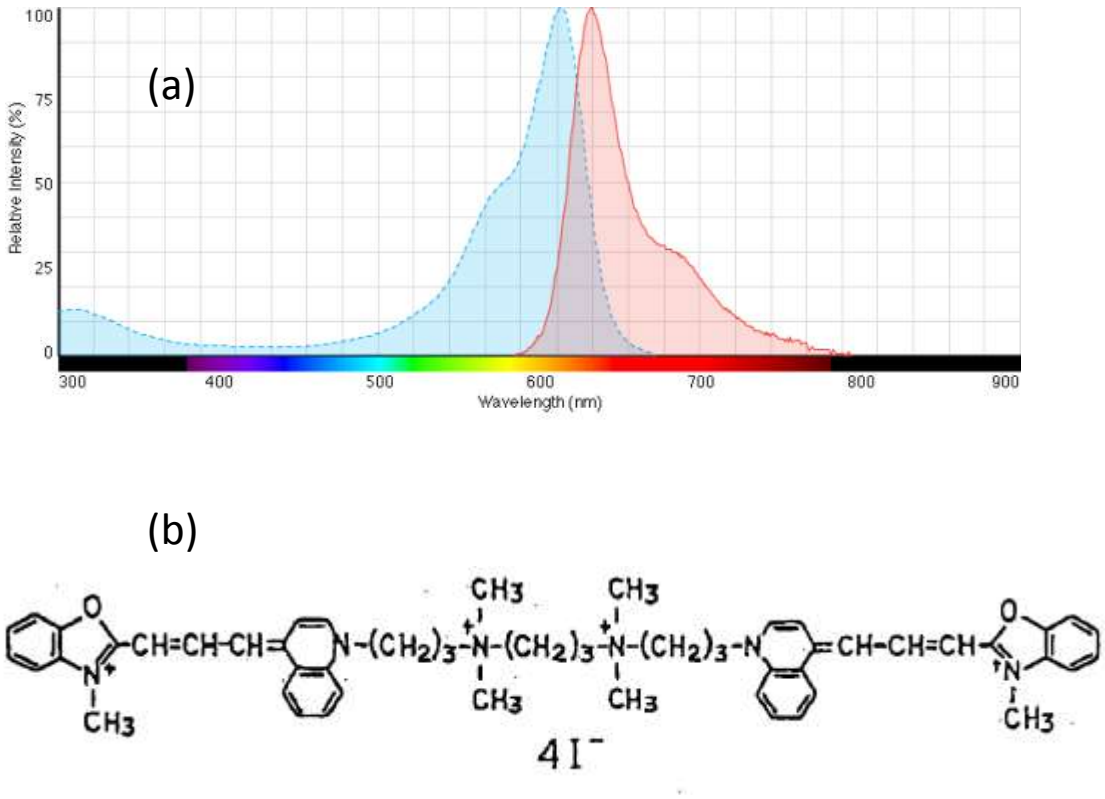

Figure 2.11: (a) Excitation (blue) and fluorescence emission (red) spectra of YOYO-3. (b) Chemical structure of YOYO-3. Image provided by Thermo Fisher Scientific.

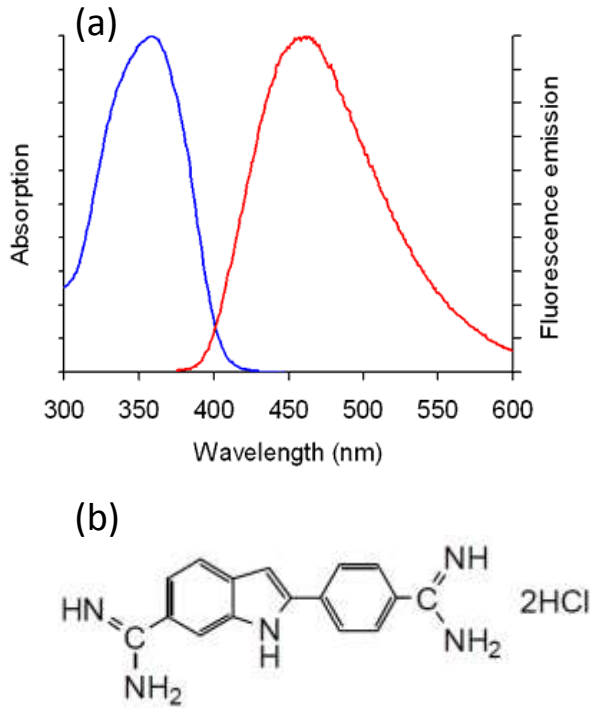

Figure 2.12: (a) Excitation (blue) and fluorescence emission (red) spectra of DAPI bound to DNA. (b) Chemical structure of DAPI. Image provided by Thermo Fisher Scientific.

4. Buffer Solutions for Fluorescence Imaging

The conformation of DNA and proteins depends on the buffer conditions [12], [29]. To image DNA molecules, we used 0.5xTBE buffer (Tris/Borate/ETDA, pH≈8). TBE buffer is a good buffer for nucleic acids. In particular it is suited our purposes because it maintains DNA deprotonated in solution. In our experiment, the salt concentration of buffer is an important factor because many physical characteristics of DNA are dependent on salt concentration of buffer. For example, it has been shown that salt concentration of buffer changes the Debye length, which can alter DNA length [12].

For this work, prepared stock 10x TBE buffer solution, which consisting of 108 g of Tris base, 55 g of Boric Acid, and 40 ml of 0.5 M EDTA, which are dissolved in 1 liter of de-ionized water. Under this conditions the mechanical properties of DNA are well-explored [29].

In case where Tris was undesired (for example working with labeled protein), we used 1x PBS buffer solution (pH≈ 7.4). 10x PBS buffer is composed of 80 g of NaCl salt (Fisher, # 5271), 2 g KCl (sigma, # 9541), 14.4 g of Na_2HPO_4 (Sigma, # 57907), and 2.72 g of K_2HPO_4 (Sigma, # p2222), which are dissolved in one litter of de-ionized water and after that, the solution must be adjusted to pH 7.4. All our buffers were autoclaved and stored at 4 ˚C.

Ethylenediaminetetraacetic acid (EDTA) in buffers serve as chelator of divalent ions, such as magnesium. The most important thing is magnesium, because it is a co-factor of many DNA-modifying enzymes. This reducing magnesium enhances DNA stability. In addition, ETDA prevents the growth of bacteria in the buffer [30].

Bovine serum albumin (BSA) is a serum albumin protein derived from cows. It is often used as a protein concentration standard in the lab experiments. It has a single polypeptide chain of approximately 583 amino acid residues and its molecular weight is 66430 g/mol. BSA helps to prevent unspecific binding of proteins and prevents DNA sticks to the channels wall *(*Invitrogen. Retrieved 19 January 2012*)*.

We used β-mercaptoethanol (BME, Sigma Aldrich) to our DNA solution right before imaging. BME is used to reduce of bleaching of our molecules during fluorescence imaging. It is also well-known to reduce disulfide bonds in solution, and thus reduces aggregation.

High concentration of BME denatures BSA proteins that reason in this case we can use Dithiothretol (DTT) in our solution. DTT is an alternative to BME and a strong reducing agent (electron donating). Addition of DDT prevents inter-and intramolecular disulfide bonds from forming between the cysteine residues of proteins. DTT is used as reducing or "deprotecting" agent for thiolated DNA [31].

5. Fluorescent Staining of Nucleic acids

Unstained lambda DNA molecules (48 kbp) were purchased from Roche at a concentration of 263 µg/ml and stored at -80 ˚C. For staining λ-DNA with a bis-intercalating dye such as YOYO-1 or YOYO-3, dyes were ordered from Invitrogen and diluted in anhydrous Dimethyl Sulfoxide (DMSO) to 10µM. An aliquot of lambda DNA is diluted to 10 µg/ml, and then heated at 65˚C for 10 minutes, and then immediately quenched by transferring to an ice bucket. We then add dye (YOYO-1 or YOYO-3) to the DNA solution. In our experiment, we used approximately one dye molecules for twenty base pairs of DNA.

After we added our dye to DNA there are several methods to obtain homogenous stained DNA. I used incubation of the solution in the dark room temperature for four hours and subsequent transfer of the solution to a 4 ˚C fridge for overnight. After I checked whether the quality of stained DNA was good, I aliquoted the stained DNA into small amounts (10 µl each vial) and froze them quickly with liquid nitrogen and kept them at -80˚C fridge.

DAPI, unlike YOYO-1 and YOYO-3, does not need to incubate with DNA for an extended time to achieve homogenously staining. We added DAPI to DNA half an hour before DNA imaging. The DAPI concentration in DNA solution is 10µM. DAPI was ordered from Sigma Aldrich and diluted to 10µM with 200 mM PBS and aliquoted DAPI were stored at -20 ˚C fridge.

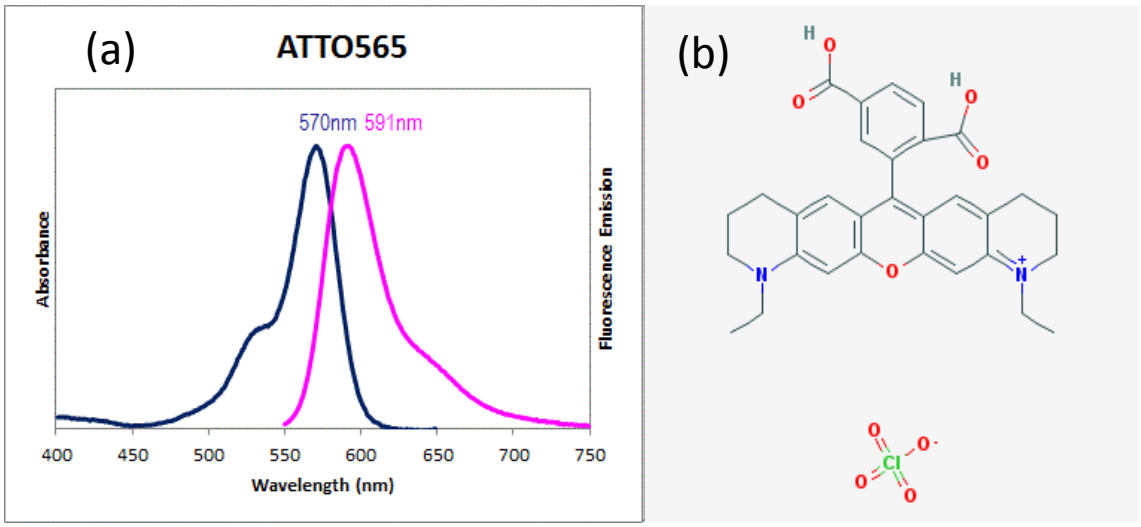

Figure 2.13: (a) Excitation (blue) and fluorescence emission (red) spectra of NHS-ester ATTO 565. (b) Chemical structure of ATTO 565. Image provided by Integrated DNA Technologies.

6. Labeling T4 DNA ligase

In chapter five, we describe a study of how T4 DNA ligase and its cofactors drive a DNA molecules in nanochannels. As part of this study, it became desirable to directly image the location of T4 DNA ligase molecules. In order to image the protein, T4 DNA ligase was labeled with ATTO 565 NHS-ester, the chemical structure and absorption-fluorescence emission spectra of which are shown in Figure 2.13.

In order to label T4 DNA ligase by attaching one dye molecule to only one lysine group of protein, we need between 40 to 60 µl of protein at a concentration of 1 to 2 mg/ml. If the concentration is below of 1 mg/ml, we would need to concentrate the protein solution prior to reaction NHS-ester is an amine- reactive cross-linker reactive group. It is the simplest and the most common and versatile techniques for crosslinking or labeling peptides and proteins such as antibodies with primary amines (–NH2).

. The labeling steps are:

1. Making bicarbonate buffer (1M) immediately, before incubating dye with the protein: 0.084 g of NAHCO3 in 1 ml of DI water add 0.88 µl of 5 M NaoH.
2. Filter this buffer with 0.1 µm syringe filter.
3. Add 10 % by volume of bicarbonate (1M) to concentrated protein.
4. Add the stock dye to the protein, such that the molecular ratio of dye to protein is 6 to 1.
5. Incubate dye with protein solution at 4˚C overnight. If the total volume of solution is more than 20µl.

We used dialysis to remove free and unreacted dyes. Specific steps are:

1. Gently rinse out dialysis micro tube with DI water, be very careful because it pops out the membrane very easily.
2. Then transfer the solution to 8 kD (depends on the molecular weight of your protein solution) dialysis tube.
3. Clean and wipe the floater with 70% ethanol.
4. Transfer the dialysis tube to cold room, make sure room is dark.
5. Place beaker with 1L of autoclaved 1X PBS at pH 7.4 with bar on stir plate.
6. Place the dialysis micro tube with floater membrane down into the buffer, into a vortex created by the stir bar. (Make sure all solution get down to the membrane, maybe need to flick the solution).
7. Dialyze for at least 30 hours (3 buffer exchange, every 9 hours)

After dialyzing protein solution, we verified that the protein was labeled properly and there was no free dye. We used microcon centrifugal filter to separate protein and free dye if present (Figure 2.14). Microcon centrifugal filter device simply and efficiently concentrate and desalt macro molecular solutions of 10–500 μL using any centrifuge that can accept 1.5 mL tubes. This filter consist of two parts: sample reservoir, which we load our solution, and the filtrate vial, which is the solutions come out from filter (Figure 2.14). We put the labeled T4 DNA ligase solution in to this filter and spin at 3000 RCF at 4˚C for 20 minutes. We then tested the filter for dye-specific absorption with UV-Vis. A dye signal in the filterate vial is indication of free dye. At the same time we expect that the ratio of protein to dye absorption in the reservoir is unchanged after filtration.

An alternative way to verify that protein labeled properly and there was no free dye is Electrophoretic Mobility Shift Assay (EMSA) gel. The speed at which different molecules move through the gel is determined by their size and charge [32]. In our case the control lane is bare dye and other lanes should be different concentrations of labeled protein. Since bare dye has a smaller size than labeled protein, we expect that by running this gel, labeled protein moves slower than the bare dye. Otherwise, it means that there is free dye in our labeled protein solution. In Figure 2.15 shows one example of labeled T4 DNA ligase with ATTO 565nm NHS-ester, which confirm that there is no free dye in the solution.

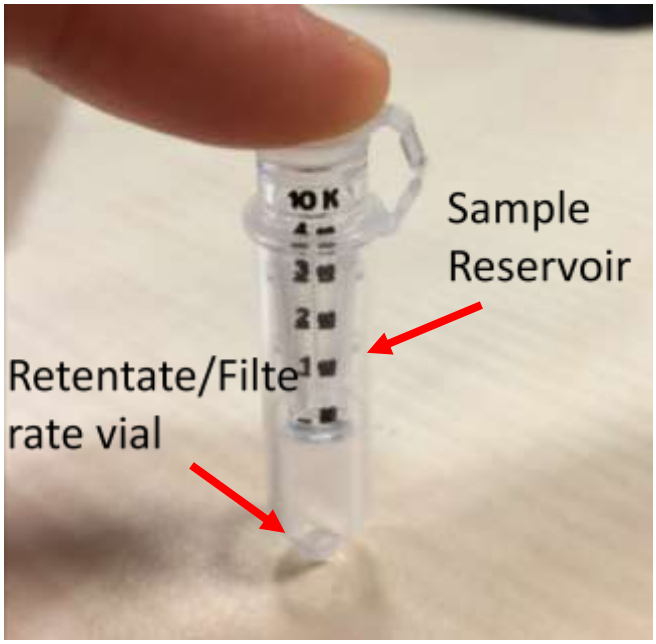

Figure 2.14: Microcon centrifugal filter device.

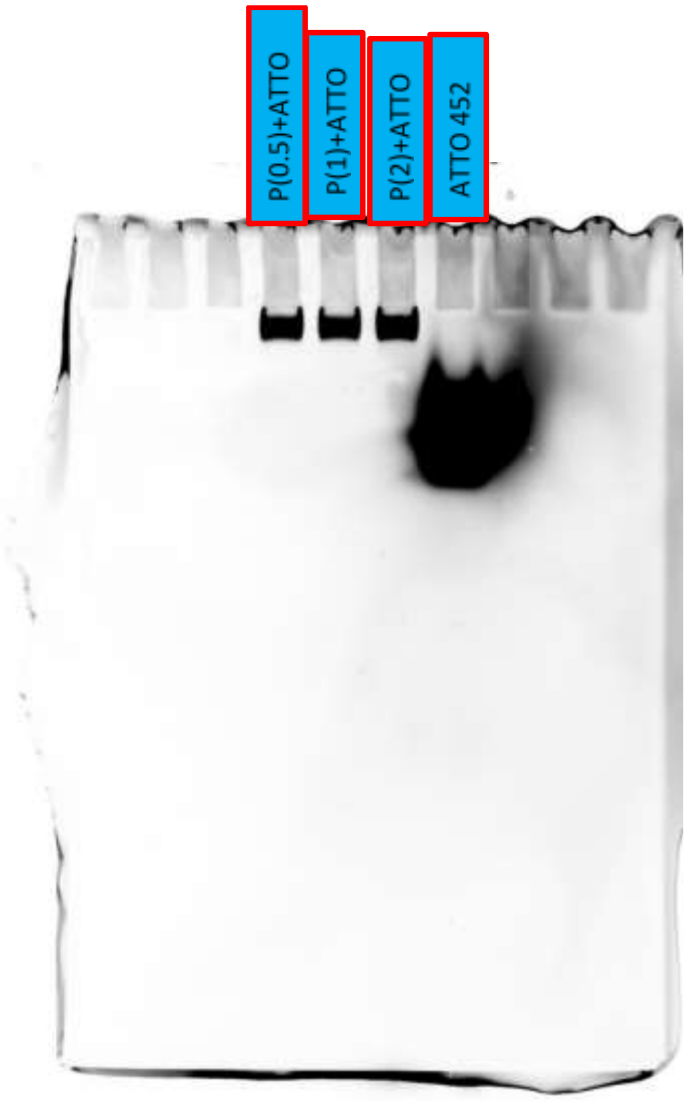

Figure 2.15: EMSA gel, bare dye is ATTO 565 nm NHS-ester and protein is T4 DNA ligase. According the gel result there is no free dye in labeled protein, otherwise had to have a band same as bare dye.

7. Gas Phase APTES modification

In chapter 3 we used Atomic Force Microscopy (AFM) to image the colocation of protein and DNA. In that method, DNA molecules need to be immobilized on surface. We follow the methods, developed by Lyubachenke et al. In that method to modify the surface with aminopropylsilane using a 3-aminopropyltriethoxysilane (APTES), which leads to an electrostatic interaction of DNA whit positive charged of amine group.

APTES reacts with hydroxyl group to make amino-functionalization. We developed a methodology to obtain APTES surface coverage by gas phase adsorption. The gas phase APTES was found to be relatively simple and effective. The modification process for mica surfaces with APTES is shown in Figure 2.16. The exposed hydroxyl reacts with hydroxyl on the mica surface, forming Si-O-Si covalent bonds, and its amino moieties remain stable on the mica surface [33]. When the DNA molecule was dropped onto this surface, its amino moieties can electrostatically adsorb negatively-charged DNA [33].

For modification of the coverslip surface with APTES by the gas phase process, we need 100 to 200 µl of APTES was dropped into small container and cleaned coverslips were

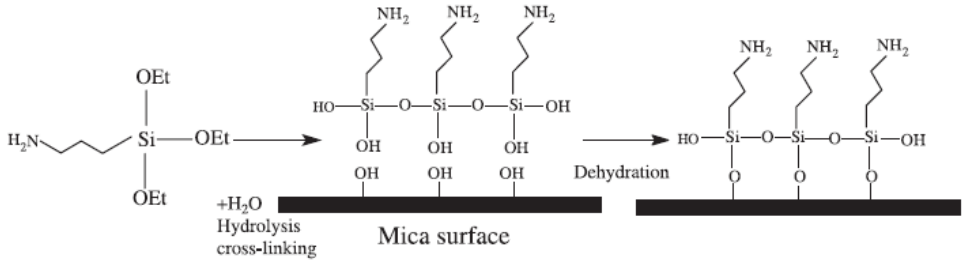

Figure 2.16: Schematic drawing of the supposed 3-aminopropyltriethoxysilane salinization process on mica surface [33]**.**

place into the Teflon rack. The rack was placed in a chamber downstream of the APTES reservoir and nitrogen was flushed through the APTES container for two hours so that the APTES 's evaporate went to our chamber. All those operations have to be performed in a fume hood (Figure 2.17). We can keep those glass-APTES coverslips in glove box for one week. In Figure 2.18 shows immobilized λ-DNA stained with YOYO-1 on an APTES surface and λ-DNA stained with YOYO-1 on normal coverslip.

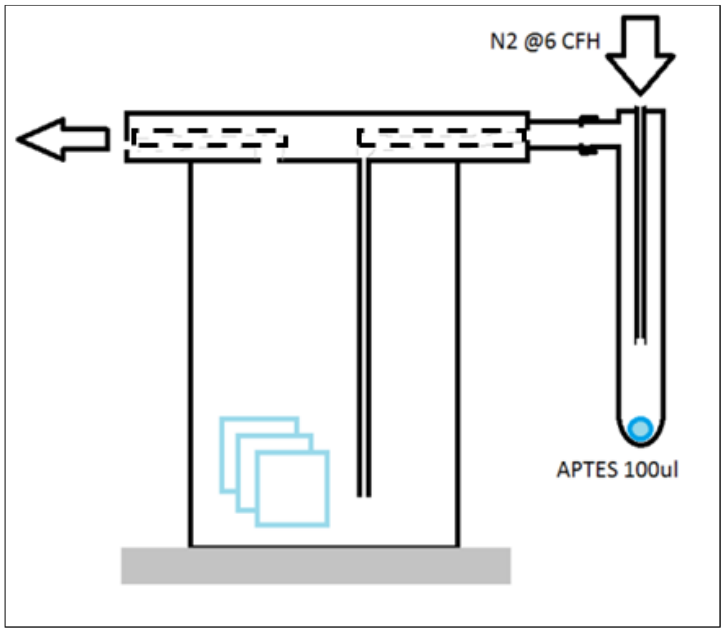

Figure 2.17: Gas phase APTES setup, consist of two major parts, first our container, which there is our liquid APTES, second our chamber, which there is our cleaned coverslips.

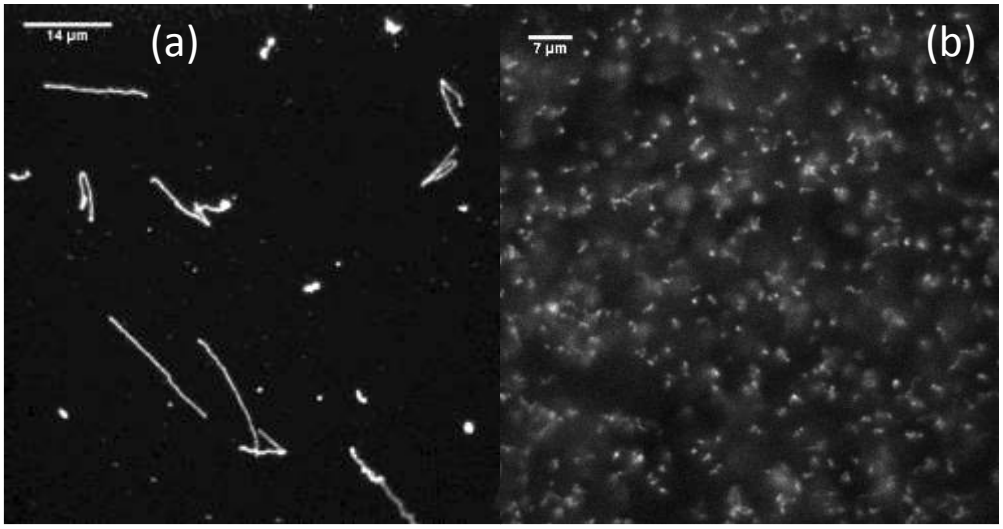

Figure 2.18: (a) Immobilized λ-DNA on APTES- coverslip. (b) λ-DNA on normal coverslip. λ-DNA was stained with YOYO-1.

3. Probing transient protein-mediated DNA linkage using nanoconfinement

We present an analytic technique for probing protein-catalyzed transient DNA loops that is based on nanofluidic channels. In these nanochannels, DNA is forced in a linear configuration that makes loops appear as folds whose size can easily be quantified. Using this technique, we study the interaction between T4 DNA ligase and DNA. We find that T4 DNA ligase binding changes the physical characteristics of the DNA polymer, in particular persistence length and effective width. We find that the rate of DNA fold unrolling is significantly reduced when T4 DNA ligase and ATP are applied to bare DNA. Together with evidence of T4 DNA ligase bridging two different segments of DNA based on AFM imaging, we thus conclude that ligase can transiently stabilize folded DNA configurations by coordinating genetically distant DNA stretches[34].

1. Introduction

Protein-mediated DNA loops play a central role in many biological processes [35], [36]. DNA looping is involved in transcription [37], repair [38], telomere maintenance [39], and gene regulation [40]. In general, protein-mediated DNA looping enables DNA regions separated by a large genetic distance to interact with each other. The formation of very large loops (10s to 100s of kbp) in the emergence of chromatin organization and the necessity of this

chromatin organization for normal cell function is an intensive focus of recent research [41]–[43]. In particular, the co-operative action of multiple protein copies in promoting DNA looping [44]–[47] and conformational change [48] has become a central question. Here we demonstrate a tool for detecting transient interactions that may be important in facilitating looping transitions (Figure 3.1).

The most established method for quantifying DNA loop formation is the gel electrophoresis mobility shift assay [49]. Protein-mediated DNA loops can also be directly visualized by atomic force microscopy (AFM) or transmission electron microscopy (TEM) [37]–[39]. These single-molecule techniques have the advantage of detecting rare states. However, only configurations of DNA molecules smaller than 10 kbp in length can be easily interpreted if molecules are randomly deposited on a surface from solution. DNA bending and looping on an even shorter scale (10s of bp) can be detected by fluorescence energy transfer, and important information about the single-molecule dynamics can be established [50], [51]. Tethered particle motion (TPM) is also able to monitor the temporal fluctuation of DNA, but does so on a larger scale [52]–[54]. However, similar to force-based measurements, it requires the modification of the DNA ends [55]–[57]. That potentially limits the utility for studying proteins that not only catalyze internal loops, but also end-to-end circularization. In principle, optical microscopy can follow the temporal course of loop formation [58], but in general it requires resolution enhancement techniques to follow loops in the range of a few kbp, which in turn lower the temporal resolution [59]. Stretching DNA in flow cells overcomes the resolution problem, but notably the extending stress is very heterogeneous along the molecule making a quantitative evaluation difficult [60].

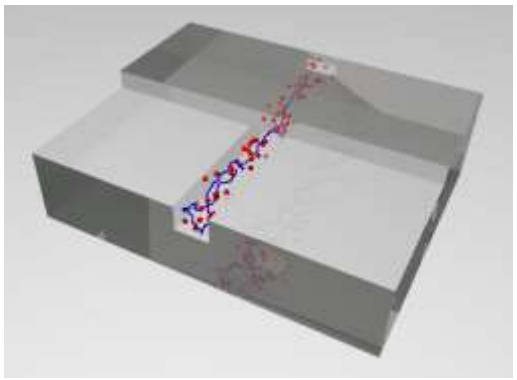

Figure 3.1: Schematic of nanochannel-stretched DNA (blue) with weakly-binding protein particles (red). Proteins are larger than actual for easy visibility. In the foreground there is a folded DNA configuration.

We will use stretching of DNA in nanochannels as the main analytic technique for following DNA loop configurations in this publication [61]. Such nanochannels have a cross-section of ~100 x 100 nm^2, and a length of 100s of micrometers. After DNA is brought into a nanochannel, it will assume an equilibrium configuration that is governed by the channel cross-section, the contour length of DNA, its persistence length, and its width [62]. The dependence on the persistence length and width make nanochannel stretching a promising probe for these parameters as a function of buffer conditions [12] or protein binding [63]–[65]. DNA is dynamic inside nanochannels and fluctuates [10], [66], [67], and can thus explore many possible configurations during a single experiment. Furthermore, the configuration of looped [68] and knotted [69] molecules can be followed in real time (Figure 3.1).

Cyclization by T4 DNA ligase is an intensively studied model system for DNA looping [70]–[73]. T4 DNA ligase displays a surprisingly large range of functionalities. T4 DNA ligase catalyzes formation of the phosphodiester bond between the adjacent $5'$-PO_4 and $3'$-OH groups at DNA ends of double-stranded DNA (dsDNA) fragments [74]. It joins dsDNA in both

blunt-ended ligation and the ligation of complimentary ends, which is the same as nick ligation. It also ligates single-stranded DNA (ssDNA), albeit with very low efficiency [75]**,** seals single-stranded 1–5-nucleotide gaps [76], and acts as a lyase by removing apurininc/ apyrimidinic (AP) sites [77]. T4 DNA ligase requires the co-factors ATP and Mg^{2+} for full activity. ATP is required for specific binding of ligase to both DNA strands, while Mg^{2+} is required for catalytic action [78], [79]. At high T4 DNA ligase concentration, non-specific binding to dsDNA was observed. Furthermore, it was proposed that the apparent persistence length of DNA drops in presence of a high concentration T4 DNA ligase [80], [81], which is likely due to ligase induced DNA kinking and local base-pair opening in transient DNA-ligase complexes [82].

In studies that focus on the mechanical properties of DNA, T4 DNA ligase is typically used at a low concentration to secure circular configurations that are at formed through hybridization of complimentary ends [70]. Thus, the cyclization rate is governed by the probability of a both ends coming together, specifically as a function of DNA length, DNA stiffness, and swelling of the coil [70], [72], [83]. While the self-interaction probability of relaxed yeast chromatin indicates the validity of the worm-like chain model [84], we note that ligase-based looping seems more efficient than predicted by that model for larger distances (> 1 kbp) [72].

We can speculate on the connection between the efficient formation of very large loops (>1 kbp) and both blunt-ended dsDNA and ssDNA ligation capability. In order to ligate distinct DNA molecules, the enzyme has to bind to two DNA molecules simultaneously and locate their ends. That means three entities (1^{st} end, 2^{nd} end, ligase or ligase multimer) have to come

together in a small volume. In analogy with search process of transcription factors and other sequence-specific enzymes, we speculate that the DNA looping rate is enhanced through a facilitated diffusion process in which the protein first binds to a nonspecific motif, and then translocates along the strand to locate DNA ends [85]. We will show evidence that non-specific DNA-protein-DNA clusters are formed even at internal DNA-DNA junctions.

In this chapter, we investigate the influence of T4 DNA ligase and its cofactor ATP on the configuration of long DNA strands under nanoconfinement. Under the Mg^{2+}-free conditions chosen by us, ligase is not capable of covalent strand-joining and is known to bind DNA independent of its catalytic action. We introduced λ-DNA molecules into nanochannels and observed extended and folded DNA configurations (Figure 3.1 and Figure 3.2). We observed a contraction of DNA in presence of T4 DNA ligase. We further recorded a strongly increased probability of folded DNA configurations in presence of T4 DNA ligase. These folded configurations gradually unfolded, and we observed that the rate of DNA unfolding reduced under ATP exposure. We attribute this slowing of unfolding to the establishment of transient, T4 DNA ligase-mediated DNA-DNA links. AFM imaging supports the hypothesized notion that transient DNA-DNA contacts are stabilized by T4 DNA ligase. We speculate that such transient stabilization of DNA-DNA contacts may be a general mechanism to increase the rate of protein-induced DNA looping.

2. Experimental

λ-DNA (Roche Diagnostics GmbH) was stained with YOYO-1 (Life Sciences) at a ratio of 1 dye per 10 base pairs. The contour length of unstained λ-DNA (48.5 kbp) is

approximately 16 µm. After staining, that length can increase by up to 30% [86]. DNA was suspended in 0.5x TBE buffer (pH 8) at room temperature. BSA (0.1 mg/ml, New England Biolabs) was added to prevent sticking of DNA to the nanochannels. For experiments requiring ATP, the final ATP concentration was 1 mM.

We chose T4 DNA ligase supplied by Roche Diagnostics (1 U_{Roche}/µl), since this vendor does not supplement their product with BSA. The latter would interfere with the interpretation of our AFM measurements. The T4 DNA ligase stock solution was expected to have a concentration of 6 µM, while we measured a concentration of 10.4 µM via absorption spectroscopy. We also observed that T4 DNA ligase is predominantly in a multimeric state using dynamics light scattering (DLS), with some large aggregates, possibly due to the fact that this vendor does not add BSA. We thus believe the concentration of active T4 DNA ligase molecules is considerably lower. Using Roches units, the final T4 DNA ligase concentration is 5 U_{Roche}/ml.

The majority of recent publications in the field use T4 DNA ligase supplied by New England Biolabs, which contains BSA. Using the same unit definition as New England Biolabs, the final concentration of T4 DNA ligase is in the range of 500 U_{NEB}/ml to 1000 U_{NEB}/ml (1 U_{NEB}/ml = 0.02 nM [82]). This compares to 250 U_{NEB}/ml used by Widom and Cloutier [87], [88], 1 U_{NEB}/ml used by low-concentration studies such as Du et al. [81], and a few 10^4 U_{NEB}/ml by Yuan et al. [82]. We verified that nanochannel measurements with an equivalent concentration of T4 DNA ligase from both New England Biolabs and Roche gave similar results.

Samples were prepared in the following sequence: DNA was suspended in buffer at 1 μg/ml and heated to 65°C for 10 minutes before being rapidly cooled on ice. BSA was added. T4 DNA ligase and ATP were added as necessary, and the sample was incubated for 15 minutes at room temperature. Then a 100 mM YOYO-1 stock solution was added, and the solution was incubated for four hours at 4°C. The solution was briefly spun down in a micro centrifuge prior to experiments.

All experiments used mixed micro- and nanofluidic devices made from fused silica, which were prepared by methods discussed elsewhere [89]. Nanofluidic channels with a 50×100 nm^2 cross-section and a length of 200 μm were placed between u-shaped microchannels that were 100 μm wide, 800 nm deep, and had about 1 cm separation between inlets and active zone [90] . Each DNA molecule is driven from microchannel to nanochannel by a hydrostatic pressure gradient. After the DNA molecule has entered the nanochannel, the pressure gradient is removed and the dynamics of molecules are observed. Molecules were observed using an inverted fluorescence microscope with a 1.3-N.A. oil-immersion microscope objective (Nikon, TE- 2000) under illumination from a metal halide lamp, and observation by emCCD camera (Andor).

We followed the conventional approach of representing the brightness of a stretched DNA molecule as the convolution of a boxcar function and a Gaussian [61]. However, since a brightness step within the molecule is present for folded molecules, two such functions are necessary. For calculating the end-to-end and the loop length of DNA molecules, we fitted the brightness along the molecule backbone to:

$$I(x) = I_b + \frac{I_f - I_u}{2}\left(\operatorname{erf}\left(\frac{x - x_f + \frac{l_f}{2}}{\sigma}\right) - \operatorname{erf}\left(\frac{x - x_f - \frac{l_f}{2}}{\sigma}\right)\right) + \frac{I_u}{2}\left(\operatorname{erf}\left(\frac{x - x_u + \frac{l_u}{2}}{\sigma}\right) - \operatorname{erf}\left(\frac{x - x_u - \frac{l_u}{2}}{\sigma}\right)\right) \quad (3.1)$$

I(x) is the intensity along nanochannel, σ is the slope of the edge, I_u, and I_f are the brightnesses of the unfolded and folded sections. x_u and l_u are the center and length of the entire molecule. x_f and l_f are the center and length of the folded stretch. I_b is a constant background term.

For AFM imaging we diluted linear DNA (3.8 kbps) in AFM deposition buffer (25mM HEPES, 25mM Sodium Acetate, pH 7.5). The final DNA concentration was 1 ng/µl for all measurements. For measurements with T4 DNA ligase and ATP, the respective final concentrations were 5 U_{Roche}/ml (Roche) and 1 mM, respectively. Solutions were incubated at room temperature for 15 min. APTES mica surfaces were prepared as described earlier [91]. A droplet of the DNA or T4 DNA ligase- DNA-ATP solution was added onto an APTES treated mica surface and incubated for 30 minutes. Surfaces were further washed with deionized water and dried with dry nitrogen. Imaging was performed in non-contact mode in air (cantilevers: Nanosensors, PPPFMR; resonant frequency: ~45-115 kHz, spring constant: 0.5-9.5 N/m) using an Asylum MFP3D AFM instrument.

3. Results

Upon introduction of λ-DNA into nanochannels, we observed two predominant configurations (Figure 3.2). The *extended configuration* (Figure 3.2a) is characterized by constant fluorescence intensity along the channel (Figure 3.2b, c, d). In the *folded configuration* (Figure 3.2e), a hairpin causes the molecule to fold back on itself. A step in the molecule brightness can be observed (Figure 3.2f, g, h). DNA molecules entered the nanochannel randomly in either an unfolded or folded configurations. The folded configurations are not simply density fluctuations of extended molecules [66], [67]. In particular, the bright region of a fold is always linked to one end, and the onset within the molecule is sudden. In contrast, thermal density fluctuations of an extended molecule are well described by Rouse modes. Their phase is in general random, so that they do not form stable step-like configurations. After observation effects are taken into account, these fluctuations also cannot reach the intensity magnitude found here.

We analyzed the intensity profiles of extended λ-DNA molecules, and found the mean end- to-end lengths by fitting to Equation (3.1) after applying the constraint $I_f=I_u$. The histogram in Figure 3.3 shows the distribution of end-to-end of lengths of extended DNA molecules for the three different datasets. A Gaussian is fit to each distribution to obtain the mean end-to-end lengths, listed in Table 3.1. We find that λ-DNA contracted in the presence of T4 DNA ligase, from 14.4 μm for bare DNA to 12.5 μm with T4 DNA ligase. We attribute the further contraction and narrowing of the distribution upon addition of ATP mainly to an interference of the dye with ATP, and not an actual effect of ATP (separate manuscript in

preparation). We have found no evidence that the increase of the ionic strength from ~15 mM lowers the extension strongly if DAPI is used for DNA visualization. Reisner reported such a reduction as funciton of ionic strength [12].

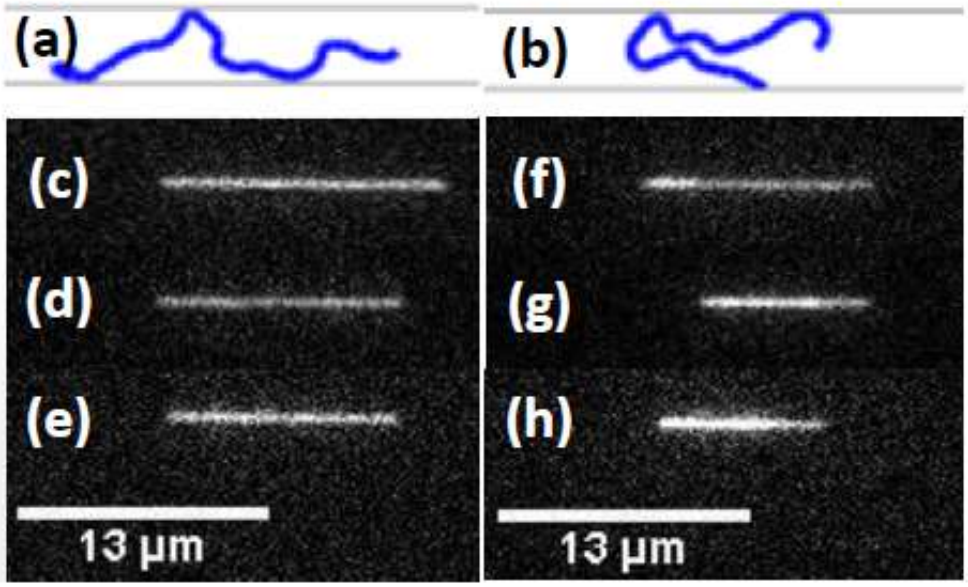

Figure 3.2: Observed configurations of λ-DNA molecules in nanochannels. (a) and (b) are schematics of extended and folded structures, respectively. (c-e) are fluorescence micrographs of extended configurations and are (f-h) fluorescence micrographs of folded configurations. (c) and (f) are bare λ-DNA, (d) and (g) are λ-DNA with T4 DNA ligase, and (e) and (h) are λ-DNA with T4 DNA ligase and ATP.

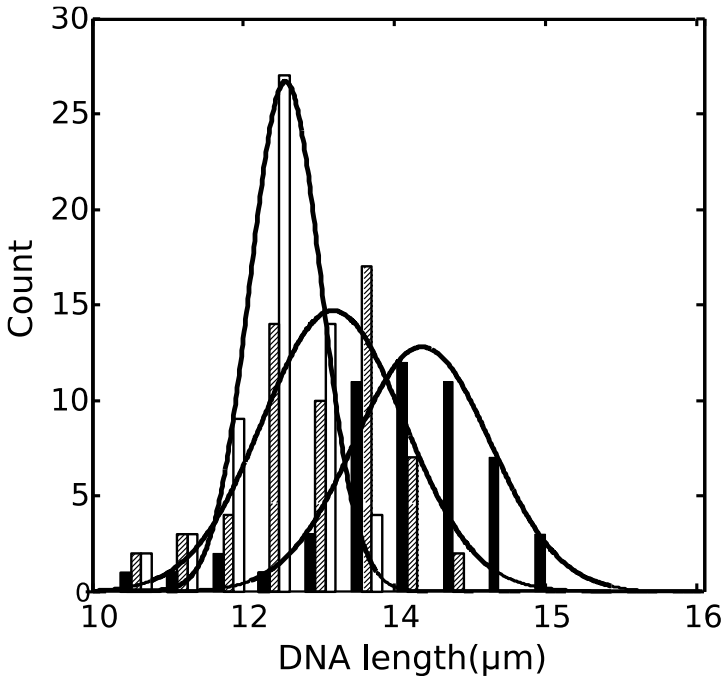

Figure 3.3: Histogram of end-to-end lengths of extended DNA molecules, bare λ-DNA (solid bars), λ-DNA with T4 DNA ligase (gray bars), and λ-DNA with T4 DNA ligase and ATP (white bars). A Gaussian was fit to each distribution to determine the mean end-to-end DNA lengths (see Table 1).

Table 3.1: Statistical characterization of DNA configurations in the presence of T4 DNA ligase and ATP. 60 extended molecules for each condition were used to find l_u (extension of a fully unfolded molecule), Δl_u^2 (mean fluctuation amplitude of fully unfolded molecules), and K (spring constant derived from the former two quantities, see discussion). 22 folded molecules for each condition were used to find γ (ratio of apparent extensions of folded and unfolded regions). The relative product of persistence length and molecule width, Pw, was found from the mean values of l_u and γ. The probability of entry in a looped configuration, p_{loop}, was found from 100 molecules for each condition. Parameter definitions are given in the discussion.

Sample	l_u (μm)	Δl_u^2 (μm^2)	K (10^{-2} N/m)	γ	Pw (rel.)	p_{loop}
Bare λ-DNA	14.4±0.1	0.218±0.02	1.9±0.2	1.26±0.15	1.00	0.27
λ-DNA + T4 ligase	13.2±0.1	0.233±0.01	1.8±0.1	1.10±0.02	0.51±0.23	0.41
λ-DNA + T4 ligase + ATP	12.5±0.1	0.223±0.02	1.9±0.2	1.06±0.02	0.39±0.18	0.43

DNA configurations are dynamic, and we followed molecules for at least 30 seconds. Folded molecules under all conditions gradually unroll until molecules reach an extended configuration, as reported by Levy [68]. We show intensity time traces of the recoil process in (Figure 3.4a-c). We quantified the configuration parameters by fitting the full form of Equation (3.1) to intensity profile of along the nanochannel (Figure 3.4d, e, f). The unrolling process occurs over 10s of seconds, and is considerably slower than the relaxation time of both density fluctuations [66], [67] and the connected relaxation of length fluctuations [10], [67] that occur within a few seconds. Thus, we feel further strengthened in applying Levy's loop interpretation [68].

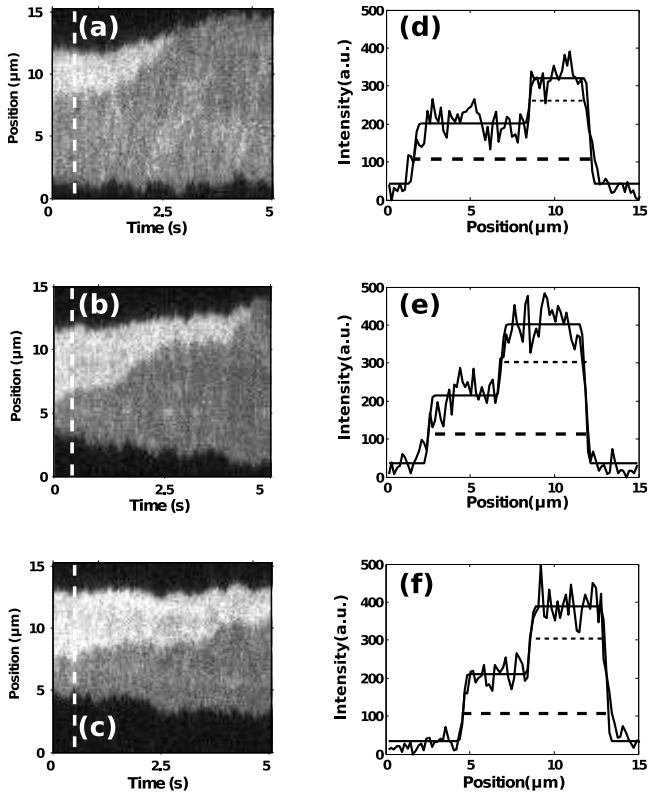

Figure 3.4: Folded λ-DNA molecules in nanochannels. (a-c) show kymographs of fluorescence intensity along channel axis as a function of time. (d-f) illustrate the projected intensity of λ-DNA molecules as a function of position along the nanochannel at 0.5 s. The end-to-end DNA length of molecules is shown with dashed line and folded length is shown with dotted lines. (a) and (d) are bare λ-DNA, (b) and (e) are λ-DNA with T4 DNA ligase, and (c) and (f) are λ-DNA with T4 DNA ligase and ATP.

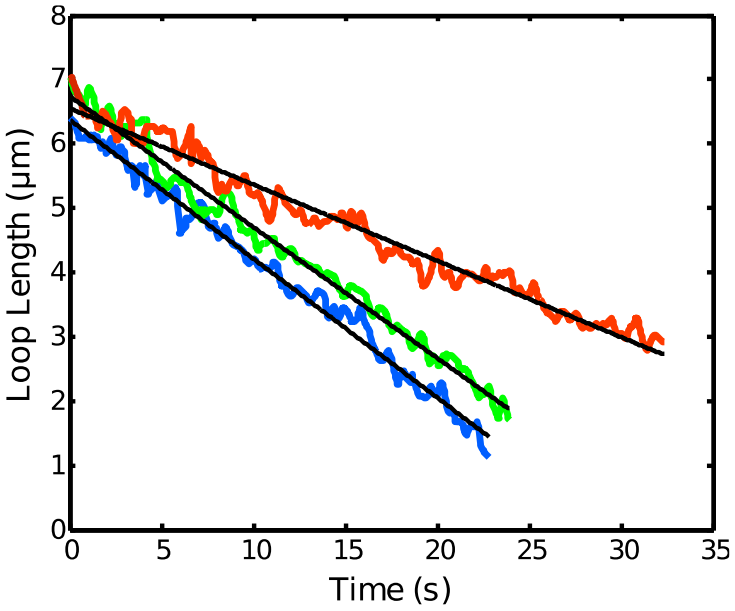

Figure 3.5: Mean aligned DNA molecule loop lengths as function of time for 22 molecules per dataset with their linear fits. Bare λ-DNA (blue), λ-DNA with T4 DNA ligase (green), and λ-DNA with T4 DNA ligase and ATP (red).

In order to quantify the speed of unrolling, we aligned molecules under equal conditions by shifting the time axis until curves overlapped. The resulting graphs of average loop length versus time are shown in Figure 3.5. We found that loops unfold with an approximately constant rate of 216 ± 5 nm/s, 204 ± 5 nm/s, and 119 ± 3 nm/s for λ-DNA, λ-DNA with T4 DNA ligase, and λ-DNA with T4 DNA ligase and ATP, respectively (ATP alone without ligase was similar to bare DNA).

To further investigate whether or not DNA ligase directly promotes DNA looping, we performed AFM imaging on DNA deposited from a solution containing bare DNA (Figure 3.6a), and a solution containing DNA, T4 DNA ligase and ATP (Figure 3.6b and c). Because of the length of the chosen DNA substrate (~1.2 μm), we anticipate that the majority of DNA

molecules form random DNA-DNA crossings that are an effect of the deposition of the 3-dimensional molecule to the 2-dimensional surface. Visual inspection of DNA-DNA crossings reveals that intersections in the presence of both T4 DNA ligase and ATP appear on average taller than those without (compare Figure 3.6a to 6b and 6c).

Along the extended DNA on the surface (away from crossings), we observed a larger variability of height of the fiber in the presence of T4 DNA ligase and ATP. In particular taller sections to occur in stretches along the molecule. We attribute this to the binding of T4 DNA ligase to DNA.

We analyzed the peak height of DNA-DNA crossings in the absence or presence of DNA ligase, and observed dramatic differences (Figure 3.7). In the case of bare DNA (Figure 3.7a), a single peak is observed (0.70±0.08 nm), while the histogram for DNA with T4 DNA ligase and ATP (Figure 3.7b) showed two peaks (0.73±0.05 and 1.07±0.15 nm). The stated uncertainties are the half-widths of the Gaussian fits; the confidence for the peak positions is higher. The lower peak in the presence of DNA ligase (Figure 3.7b) is consistent with the height for DNA-DNA crossing with bare DNA (Figure 3.7a). The second peak in Figure 3.7b corresponds to the binding of T4 DNA ligase since it is absent without DNA ligase (Figure 3.7a). The area under the two Gaussian peaks indicates that ~¾ of all DNA-DNA junctions are bound by ligase molecules. We are not able to distinguish whether these are monomers or multimers. That ratio matches the fraction of junctions with greater height that we visually estimated in Figure 3.6.

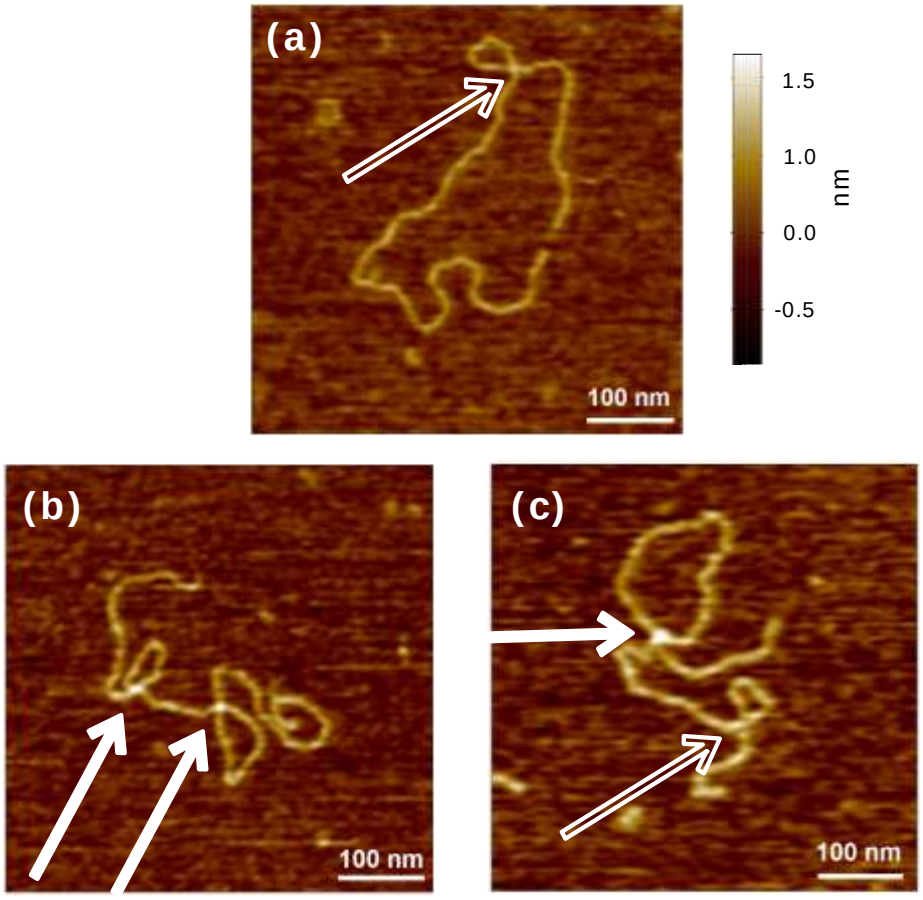

Figure 3.6: AFM images of DNA-DNA crossings. (a) Bare DNA (3.8 kbp). (b, c) DNA with T4 DNA ligase and ATP. Solid arrows indicate higher crossings consistent with ligase binding, outlined arrows indicate shallower crossings consistent with bare DNA.

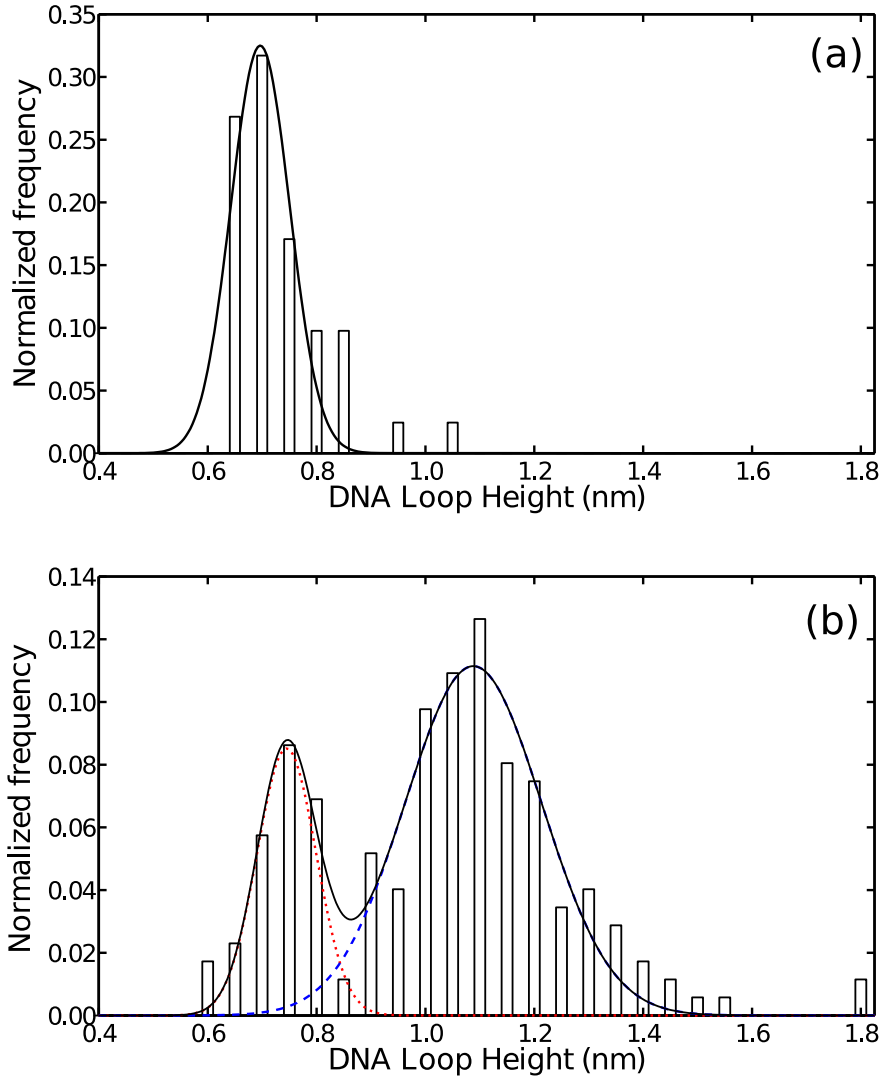

Figure 3.7: Histograms of heights of DNA-DNA crossings. (a) Bare DNA (N=41). (b) DNA with T4 DNA ligase and ATP (N=174). The red dotted line corresponds to unoccupied crossings, the blue dashed line to occupied crossings, and the solid line is the sum of both.

4. Discussion

It is apparent that the addition of T4 DNA ligase and the further addition of ATP modify the behavior of DNA significantly. In order to interpret the measurements, we will have to discuss them in the framework of confined polymers.

Although the theory of DNA extension under 1-d confinement is still an active field of research [92], [93], a good experimental understanding exists [10], [94]. Broadly, the extension of confined DNA molecules results from a balance between entropy and excluded volume interactions within the DNA [95]. A DNA molecule of contour length *L*, width *w*, and persistence length *P* that is confined to a nanochannel of width *D* will elongate due to excluded volume interaction between segments of the polymer that are separated in genetic position along the backbone. The de Gennes theory predicts an extension *l* that scales as [95], [96]

$$\boldsymbol{l \cong L\left(\frac{wP}{D^2}\right)^{1/3}} \tag{3.2}$$

However, experimental tests have shown that the scaling in *D* is stronger than indicated [10]. Recently, the importance of a minimum scale for self-avoidance [97], and the alignment of polymer segments [98] have been demonstrated. Interestingly, the ideal scaling of Equation (3.2) is recovered for circular DNA [94]. We thus anticipate that the dependence of *l* on *P* is higher than that on *w* in channels with a width of 100 nm, with an exact functional relationship not clear for the extended configuration.

There are two distinct mechanisms that can lead to an apparent shortening of DNA in nanochannels upon protein binding. The first mechanism is the formation of stable compacted

DNA configurations that change the effective available contour length of the DNA. Examples include the binding of histones [63] or nucleoproteins [64]. The second mechanism is the modification of p and w, which leads to more dramatic effects under nanoconfinement than in free solution [12], [99]. Decreasing l in identical channels could be effect of w or P. Neither mechanism are related to the osmotic pressure effects that can collapse DNA which occurs at higher concentration of proteins than considered here [18], [100], [101].

To the first approximation, the effective spring constant K of unfolded molecules can be found from the fluctuation amplitude through $K=k_BT/\langle \Delta l_u^2 \rangle$ [10], where k_B is the Boltzmann constant and T is the temperature. If the scaling of Equation (3.1) is combined with the free energy of deformation of the de Gennes model such as given by Jun et al. [102], one can predict that the spring constant is invariant under changes in (Pw) as long as the contour length is conserved. Refinements to the determination of the length fluctuation amplitude that take the measurement process and all Rouse modes into account [67] do not change this result as it applies to all modes independently. We tested whether the reduction in l was connected to a change of w and P or to a more fundamental change in molecule configuration by determining the effective spring constant witnessed by the fluctuation amplitude in l (Table 3.1). Addition of T4 DNA ligase to DNA as well as further addition of ATP did not change the spring constant significantly. We thus believe that all extended configurations are essentially wormlike chains of similar contour length, and that no permanent links between genetically distant loci are established.

We define α as the extension factor (length of occupied channel segment divided by contour length) of an unfolded segment of DNA. β is the extension factor of a folded segment (two times length of occupied channel segment divided by contour length). Interestingly, we can determine $\gamma = \beta/\alpha$ alternatively from the ratio of brightness's $\gamma = 2 \cdot I_u/I_f$. The γ-factor is a demonstration of the excluded volume effect, since an ideal chain should show γ=1. Levy et al. reported γ=1.3 in a configuration similar to ours [68]. We find a similar γ for bare DNA (Table 3.1), but a strong reduction once T4 DNA ligase is introduced, and a further reduction upon ATP addition. Since the relative magnitudes of both α and γ are experimentally accessible, we can find β. Since the scaling predicted by de Gennes holds for folded segments [94], we can assume that Equation (3.2) holds and determine the product *wP*. We find that it is reduced to 50% upon addition of T4 DNA ligase and to 40% in the presence of ATP. This is a remarkable reduction. We are however not able to measure *w* and *P* independently, even though detailed numerical studies exist [93], [103].

Levy et al. have described a model for the unfolding of the folded geometry that utilizes a constant driving force due to excluded volume interaction and a drag force dominated by the drag between channel walls and DNA [68]. In the framework of this model, the decreased unfolding rate in the presence of T4 DNA ligase and ATP could be interpreted as a reduction of the effective width of the chain. The looping and unfolding process in nanochannels has numerically been treated by Cifra and Bleha [104], but for relatively short chains and without hydrodynamic interactions. Račko and Cifra [105] have treated kinetics of the segregation two independent chains in nanochannels, which is interesting, but topologically different. A recent

study by Chen did note that some folded molecules can become trapped in a folded state for extended times [106].

We have found two potential problems with Levy's model [68]. Firstly, the model is missing a force term for γ>1. We have modified the model by changing to discrete model and numerical integration, and find a small correction for γ=1.3. Secondly, neither the original nor the modified model appears to fit the data in our data set. Instead of a concave curve as claimed by Levy, we find essentially a straight line. Indeed, if the last two data points of their data set are removed, their result also is consistent with a straight line.

In order to illuminate the apparent inconsistency of our fit with Levy's model, we calculated the histogram of frame-to-frame steps. For bare DNA, the result is shown in Figure 3.8a. A single Gaussian fit (not) shown showed a considerable under fitting in the region of -1.0 to -0.5 μm. We thus fitted to two Gaussians, where one Gaussian has mean displacement of approximately 0 with 208±5 counts attributed. A secondary feature emerges at -0.75 μm displacement (frames are spaced by 50 ms). However, since only 1/10th of all counts are attributed to the secondary feature (22.8±4.5), the location and width of the feature carry large uncertainties. Upon inspection of the original image data (Figure 3.4), we observe that it appears to contain long phases of relatively little change that are interrupted by short periods of rapid shortening of the looped region. Inspection of Levy's data shows the same dynamics. Note that the secondary feature leads to a very large effect on the total movement of the chains as these periods carry a high weight due to the large displacement (Figure 3.8b).

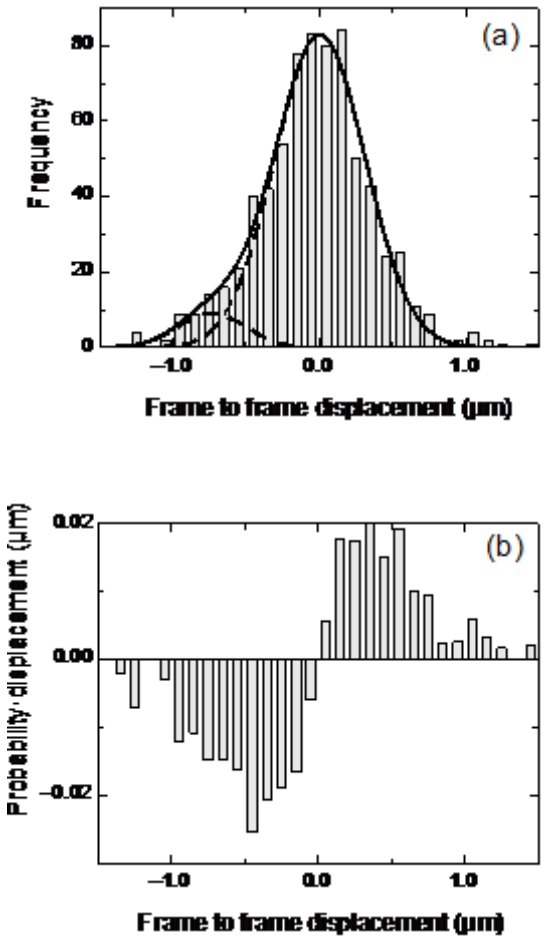

Figure 3.8: Statistical properties of folded length for bare DNA. (a) Frame to frame statistics of displacements of folded length. The solid line is the composite fit, while the dashed lines are the individual Gaussians. The fit parameters (with 1 σ error) for the main peak are center position 0.003±0.025 μm, standard deviation 0.308±0015 μm, number of molecules 208±5. The fit parameters for the weaker feature are center position -0.734±0.118 μm, standard deviation 0.231±0.097 μm, and number of molecules 22.8±4.5 (b) Probabilities in (a) weighted with displacements, i.e. a histogram of the probability-displacement product.

We speculate that the unrolling does not progress through a continuous process, but rather one that is characterized by starts and stops which is linked to entanglement of the two chains occupying the same channel segment. In particular, the central feature appears to correspond to the relatively stable folded configurations that Chen observed [106], and we

suggest that the importance of the feature in our data is due to the fact that our molecules are 8 times longer than in their publication. We can probe whether the displacement in the histogram is due to random motion, or the effect of a hypothetical two-state motion. To this end, we form the mean over three consecutive displacements, and the re-calculate the histogram. We find that the central peak has narrowed approximately by a factor of $\sqrt{3}$, as expected for thermal fluctuations with a short relaxation time, or errors in fitting. However, the negative displacement feature did not shift significantly, and became even more distinct. Thus, we conclude that steps of rapid unrolling are typically occurring together. We believe that the local rate of unlooping within these should follow Levy's model.

We now turn to the histogram obtained when T4 DNA ligase and ATP are added (Figure 3.9a). We chose the three-step averaged form since the narrower distribution makes visual comparison easier. We find that upon adding T4 DNA ligase to DNA, the shape and distribution of the central peak does not shift significantly. The secondary feature disappears in the isolated form, but is possibly reflected by a large weight at about -0.15 μm in Figure 3.9b. Since the rapid unrolling typical of the 'jumps' occurred in irregular intervals, the alignment of the unrolling curves in Figure 3.5 does typically "grab onto" the slow creep phases. Thus, the similar shape of the main feature for bare DNA and that bound to T4 DNA ligase leads to a similar numerical measure of relaxation.

Upon addition of ATP to DNA and T4 DNA ligase, the mean displacement of the central peak is considerably reduced, and the peak width apparently is reduced. No secondary feature is discernable. The reduction in mean displacement is directly reflected in the mean

unrolling speed in Figure 3.5. We believe that the reduction in peak width indicates that DNA segments are not free to move past other segments. Note that the length fluctuations for fully extended DNA molecules in Table 3.1 showed no change at the same time.

We will now attempt to attribute the differing dynamics in the light of the likely biological function of T4 DNA ligase and DNA polymer behavior. Above we have hypothesized that the creeping motion is an effect of mutual entanglement of the two strands occupying the same volume, while the jumps are in an untangled state. Following this hypothesis, we conclude that addition of T4 ligase either reduces the likelihood of disentanglement dramatically, or increases the likelihood of re-entanglement. Both the reduction in persistence length, as well as the reduction in effective polymer width would lead to such an effect, due to the likelihood of entanglement, and the lowering of the effective driving force.

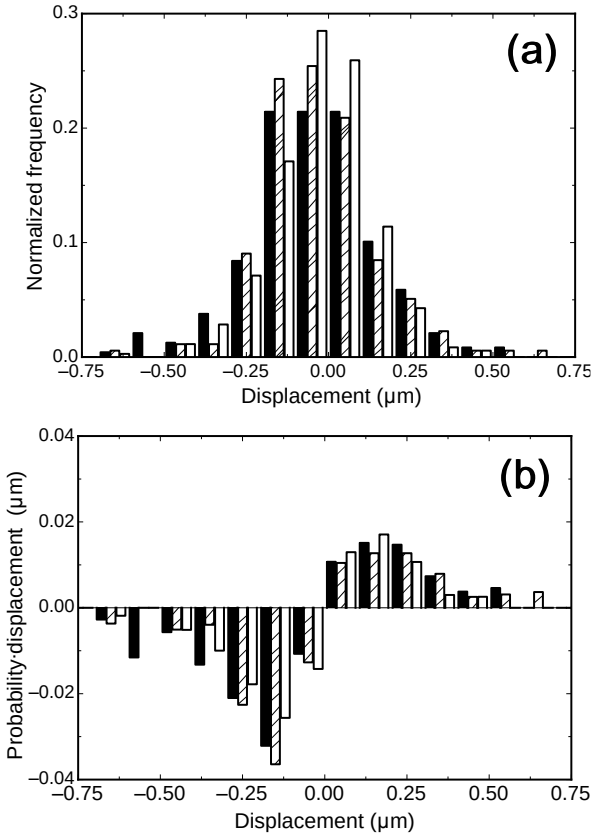

Figure 3.9: Histograms of 3-frame averaged displacement of folded length. (a) Histogram showing bare DNA (solid), after addition of T4 ligase (diagonal stripes), and with T4 ligase and ATP (outlined dots). (b) Product of probabilities in (a) and displacement.

Upon binding of ATP, we anticipate that the interaction between DNA and T4 DNA ligase becomes considerably more specific. The uniform modification of γ has already demonstrated that ligase binds uniformly along the molecule. We thus believe that the significant reduction of the mean displacement in Figure 3.9b is a testament of increased binding stability of T4 DNA ligase to DNA, and dimerization of T4 DNA ligase molecules on neighboring strands. T4 DNA ligase could potentially slide along the DNA, but we believe that

it is likely to stall at intercalating dyes and single-stranded DNA defects induced by oxidative damage during dye bleaching [107], [108]. ATP has previously been identified as being necessary for specific binding to single-site defects. Since multiple bound enzymes can act to stabilize the same loop, the ability of ligase oligomers to stabilize folded configuration is a function of both binding constant of ligase and the coverage.

This picture is further solidified by our finding that the majority of DNA-DNA crossings were occupied by T4 DNA ligase in AFM measurements. Based on the dynamic light scattering data, this T4 DNA ligase is likely in not in a monomeric state. Thus it appears that one T4 DNA ligase is bound to each DNA strand, and the oligomerization drives the coordination of the strands.

We further believe that the DNA-DNA crossings observed in AFM are present before the DNA is deposited on the substrate, and not simply a result of the deposition of a 3-dimensional molecule onto the 2-dimensional substrate. We base this statement on the statistics of molecule entry into nanochannels (Table 3.1). At the pressures used for the majority of experiments, the fraction of DNA molecules entering channels was considerably lower for bare DNA when compared to both samples with T4 DNA ligase. This increase upon ligase binding could be due to a reduction in w and P, but also the formation of a looped structure prior to insertion into the nanochannel. While the first factor doubtlessly plays a role, we have concrete evidence for the second one as well.

For this, we lowered the injection pressure, which resulted in near complete disappearance of folded configurations for bare DNA, while DNA in the presence of T4 DNA

ligase still entered with loops. However, the configuration was such that the folded segment trailed the molecule through the channel. That in stark contrast to loops at high driving pressure [109], and in particular loops in the absence of T4 DNA ligase, where we see almost exclusively folded segments leading the molecule. The only explanation for this asymmetry is the formation of transient loops in solution. Remarkably, this occurs even in the absence of Mg^{2+} (although a small number of Mg^{2+} ions could be remaining from expression of the protein).

5. Conclusion

We have presented evidence that the physical behavior of nanoconfined DNA is significantly altered in the presence of T4 DNA ligase. In particular, the characteristic stretching of DNA in nanochannels is reduced. We have found evidence of dense binding of protein along the molecule. T4 DNA ligase binding reduced the product of effective DNA width and persistence length by more than a factor of 2, and greatly increased the stability of folded geometries within nanofluidic channels. We hypothesize that bound ligase molecules on neighboring strands can dimerize, and that they in essence stabilize parallel configurations of two DNA strands. We further found evidence for temporary loops in solution that are stabilized by transient ligase-induced links. We believe that such transient protein loops are mobile, and may form an important pathway for the efficient formation of specific large-scale DNA loops.

4. Interference of ATP with the Fluorescent Probes YOYO-1 and YOYO-3 Modifies the Mechanical Properties of Intercalator-Stained DNA Confined in Nanochannels

Intercalating fluorescent dyes are widely used to visualize DNA in studies on DNA-protein interactions. Some require the presence of adenosine triphosphate (ATP). We have investigated the mechanical properties of DNA stained with the fluorescent intercalating dyes YOYO-1 and YOYO-3 as a function of ATP concentrations (up to 2 mM) by stretching single molecules in nanofluidic channels with a channel cross-section as small as of roughly 100×100 nm^2 including. The presence of ATP reduction the length of the DNA by up to 11%. On the other hand, negligible effects are found if DNA is visualized with the minor groove- 4', 6-diamidino-2-phenylindole (DAPI). The apparent drop in extension under nano- confinement is attributed to an interaction of dye and ATP, and the resulting expulsion of YOYO-1 from the double helix [110].

1. Introduction

Single-molecule fluorescence microscopy is a powerful tool to explore the statistical, mechanical, and transport properties of DNA [111]–[115]. It in particular enables nanofludic methods for genome analysis that aid rapid sequence assembly and elucidate structural variations as well as haplotype. Since DNA is not fluorescent, it must be stained with fluorescent dyes. One of the most commonly used dyes in such experiments is the bis-intercalator YOYO-1. YOYO-1 forms a very stable complex with double-stranded DNA (dsDNA) and undergoes about 500-fold fluorescence enhancement upon binding, thus providing high signal to noise ratio [116].

Intercalating dyes affect both the mechanical and structural properties of DNA [117]–[119]. Generally, YOYO-1 causes DNA elongation, and it is assumed that the contour length of dsDNA complex with YOYO-1 increases linearly with increasing staining ratio by up to 35% compared to native DNA [86], [118], [120]. This lengthening effect originates from the fact that each YOYO-1 molecule separates two pairs of neighboring DNA base pairs by ~0.4 nm [121], [122].

Currently, contradicting ideas exist how YOYO-1 binding alters DNA rigidity, with results ranging from a decreased persistence length [118], over unchanged persistence length [120],[123],[28] to an assumed increase in persistence length [112]. The more recent studies favor a persistence length that is independent of YOYO-1 concentration [28].

An alternative fluorescent dye is DAPI (4′, 6-diamidino-2-phenylindole). It attaches inside the minor groove of A-T rich DNA sequences [124]. DAPI is a useful fluorescent dye

to visualize DNA molecule as it shows insignificant effect on the local structure of DNA. In particular, DAPI does not inhibit the enzymatic activities of many restriction endonucleases [125]. However, it was found that DAPI exhibits a marked effect on the higher order structure of DNA [126].

Many factors such as proteins and coenzymes can alter the stability of fluorescence dye binding and therefore exert an effect on DNA contour length. In our previous work we showed that T4 DNA ligase can change the DNA configuration in nanochannels [34]. This protein requires ATP as a cofactor. Given the near ubiquity of ATP as a coenzyme, it is useful to know how it interacts with staining agents in order to decouple that interaction from observations and extract the true phenomena of interest. Therefore, we are studying the effect of ATP on YOYO-1, YOYO-3, and DAPI stained λ-DNA in this chapter.

Stretching of DNA in nanochannels is applied here as the main analytical technique for allowing DNA configuration [61]. Such nanochannels have a cross-section on the order of ~100×100 nm^2, and a length of 100s of micrometers. After DNA is brought into a nanochannel, it will assume an equilibrium configuration that is governed by the channel cross-section, the contour length of DNA, its persistence length, and its width [92]. Example data is shown in Figure 4.1. The dependence on the persistence length and width make nanochannel stretching a promising probe for these parameters as a function of buffer conditions and protein binding [12]. DNA inside nanochannels fluctuates [10], [127], and can thus explore many possible configurations during a single experiment.

We present an investigation of the influence of ATP on the configuration of long DNA strands under nanoconfinement. We introduced λ-DNA molecules into nanochannels and observed extended DNA configurations fluctuating around the equilibrium point. A contraction of bis-intercalator stained DNA in the presence of ATP is found. In contrast, DAPI-stained DNA is not affected by ATP.

2. Experimental

λ-DNA (Roche Diagnostics GmbH, 1 μg/ml) was stained with YOYO-1 or YOYO-3 (Life Sciences) at a ratio of 1 dye per 10 base pairs. We also investigated DNA stained with DAPI (10 μM). The contour length of unstained λ-DNA (48.5 kbp) is approximately 16.5 μm. After staining, that length can increase by about 35% [86], where a linear interpolation would predict about 14% extension for our staining. DNA was suspended in ½ x TBE buffer (pH 8) at room temperature. BSA (0.1 mg/ml, New England Biolabs) was added to prevent sticking of DNA to the nanochannels. Adenosine triphosphate (ATP) at concentrations of 0.5 mM, 1 mM, and 2 mM were investigated. For preparing "quick-stained" DNA, DNA and YOYO-1 were incubated for 30 minutes at room temperature. For preparation of an "equilibrated" stained DNA, solutions were incubated for 48 hours at 4°C.

All experiments used mixed micro- and nanofluidic devices made from fused silica, which were prepared by methods discussed elsewhere [89]. Nanofluidic channels with 80×80 nm^2, 100×100 nm^2, 130×130 nm^2, and 150×150 nm^2 cross-sections and a length of 200 μm were placed between microchannels [90]. Each DNA molecule is driven from microchannel to nanochannel by a hydrostatic pressure gradient. After the DNA molecule has entered the

nanochannel, the pressure gradient was removed and the dynamics of molecules were observed. Molecules were observed using a fluorescence microscope with a 1.3-N.A. oil-immersion microscope objective under illumination from a metal halide lamp, and images were recorded by an emCCD camera (Andor).

For calculating the end-to-end extended length of DNA molecules, we fitted the brightness along the molecule backbone to:

$$I(x) = I_b + \frac{I_0}{2}\left(\mathrm{erf}\left(\frac{x - x_c + \frac{l}{2}}{\sigma}\right) - \mathrm{erf}\left(\frac{x - x_c - \frac{l_u}{2}}{\sigma}\right)\right) \tag{4.1}$$

Here $I(x)$ is the intensity along nanochannel, σ is the slope of the edge, I_0, x_c, l, and I_b are the brightness, center position, length, and background signal, respectively. Only hairpin-free molecules were considered for analysis.

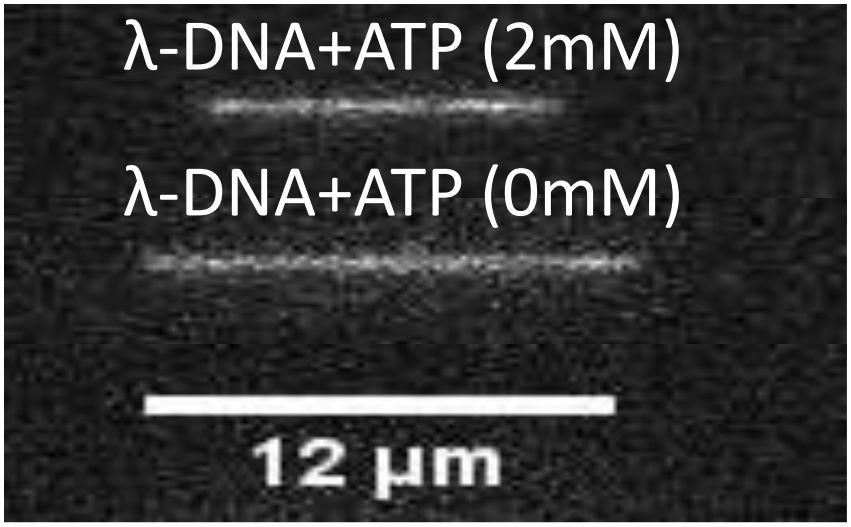

Figure 4.1: Nanochannel-stretched DNA (48.5 kbp) stained with YOYO-1 is sensitive to ATP concentration in buffer. Nanochannels with a cross-section of 80×80 nm² were used to stretch DNA.

3. Results and Discussion

In Figure 4.2a, b we show the extension of YOYO-1 “quick-stained” DNA inside nanochannels with and without added ATP, at the same conditions as in our previous publication [128]. We observed a significant shortening of DNA upon addition of 1 mM ATP (Table 4.1). This shortening could be an effect peculiar to quick stained DNA, because quick staining produces inhomogeneous fluorescence along the length of the DNA. In comparison, longer equilibration times promotes uniform stating, which indicates that dye-interaction is a dynamic process [129].

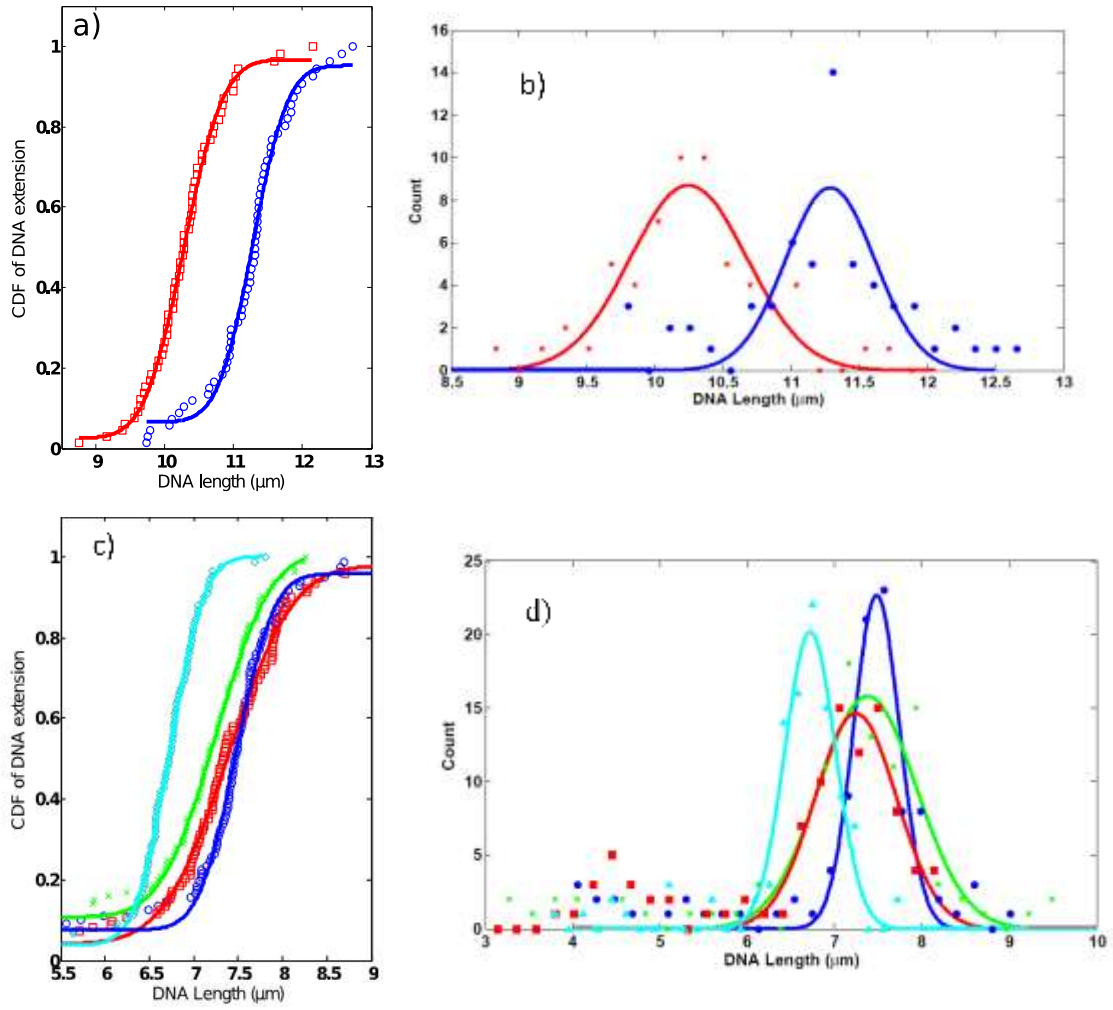

Figure 4.2: a) Cumulative distribution function (CDF) of extensions of "quick-stained", YOYO-1 bearing DNA without ATP (blue ○), and with 1 mM (red □). Measurements were performed in channels with 100×100 nm^2 cross-section and 60 molecules for each condition. b) Histograms of extensions of unfolded λ-DNA molecules in nanochannels with and without ATP visualized by YOYO-1. Bare λ-DNA (blue circle), λ-DNA with ATP (1 mM) (red star). c) CDF of DNA with equilibrated YOYO-1 stain at 0 mM ATP (blue ○), 0.5 mM ATP (red □), 1 mM ATP (green ×), 2 mM ATP (cyan □). Measured over 100 molecules each condition, and in a channel cross-section of 130×130 nm^2.d) Histogram of same molecules and same conditions of c), Bare λ-DNA (blue circle), λ-DNA with ATP (0.5 mM) (green star), λ-DNA with ATP (1 mM) (red square), and λ-DNA with ATP (2 mM) (light blue triangle).

Table 4.1: Numerical results of fitting cumulative distribution functions in all figures to a single error function model. *l* is the extension defined in Equation (3.1).

Fig. #	Dye	[ATP] (mM)	Channel cross-section (nm^2)	l (μm)*
1a	YOYO-1	0.0	100×100	11.28 ±0.06
		1.0		10.27 ±0.05
1b	YOYO-1	0.0	130×130	7.46 ±0.03
		0.5		7.37 ±0.05
		1.0		7.17 ±0.05
		2.0		6.71 ±0.03
2	YOYO-1	0.0	100×100	10.84 ±0.05
		2.0		9.67 ±0.03
		2.0 (AMP)		9.42 ±0.04
		2.0 (GTP)		9.24 ±0.05
3a	DAPI	0.0	150×150	7.14 ±0.08
		1.0		7.31±0.12
		2.0		7.08 ±0.1
3b	YOYO-3	0.0	80×80	14.38 ±0.08
		2.0		12.75 ±0.09

To investigate whether the shortening effect in Figure 4.2a, b is specific to quick-stained DNA or whether it is a general property, we exposed DNA with an equilibrated YOYO-1 stain to a range of ATP concentrations (Figure 4.2c,d). We observed that concentrations as low as 0.5 mM alter the DNA length (Table 4.1). Furthermore, as we increased the concentration, the apparent shortening became more dramatic, i.e. the strength of the ATP effect depends on its concentration. Thus it appears that ATP alters both quick and equilibrated stained DNA, but that its effect on quick-stained DNA is stronger. This would suggest that ATP's effect is stronger when the dye has not had time to fully thermalize and that it may be linked to the some redistribution of dye along the DNA. The extension observed in Figure 4.2c,

d was slightly smaller than that in Figure 4.2a, b because wider nanochannels (130×130 nm^2) were used.

One possible causes for shortening DNA length in the presence of ATP is ATP hydrolysis, because ATP hydrolysis can change pH of solution and DNA length is function of pH [130]. For testing this hypothesis, we explored whether ATP's effect is time dependence or not. We measured DNA length after list the times incubation with ATP (see Table 4.2). We did not observe any statistically significant dependence at these time scales, indicating the effect occurs quickly (Figure 4.3). Apparently, ATP hydrolysis does not affect DNA length, chiefly, because we are using ½ x TBE buffer and ATP hydrolysis can hardly change pH of solution in this buffer.

Table 4.2: Extended length of YOYO-1 stained DNA after different times of incubation with ATP.

100×100 nm^2	Mean±$\boldsymbol{\sigma}/\sqrt{N}$
λ-DNA+ ATP (0mM)	11.19±0.091
λ-DNA+ATP (1mM)+0 hour	10.45±0.064
λ-DNA+ATP (1mM)+1hour	10.45±0.101
λ-DNA+ATP (1mM)+2 hours	10.38±0.035
λ-DNA+ATP (1mM)+3hours	10.35±0.12
λ-DNA+ATP (1mM)+4 hours	10.47±0.101

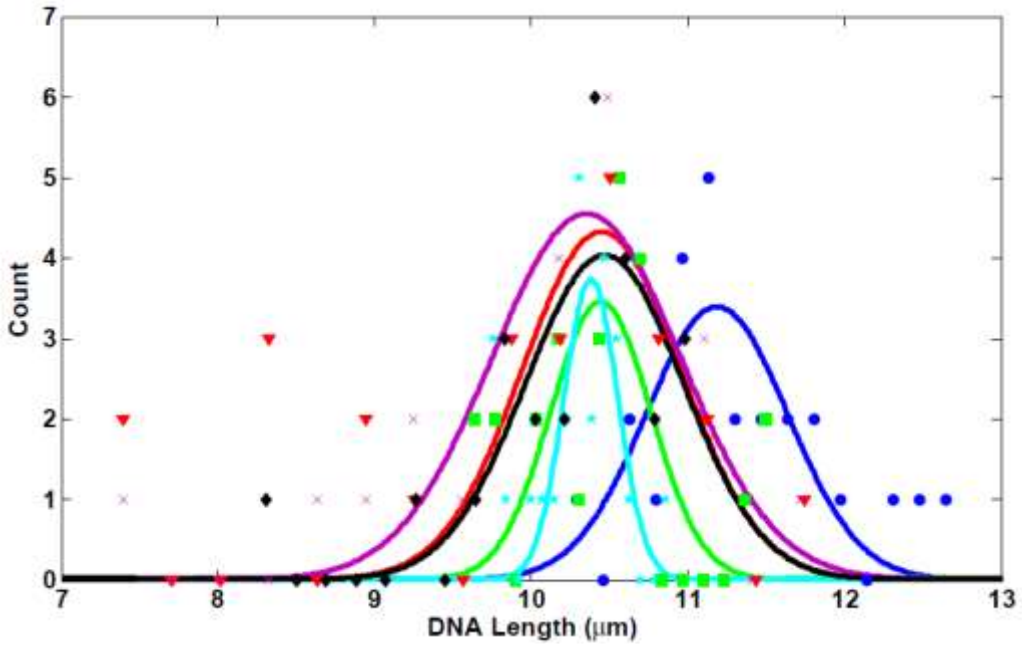

Figure 4.3: Histograms of extensions of unfolded λ- DNA molecules with and without ATP at different times. Bare λ-DNA (dark blue circle), λ-DNA with ATP (1mM) right away after added ATP (green square), λ-DNA with ATP (1mM) after one hour (red triangle), λ-DNA with ATP (1mM) after two hours (light blue star), λ-DNA with ATP (1mM) after three hours (purple cross), and λ-DNA with ATP (1mM) after four hours (black diamond). Channels were about 100 nm wide and deep. Total DNA molecules for each solution is 25 molecules.

ATP's molecular structure consists of a phosphate chain, a sugar, and a nucleoside base. To explore which part of ATP is interacting with DNA or YOYO-1, we repeated the same experiment with GTP (Guanosine triphosphate), which has the same phosphate group as ATP, and AMP (adenosine monophosphate), which has the same nucleoside as ATP (Figure 4.4). It is apparent that all of those nucleosides alter DNA length (Table 4.1). In particular the effect of GTP and ATP are quite similar.

In contrast, the effect of AMP is less pronounced, pointing to a dependence on the size of the phosphate chain. We would naively anticipate an ionic strength of ~15 mM in the absence of ATP, and of ~25 mM in the presence of 2 mM ATP, which according to Reisner et al. led to a reduction of up to 8% in extension along the channel axis [12]. Given the complex behaviour of ATP and AMP, the prediction of the buffer strength effect is fraught with considerable uncertainty, but it is safe to assume that AMP should carry at most half the contribution of ATP. However, the differences between the lengths are far less than half the amplitude of the peak shift, and so it does not appear that the ionic strength effect makes the leading contribution.

One of the possibilities for the apparent shortening could be an interaction between ATP and YOYO-1 in solution leading to less free dye available for staining of DNA. Such an interaction could be driven by the high positive and negative charges, respectively. The drop in the staining ratio would result in shorter molecules.

To further support our hypothesis of ATP-YOYO-1 interaction instead of an ATP-DNA interaction, we repeated the measurement on DNA stained with DAPI, a minor groove binder (Figure 4.5a). It is apparent that the DAPI- stained DNA is not affected by ATP to the same extent that YOYO-1 stained DNA is (Table 4.1). This strongly suggests that the hypothesis of ionic strength-driven contraction is not correct.

In order to confirm that ATP does affect bis-intercalated dyes other than YOYO-1, we repeated the same experiment with YOYO-3, which is also a bis-intercalating dye. We

observed an effect similar to what we observed on YOYO-1 stained DNA Figure 4.5c, d, (Table 4.1).

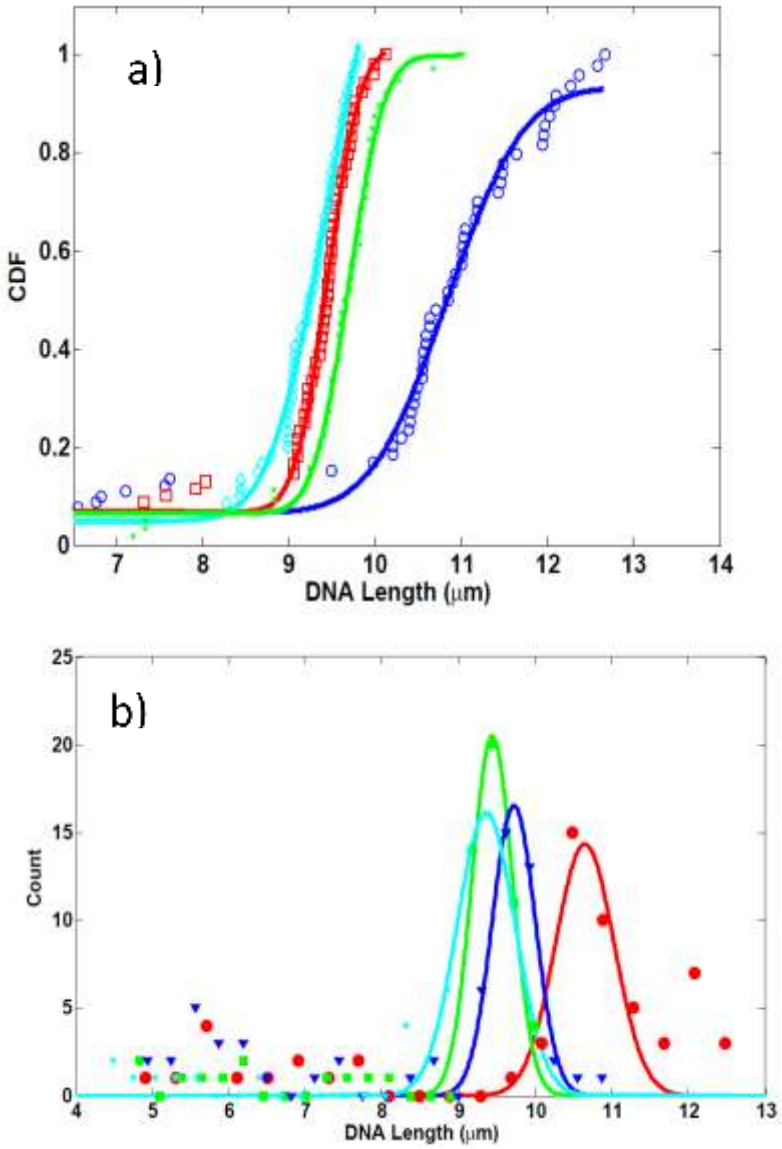

Figure 4.4: a) Cumulative distribution function of extensions of DNA without nucleotide triphosphate (blue ○), 2 mM ATP (red □), 2 mM AMP (green ×), 2m M GTP (cyan ◇). b) Histograms of extensions of unfolded λ- DNA molecules with and without ATP, AMP, and GTP. Bare λ-DNA (red circle), λ-DNA with ATP (2mM) (green square), λ-DNA with AMP (2mM) (blue triangle), and λ-DNA with GTP (2mM) (light blue star). Sixty molecules each condition. Channel cross-section was 80×80 nm^2.

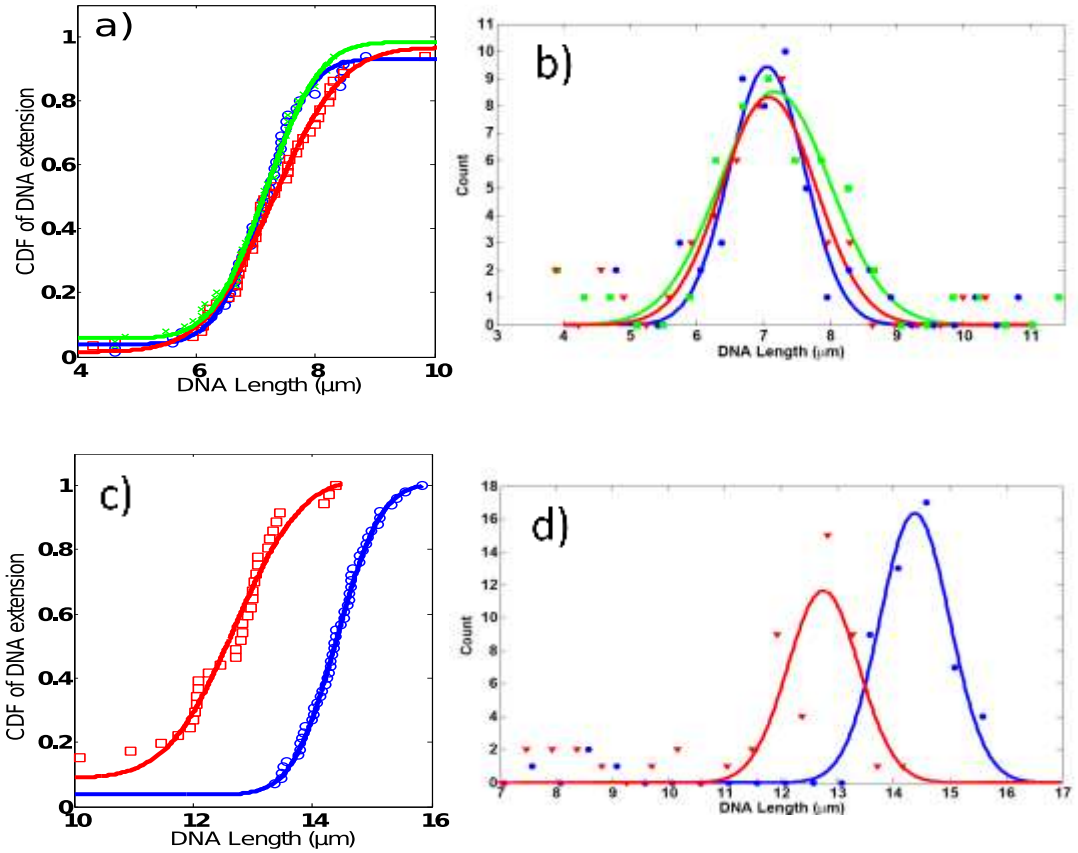

Figure 4.5: a) Cumulative distribution function of extension of DNA stained with DAPI without ATP (blue ○), 1mM ATP (red □), and with 2 mM ATP (green ×). Measured in channels with 150×150 nm² cross-section and 50 molecules for each condition. b) Histograms of extensions of unfolded λ-DNA molecules in nanochannels with and without ATP visualized by DAPI. Bare λ-DNA (blue circle), λ-DNA with ATP (1mM) (green square), and λ-DNA with ATP (2 mM) (red triangle). c) CDF of DNA with equilibrated YOYO-3 stain at 0 mM ATP (blue ○), and with 2 mM ATP (red □). d) Histograms of extensions of unfolded λ-DNA molecules in nanochannels with and without ATP visualized by YOYO-3. Bare λ-DNA (blue circle) and λ-DNA with ATP (2mM) (red triangle) 55 molecules each condition, and channel cross-section of 80×80 nm².

4. Conclusion

We have investigated the physical behavior of nanoconfined, bis-intercalator-stained DNA in the presence of ATP. In particular, the extensions of DNA molecules reduced when more than 1 mM ATP was added to YOYO-1 and YOYO-3 stained DNA. By comparing ATP, AMP, and GTP, we concluded that that the action of ATP is through an action of the nucleoside on the dye that is intercalated into the DNA. On the other hand DAPI- stained DNA is not affected by ATP to the same extent as YOYO-1 stained DNA. We believe that this result is important because it could lead to a considerable artifact when studying the interaction of DNA and ATP-dependent proteins on YOYO-1 stained DNA.

5. Protein-directed motion of DNA in nanochannels driven by ATP

Inside the confined environment of the nanochannel, long DNA molecules stretch out due to self-avoiding interactions. The individual molecule remains stationary, randomly fluctuating about its central position. However, cooperative interactions of proteins with the DNA and the channel walls can break the symmetry and induce directed motion of the DNA molecule inside the nanochannel. Here we show directed motion in this configuration for three different proteins (T4ligase, MutS, E.Coli Ligase) in the presence of their co-factors (ATP, NAD^+) and driven by their respective energy cycles. The motion is characterized by a smooth transition from a slightly sub-diffusive motion at short time scales to a super-diffusive regime at longer time scales. We propose a self-maintained osmotic pressure gradient between the left and the right terminal of the elongated DNA molecule inside nanochannel, which linked to the change of molarity of a solution during hydrolysis of ATP causes this drift. Also, we consider DNA molecules acts as an ion-selective membrane.

1. Experimental Method

λ-DNA (Roche Diagnostics GmbH, 5μg.mL^{-1}), was stained with YOYO-1 (Invitrogen) at a ratio of 1 dye per 20 base pairs. The contour length of unstained λ-DNA which

has 48.5 kbp, is around 16.5 μm. After staining, that length can increase by about 30% [131]. DNA was suspended in ½ x TBE buffer, pH 8 at room temperature with concentration of 5 μg/ml. For preparation of an "equilibrated and homogeneous" stained DNA solution were incubated for 48 hours at 4 ^{o}C. We labeled T4 DNA ligase with ATTO 565 nm NHS-ester (I explained in chapter 2 how to label T4 DNA ligase) and we observed that labeled proteins stick to our channels wall (Figure 5.5). BSA (0.6 mg/ml) was added to prevent sticking of proteins to the nanochannels, because BSA is well-known protein, which prevents sticking DNA to the nanochannels.

We used 4% by volume T4 DNA ligase (100U (1U/μl), Roche Diagnostics GmbH), 1 mM ATP (Roche Diagnostics GmbH), and 5mM $MgCl_2$ as T4 DNA ligase cofactors in our solutions (λ-DNA, 5μg.mL^{-1}). This solution was incubated 1 hour at 16 ^{o}C. After that we add 2 mM EDTA (widely are used for the formation of chelates) to our solutions to get rid of free Mg^{+2} in our solution for 2 hours at 20˚C.

All experiments used mixed micro- and nanofluidic devices made from fused silica, which were prepared by methods discussed elsewhere [11]. Nanofluidic channels with a 120×150 nm^2 cross- section and a length of 200μm were placed between microchannels [132]. Each DNA molecule is driven from microchannel to nanochannel by a static pressure gradient. After the DNA molecule has entered the nanochannel, the pressure gradient was removed and the dynamics of molecules are observed. Molecules were observed using an inverted fluorescence microscope with a 100 X, 1.3 N.A. oil-immersion microscope objective (Nikon, TE- 2000) under illumination from a metal halide lamp, and observation by EM-CCD camera

(iXon, Andor). The mean square displacement of central of mass as a function of time is given by:

$$MSD(n\Delta t) = \frac{1}{N - n}\sum_{i=1}^{N-n}\left[\left(X_{i+n} - X_i\right)^2\right] \quad (5.1)$$

Where N is the total number of frames, n is the number of frames for different intervals, Δt is the time between frames, and x_i is the position of the CoM of DNA molecule in the frame i.

2. Results

Figure 5.1 shows an example of an optical measurement of fluorescently stained λ-DNA inside a nanofluidic device. We find a qualitatively different behavior for DNA in an inert buffer (Figure 5.1 a) and DNA exposed to the T4 DNA ligase protein and its cofactors (Figure 5.1 b). In each experiment, the DNA molecule has been driven into a nanochannel from a microchannel by a static pressure difference. After the DNA molecule had entered the nanochannel, external pressure was removed and the dynamics of molecule were recorded. Inside the nanochannel, DNA molecules fluctuate freely, displaying diffusive motion, such that the center of mass (CoM) of the DNA molecule moved slowly (Figure 5.1a and Figure 5.1 c, red curve). For DNA in the presence of the protein and its cofactors, the motion is much

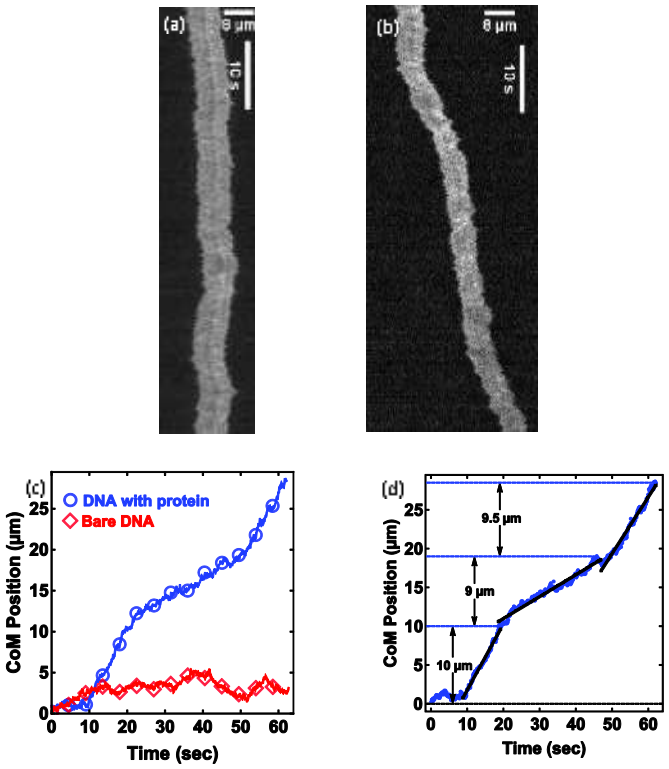

Figure 5.1: λ-DNA molecules inside nanochannel. (a,b) Kymographs showing the fluorescent intensity along channel axis as a function of time for bare λ-DNA (a) and λ-DNA with active protein (b), respectively. (c) Position of center of mass (CoM) of the molecules in a (red, diamonds) and b (blue, circles) as function of time. (d) CoM position of λ-DNA with active protein. Three distinct motion regimes are clearly visible, covering the length of the molecule. Linear fits were made to each segment, indicating constant speed.

faster. For this treated DNA, we observe a clear net displacement along the channel (Figure 5.1b and Figure 5.1c, blue curve) resembling motion with a stepwise constant speed (Figure 5.1d).

Figure 5.2 shows the distribution of velocities for 20 DNA molecules in the presence of the protein and its cofactors. Distinct peaks in the forward and backward directions with possible higher order peaks are observed, suggesting that in the presence of the active protein

the motion is directed with a displacement proportional to time squared. To examine this hypothesis, the mean-square displacement (MSD) was calculated for each molecule from its CoM position.

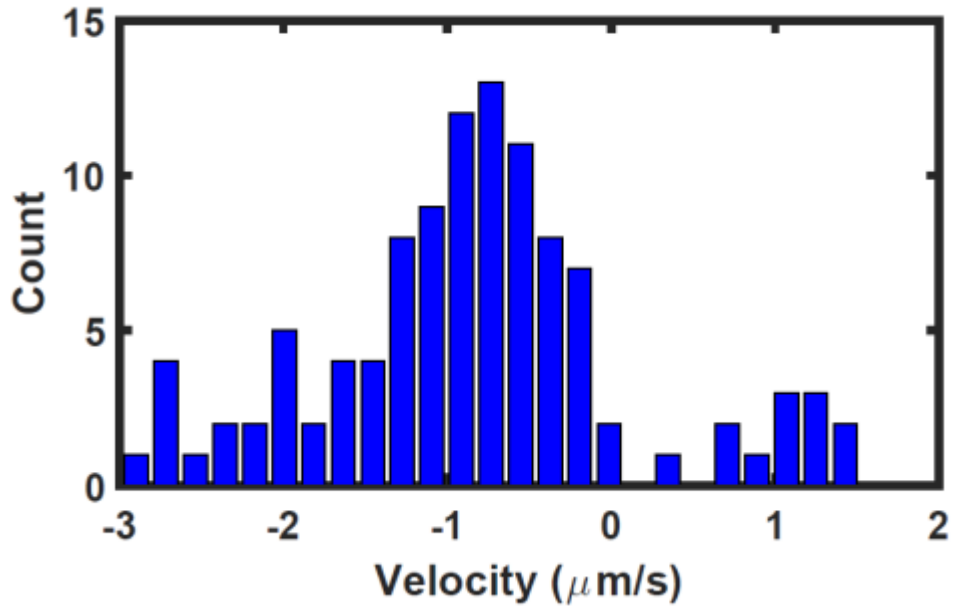

Figure 5.2: Distribution of segment velocities for 22 extended molecules. The velocity for each molecule inside the channel was calculated from the displacement curves, as in Figure 5.1d.

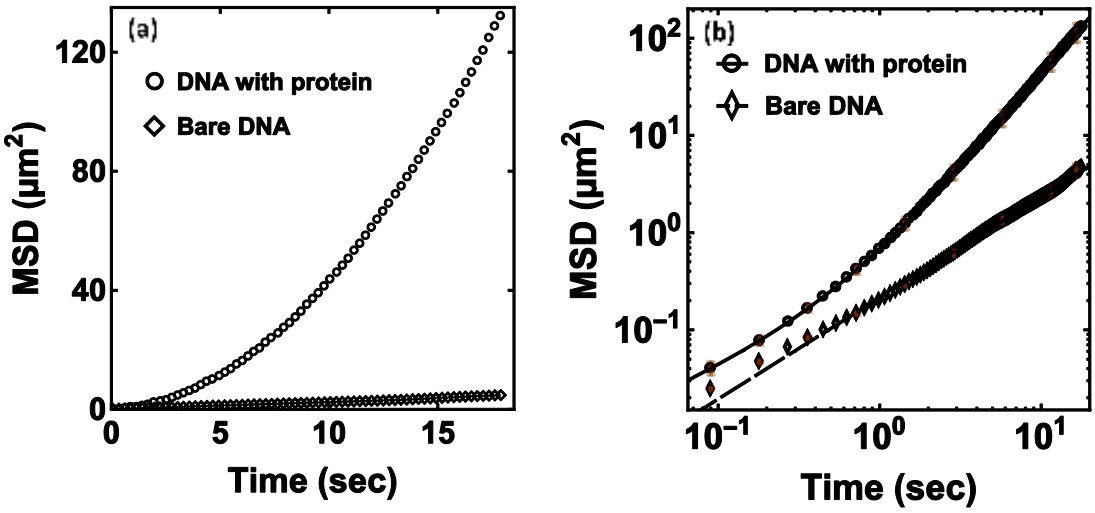

Figure 5.3: Average mean-square displacement (MSD) curves (linear scale, a; log-log scale, b) calculated from the CoM position of λ-DNA inside the nanochannel for 20 molecules. Circles correspond to data of DNA with T4ligase in the presence of its cofactors, while diamonds indicate bare DNA. Error bars in b are calculated from the standard deviation, and are depicted from select data points to illustrate the trend. The continuous and dashed curves in b correspond to the two-stage diffusion model, $(\mathbf{0.23} \pm \Delta)\boldsymbol{t}^{\mathbf{0.77}\pm\Delta} + (\mathbf{0.45} \pm \Delta)\boldsymbol{t}^{\mathbf{1.96}\pm\Delta}$ **and the one-stage diffusion model**$(\mathbf{0.21} \pm \Delta)\boldsymbol{t}^{\mathbf{1.04}\pm\Delta}$**, respectively.**

In Figure 5.3, the average MSD curves (calculated for 20 molecules) are plotted in a linear (Figure 5.3a) and log-log scales (Figure 5.3b). In Figure 5.3a, the untreated DNA (red curve) displays an MSD proportional to *t*, obeying the single process step of classical diffusion at longer time scales. On the other hand, treated DNA displays a more complicated process. We have fitted the data to a four-parameter two-step process. Combining diffusion and drift produces a sum of two power laws, $\alpha_1 t^{\beta_1} + \alpha_2 t^{\beta_2}$ with $\alpha_2 = 0.45 \approx 2\alpha_1, \beta_1 \approx 0.8$ and $\beta_2 = 2$.

To test whether the molecule had some preferential direction, we performed several experiments in which the moving molecule was pushed backwards in the opposite direction to

its motion (Figure 5.4). We observed that each time, the molecule returned to drift in the original direction with a nearly identical velocity, suggesting that the perturbation does not overcome internal order of the protein collective and the associated chemical composition. Based on this observation, we conclude that once the initial direction of motion has been set (stochastically), it is well-established, suggesting the system is endowed with a degree of memory.

Figure 5.4: Kymograph of DNA molecule with T4 DNA ligase and its cofactors. Show the molecule is drifting along the nanochannel without any pressure and even after the same molecule was pushed back in the opposite direction by ultralow pressure (5 psi), the molecule returned to drift in the original direction.

In order to understand the origin of this directed motion, several experiments were carried out (Table 5.1). Firstly, the role of the cofactors (ATP, Mg^{+2}) was assessed by a series of control experiments. By varying concentrations and species in solution, we established that only a combination of both ATP [1 mM] and Mg^{+2} [5 mM] produces the observed directed motion (Figure 5.4). This is consistent with the necessary conditions for ATP hydrolysis [133]. These suggest that the directed motion is driven by ATP hydrolysis. Experiments were carried out to determine the position of the protein during the actual drift. Fluorescent labeling of T4 DNA ligase (Figure 5.5) revealed the proteins were sticking to the walls as well as to the DNA itself. We further observed that adding bovine serum albumin (BSA) at a concentration sufficient to stop the transport phenomenon also prevented adhesion of fluorescently labeled T4 DNA ligase to glass surfaces (Figure 5.6).

Table 5.1: Summary of experimental results for different solutions inside the nanochannel. No motion was observed for DNA molecules inside the nanochannel without protein and its cofactors.

Solution	Drift
Bare λ-DNA	No
λ-DNA + ATP	No
λ-DNA + ATP+ Mg+ EDTA	No
λ-DNA + T4 ligase+ ATP	No
λ-DNA + T4 ligase+ ATP+ Mg^{+2}+ EDTA	Yes
λ-DNA + T4 ligase+ ATP+ Mg^{+2}+ EDTA+BSA	No
λ-DNA +E-coli DNA ligase+ NAD^{+} + Mg^{+2}+ EDTA	yes
λ-DNA +E-coli DNA ligase+ ATP + Mg^{+2}+ EDTA	No

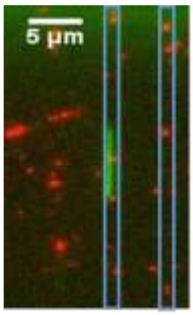

Figure 5.5: Labeled protein (T4 DNA ligase with ATTO 565, red dots) and λ-DNA (stained with YOYO-1) inside nanochannel.

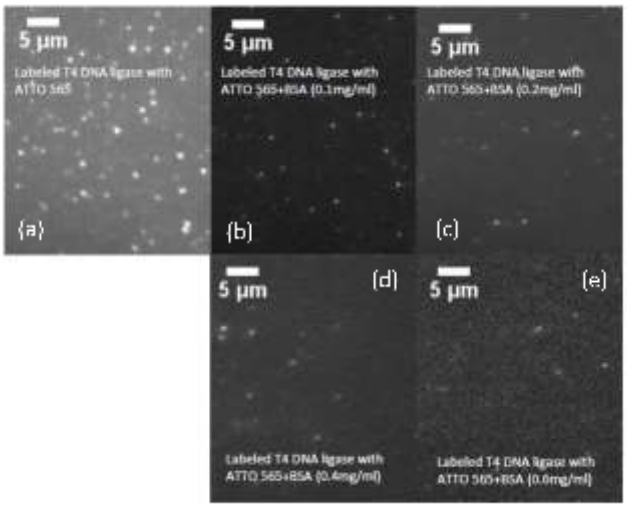

Figure 5.6: labeled T4 DNA ligase with ATTO 565 NHS-ester and different concentrations of BSA on normal coverslip. Labeled T4 DNA ligase proteins stop to stick to the normal coverslip surface by increasing BSA concentration. (a) Just bare labeled protein, (b) labeled protein with BSA (0.1 mg/ml), (c) labeled protein with BSA (0.2 mg/ml), (d) labeled protein with BSA (0.4 mg/ml), (d) labeled protein with BSA (0.6 mg/ml).

3. Discussion

We present two possible models for the observed transport phenomenon. The first model is based on a self-maintained osmotic pressure difference between the left and right terminal of the elongated DNA molecule. The DNA molecule here acts as an ion-selective membrane [134]. The osmotic pressure gradient is linked to the change of molarity of a solution during hydrolysis of ATP and release of the Magnesium that was bound to ATP. Importantly, we assume that channel-bound proteins are in contact with ATP prior to the introduction of the DNA molecule into the channel. Physical contact with the proteins enables hydrolysis.

We can estimate the change in molarity that can cause a drift of the magnitude observed here. The effective friction coefficient per unit length of DNA within a nanochannel is on the order of $\sim 2 \times 10^{-4}$ Ns/m^2 (Experimental) or $\sim 1 \times 10^{-3}$ Ns/m^2 (theoretical) [135]. The observed drift velocity here ($\sim 10^{-6}$ m/s), leads to a required pressure difference on the order of 0.05 Pa for our channel diameter (based on experimental drag [135], [127]. That would require a molarity differential of about 15 µM between the termini of the molecule. That corresponds to an average of one molecule difference per six micrometers of channel length. Even if the effective friction coefficient per unit length is given by the theoretical value, a molarity difference of 150 µM does not appear excessive. We argue that such concentration and pressure differences between the leading and trailing ends of the molecule can be self-maintaining if energy is constantly provided by the hydrolysis of ATP. In the model, we consider that surface-bound protein already is associate to ATP if ATP is present in sufficient excess. In the next

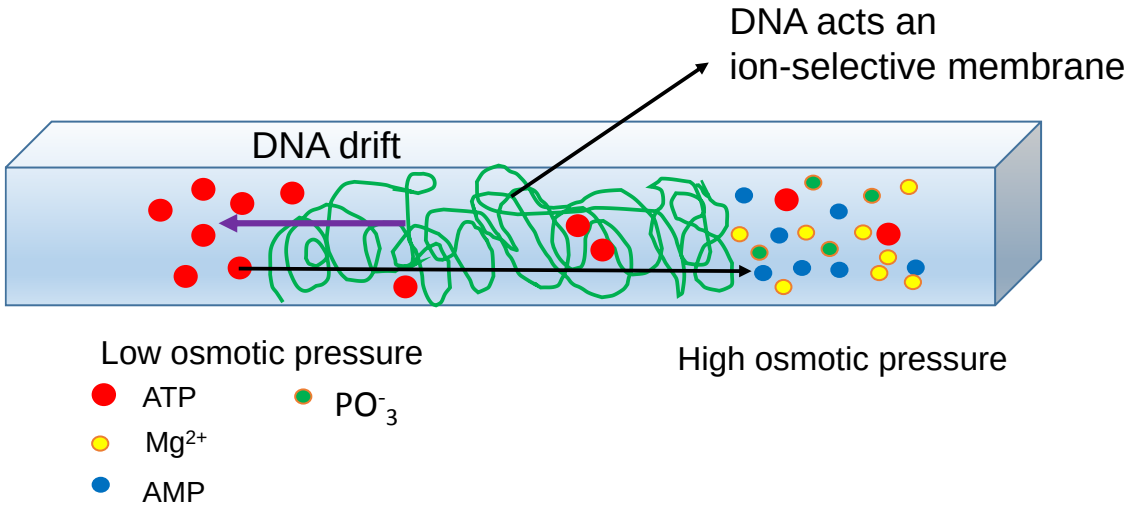

Figure 5.7: Cartoon of DNA inside of nanochannel acting as an ion-selective membrane and drifting based on osmotic pressure gradient between the right and the left terminal of the elongated DNA molecule.

step, DNA moves over the protein (due to the osmotic pressure difference), and makes random contact with the DNA. If a specific interaction between protein and DNA is obtained that enables hydrolysis of ATP, three freely diffusing products (AMP, Mg^{+2}, $(PO_3^-)_2$) are created for every "loaded protein". Within the polymer coil, there is a net flow of liquid against the direction of the osmotic pressure drop, and thus the reaction products are swept to the trailing end of the molecule. Here they join the present population of AMP and PO_3^-. Note that back-diffusion of AMP and PO_3^- through the DNA coil is hindered by the ion-selective nature of DNA (Figure 5.7). Therefore the concentration gradient is self-maintaining.

Beyond this kinetic mechanism for observing the motion of DNA inside nanochannels under ATP hydrolysis, we note that there is a certain possibility that a molecular motor action of a protein could give rise to an effect similar to the one observed. In this framework, surface bound proteins act as molecular motors that transport DNA in a fashion that is entirely

analogous to the mono-directional transport of actin filaments by surface-bound myosin motors in shallow microchannels (Figure 5.8) [136], [137]. The motion becomes observable because the high degree of DNA alignment along the channel axis renders it effectively stiff over distances more than a few channel diameters.

We believe at this time that the first model (osmotic pressure difference) is a better candidate for the explanation of the drift effect. The strongest criticisms of the "molecular motor" hypothesis is that none of the three enzymes tested (T4 DNA Ligase, E. coli DNA ligase, MutS) has been previously reported to possess the ability to undergo directed search. However, a common contamination of all proteins stemming from a similar expression system is possible. We repeated the experiment with different DNA sources (lambda DNA, human genomic DNA), and believe that the drift is not caused by a contamination of the DNA stocks. Furthermore, we have previously provided evidence that T4 DNA is a protein with low processivity [34].

Over the time-scales considered here (5 sec), which would make it impossible to maintain memory of the polarity of the substrate. Lastly, we performed experiments where we attempted to reverse the direction of transport by forcing backward using a very weak pressure driven flow. As soon as the flow was removed, flow proceeded in the original direction.

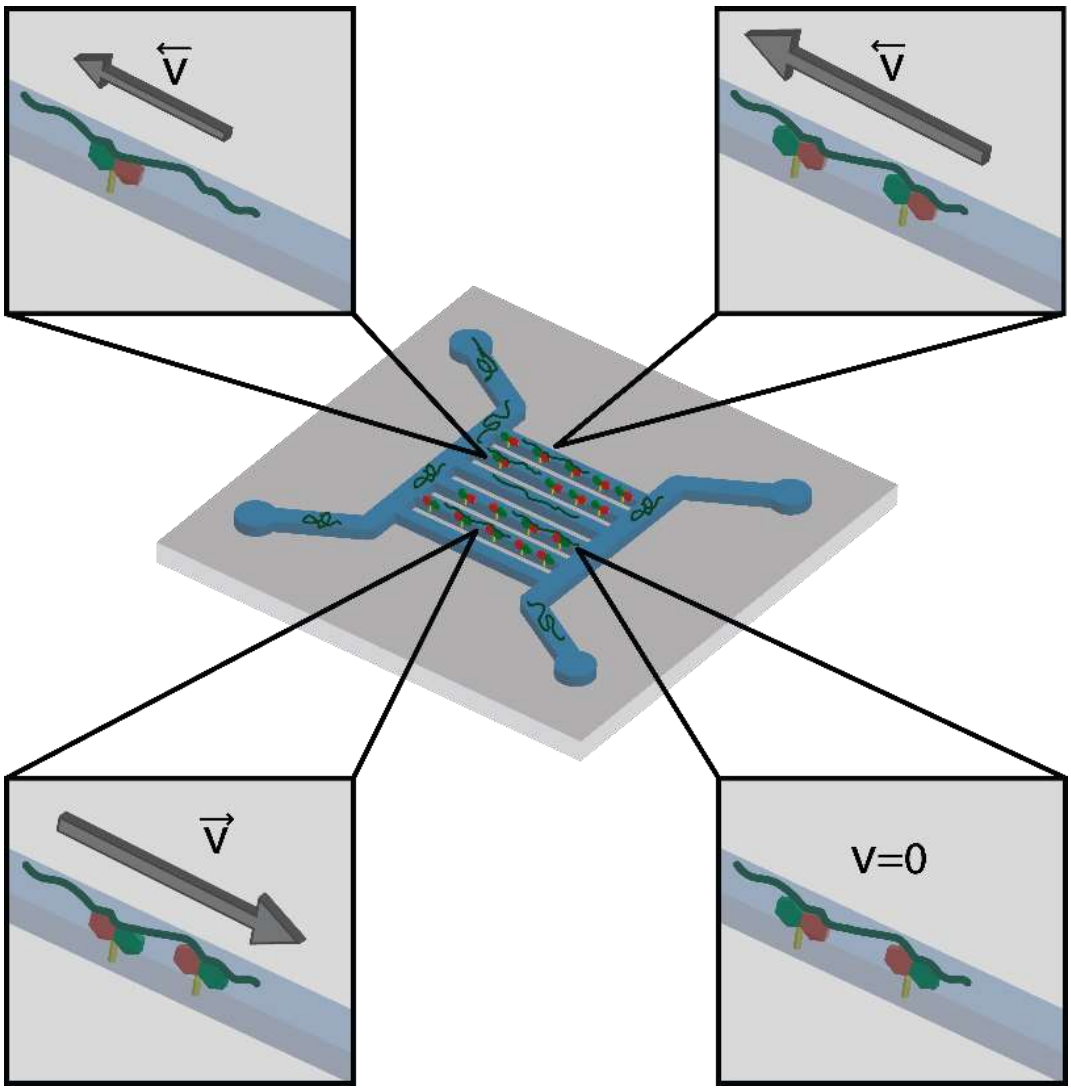

Figure 5.8: Cartoon of DNA inside nanochannels and bound proteins on surface act as molecular motor.

We would like to point out that in both models, the transport is only observable under nano-confinement. For the osmotic pressure hypothesis to be correct, we require the DNA to act as an ion-selective membrane, which has a one-dimensional of transport direction. This cannot be obtained on a DNA molecule in free solution, where liquid and ions can travel around the molecule. The nanochannel renders the transport essentially one-dimensional. Similarly, the observation of the molecular motor hypothesis by fluorescence microscopy is impossible because the diffraction limit is larger than the persistence length of double-stranded DNA. However, in nanochannels, the orientation of the molecule is conserved over very long distances, thus making the effect observable.

4. Conclusion

In conclusion, we have demonstrated that a range of DNA-binding proteins that undergo ATP or NAD hydrolysis cause mono-direction motion of nanochannel stretched DNA. The motion appears directly linked to the hydrolysis of ATP. We have proposed two models, both of which would have far-reaching implications. If the hypothesis of a self-maintaining osmotic pressure gradient is applicable, we anticipate that a wide range of polymer-linked catalysts under nano-channel confinement will lead to a similar motor-like action. That could either be exploited directly as an actuation mechanism, or be used as an analytic technique to detect any possible activity. If the motor hypothesis is correct, it would similarly be a very powerful technique since it requires no modification of either protein or DNA to detect the action. In a larger context, the ability to test for the activity of a candidate DNA-modifying protein without any protein and DNA modification or the need for inert ATP

derivatives appears promising for exploratory studies, or screening of possible activity of mutant libraries of previously characterized proteins.

6. Conclusion and possible further work

During my Ph.D., I have investigated the kinetic evolution of DNA loops (~50 kbp) stabilized by T4 DNA ligase (as a model system for DNA cyclization) and T-loop forming proteins inside a nanofabricated channel system with a channel cross-section of 100 ×100 nm^2, and a few hundred microns channel length. In these nanochannels, DNA is forced in a linear configuration that makes loops appear as folds, whose size can easily be quantified.

We observed that the static physical behavior of nanoconfined DNA is significantly altered in the presence of T4 DNA ligase. We have found dense binding of protein along the DNA. T4 DNA ligase binding reduced the product of effective DNA width and persistence length. A similar modification of static properties through an interaction of intercalating dyes and ATP was also observed. We further demonstrate that T4 DNA ligase has effects on the dynamic properties of folded DNA. Both static and dynamic effects were interpreted in a framework in which T4 DNA ligase mediates multiple transient links between the two arms of a folded molecule.

A second study using T4 DNA ligase presented a sensitive assay for enzyme activity coupled to ATP hydrolysis that is based solely on an induced motion of DNA molecules when confined to nanochannels. This essay also makes use of the dynamic nature of nanochannel measurements.

1. Possible Future Work

In chapter 3 through 5 we developed a model of protein binding to DNA and its activity solely by observing only the DNA configurations, without any direct observation of the protein itself. We believe that this concept can be extended to other proteins and other protein binding modes.

In particular we believe that it should be possible to determine whether proteins form dense or sparse binding patterns and whether bonding is tight or transient. Again, no protein labeling is required for this detection. In particular, we have hypothesized that the modification of the ratio of extension between singly- and doubly-occupied channel segments is a bulk property that indicates a dense binding of protein to DNA. In Figure 6.1, we demonstrate preliminary measurement on two proteins associated with the telomere (TRF1 and SA1). We find that TRF1 leads to a compaction of folded segments, even stronger than T4 DNA ligase. We thus believe it is a dense binder similar to T4 DNA ligase. However, we find that SA1 does not lead to a compaction of DNA. We attribute this to SA1 being a sparse binder. This sensing mechanics is based on the static mechanical properties of DNA which can be detected with high sensitivity using nanochannels.

We furthermore observed the influence of proteins on the dynamics of DNA loops in real time, and found that different protein binding modes lead to unique signatures in the configuration dynamics (Figure 6.1). TRF1 completely stabilizes the loop, meaning that contacts are not transient. SA1 appears to stabilize a loop at first, but at later times fails to do

so. We interpret this behavior as that of a tightly binding protein that cannot recapture a link after an initial link is broken because its binding density is too low.

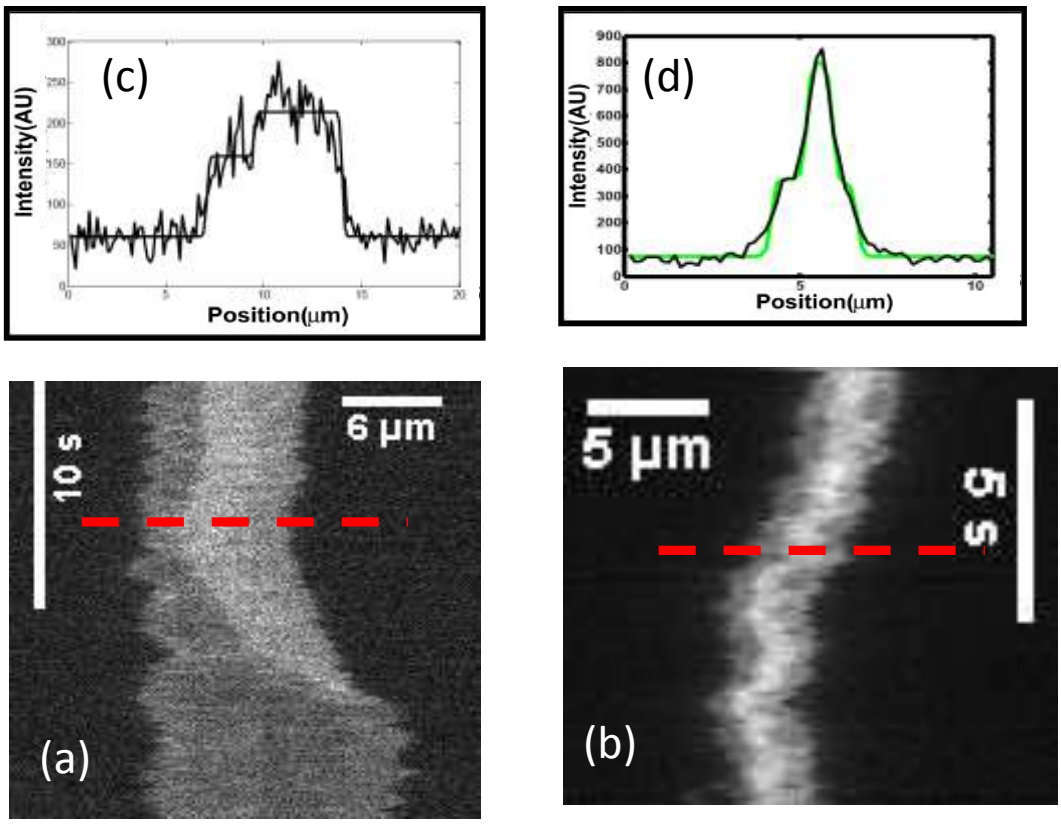

Figure 6.1: Kymograph of DNA molecules. (a) and (b) show kymograph of fluorescence intensity along nanochannels axis as a function of time. (c) and (d) illustrate the projected intensity of DNA molecules as a function of position along the nanochannels. (a) and (c) are λ-DNA with SA1 protein. (b) and (d) are ligated telomere DNA with TRF1 protein.

Based on both of these experiments, I propose that dynamic measurement of DNA loops could be used to elucidate T-loop formation. The T-loop stabilizes telomeres and is important in ageing and cancer. In vivo the T-loop is protected by a protein complex that consist of six core proteins, which are called sheltering proteins. The loop size is typically a

few to ten of kilobasepairs, similar to the loops describe in chapter 3. The mechanism and dynamics of the T-loop formation are unknown.

We fabricated a device is shown in Figure 6.2. The device contains independent channels for DNA and proteins, which will be moved through the devices with a combination of hydrodynamic flow and electrophoresis. In order to observe the response of DNA to step-wise recruitment of multiple proteins, the device contains a nanochannel region with a shallow shunt channel that enables a very localized and controlled exposure of DNA to shelterin proteins.

DNA will be forced into a feeding nanochannel. Once DNA has been located within the channel, a succession of different protein-carrying buffers can gently be flushed over it under constant observation by the microscope. On real time we are able to observe the dynamics of T-loop. In particular, we will be able to observe whether it is formed in a single capture event or formed through distributed binding of binding of multiple copies of a number proteins, which are mobile on DNA. Also we can observe, whether binding of multiple proteins is cooperative. If cooperative behavior is found we will be able to determine which proteins

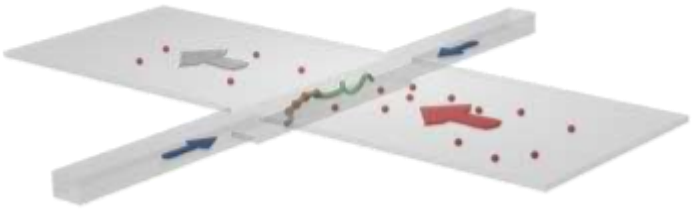

Figure 6.2: Nanochannel device with shallow gap. DNA (green) will be flushed in by nanochannel flows (blue arrows). The nanochannel flow rate then is dropped to prevent other more DNA from entering, and keep the present DNA centered in the channel. Protein (red balls) will be flushed over DNA through the shallow region (red arrow). Surplus liquid escapes through the waste flow (white arrow).

Figure 6.3: Binding of fluorescently tagged TRF2 (green) to DNA (red) in nanochannels.

are required to interact with each other for fully functionality, and what the order of recruitment is. Because we are working more than one protein, it will become necessary to label proteins to conclusively prove or disprove colocation of multiple protein species. DNA and proteins will be observed by inverted fluorescence microscope, which has an image splitter and multiple laser. In preliminary work, I was able to label and observe TRF2 and RAP1 proteins bound to DNA within nanochannels.

A particular challenge for using protein labeling is that the labeled protein is required to be as active as unlabeled protein. Preliminary data for the binding of Alexa 488-tagged TRF2 on stained λ-DNA is shown in Figure 6.3. In contrast to the proposed experiments, DNA and TRF2 were incubated off-chip. We observed co-localization of TRF2 and condensed DNA regions when introduced into nanochannels, in confirmation of the larger theme of this dissertation that protein binding to DNA can be observed through a modification of the configuration of DNA within nanochannels.

REFERENCES

[1] W. Reisner, J. N. Pedersen, and R. H. Austin, "DNA confinement in nanochannels: physics and biological applications," *Reports Prog. Phys.*, vol. 75, no. 10, p. 106601, 2012.

[2] T.-H. Wang, C. Puleo, and H.-C. Yeh, "Single Molecule DNA Detection," in *Integrated Biochips for DNA Analysis SE - 11*, R. Liu and A. Lee, Eds. Springer New York, 2007, pp. 139–150.

[3] S. Nie and R. Zare, "Optical detection of single molecules," *Annu. Rev. Biophys. Biomol. Struct.*, vol. 26, pp. 567 – 596, 1997.

[4] F. Kulzer and M. Orrit, "Single-molecule optics.," *Annu. Rev. Phys. Chem.*, vol. 55, no. 3, pp. 585–611, 2004.

[5] W. E. Moerner and D. P. Fromm, "Methods of single-molecule fluorescence spectroscopy and microscopy," *Rev. Sci. Instrum.*, vol. 74, no. 8, pp. 3597–3619, 2003.

[6] S. Weiss, "Fluorescence spectroscopy of single biomolecules.," *Science*, vol. 283, no. 5408, pp. 1676–1683, 1999.

[7] J. A. Schellman and D. Stigter, "Electrical Double-Layer, Zeta Potential, and Electrophoretic Charge of Double-Stranded DNA," *Biopolymers*, vol. 16, no. 7, pp. 1415–1434, 1977.

[8] R. C. Rubinstein Micheal, *Polymer Physics*. OUP Oxford, 2003.

[9] T. Odijk, "On the Statistics and Dynamics of Confined or Entangled Stiff Polymers," *Macromolecules*, vol. 1344, no. 3, pp. 1340–1344, 1983.

[10] W. Reisner, K. J. Morton, R. Riehn, Y. M. Wang, Z. Yu, M. Rosen, J. C. Sturm, S. Y. Chou, E. Frey, and R. H. Austin, "Statics and dynamics of single DNA molecules confined in nanochannels," *Phys Rev Lett*, vol. 94, no. 19, p. 196101, 2005.

[11] R. Riehn, W. W. Reisner, J. O. Tegenfeldt, V. M. Wang, C. Tung, S. Lim, E. C. Cox, C. Sturm, K. Morton, and R. H. Austin, "Nanochannels for Genomic DNA Analysis: The Long and the Short of lt," in *Integrated Biochips for DNA Analysis*, 2007, pp. 151–186.

[12] W. Reisner, J. Beech, N. Larsen, H. Flyvbjerg, A. Kristensen, and J. O. Tegenfeldt, "Nanoconfinement-Enhanced Conformational Response of Single DNA Molecules to Changes in Ionic Environment," *Phys Rev Lett*, vol. 99, no. 5, p. 058302, Aug. 2007.

[13] A. Press, "INTERMOLECULAR AND SURFACE Tbe Forces Between Atoms and Molecules : Principles and Concepts," *Interactions*, pp. 3152–3158, 2010.

[14] C. Bustamante, S. B. Smith, J. Liphardt, and D. Smith, "Single-molecule studies of DNA mechanics.," *Curr. Opin. Struct. Biol.*, vol. 10, no. 3, pp. 279–85, 2000.

[15] a Y. Grosberg and a R. Khokhlov, "Statistical Physics of Macromolecules," *AIP Woodbury, NY*, vol. 171, p. 350pp, 1994.

[16] A. Vologodskii and N. Cozzarelli, "Modeling of long-range electrostatic interactions in DNA.," *Biopolymers*, vol. 35, no. 3, pp. 289–296, 1995.

[17] D. E. Streng, S. F. Lim, J. Pan, A. Karpusenka, and R. Riehn, "Stretching chromatin through confinement.," *Lab Chip*, vol. 9, no. 19, pp. 2772–4, Oct. 2009.

[18] C. Zhang, Z. Gong, D. Guttula, P. P. Malar, J. A. van Kan, P. S. Doyle, and J. R. C. van der Maarel, "Nanofluidic compaction of DNA by like-charged protein.," *J. Phys. Chem. B*, vol. 116, no. 9, pp. 3031–6, Mar. 2012.

[19] S. Fang Lim, A. Karpusenko, J. J. Sakon, J. a. Hook, T. a. Lamar, and R. Riehn, "DNA methylation profiling in nanochannels," *Biomicrofluidics*, vol. 5, no. 3, p. 034106, 2011.

[20] S. E. Halford, A. J. Welsh, and M. D. Szczelkun, "Enzyme-mediated DNA looping.," *Annu. Rev. Biophys. Biomol. Struct.*, vol. 33, no. 35, pp. 1–24, Jan. 2004.

[21] R. Schleif, "DNA looping.," *Annu. Rev. Biochem.*, vol. 61, pp. 199–223, Jan. 1992.

[22] M. Alizadehheidari, E. Werner, C. Noble, M. Reiter-Schad, L. K. Nyberg, J. Fritzsche, B. Mehlig, J. O. Tegenfeldt, T. Ambjörnsson, F. Persson, and F. Westerlund, "Nanoconfined Circular and Linear DNA: Equilibrium Conformations and Unfolding Kinetics," *Macromolecules*, vol. 48, no. 3, pp. 871–878, 2015.

[23] T. de Lange, "T-loops and the origin of telomeres.," *Nat. Rev. Mol. Cell Biol.*, vol. 5, no. 4, pp. 323–329, 2004.

[24] L. Saiz and J. M. Vilar, "DNA looping: the consequences and its control," *Curr Opin Struct Biol*, vol. 16, no. 3, pp. 344–350, 2006.

[25] A. Karpusenko, “Physics and Application of Nanofluidic System,” North Carolina State University, 2013.

[26] P. C. H. Li, *Microfluidic lab on a chip for chemical and biological analysis and discovery*. 2008.

[27] I. I. Smolyaninov, “Optical microscopy beyond the diffraction limit.,” *HFSP J.*, vol. 2, no. 3, pp. 129–131, 2008.

[28] K. Günther, M. Mertig, and R. Seidel, “Mechanical and structural properties of YOYO-1 complexed DNA.,” *Nucleic Acids Res.*, vol. 38, no. 19, pp. 6526–32, Oct. 2010.

[29] C. C. Hsieh, A. Balducci, and P. S. Doyle, “Ionic effects on the equilibrium dynamics of DNA confined in nanoslits,” *Nano Lett.*, vol. 8, no. 6, pp. 1683–1688, 2008.

[30] J. R. Hart, W. R. Grace, and U. States, “Ethylenediaminetetraacetic Acid and Related Chelating Agents,” 2000.

[31] W. W. Cleland, “Dithiothreitol, a New Protective Reagent for Sh Groups.,” *Biochemistry*, vol. 3, no. 1960, pp. 480–482, 1964.

[32] L. M. Hellman and M. G. Fried, “Electrophoretic mobility shift assay (EMSA) for detecting protein–nucleic acid interactions,” *Nat. Protoc.*, vol. 2, no. 8, pp. 1849–1861, 2007.

[33] Z. Liu, Z. Li, H. Zhou, G. Wei, Y. Song, and L. Wang, “Immobilization and condensation of DNA with 3-aminopropyltriethoxysilane studied by atomic force microscopy,” *J. Microsc.*, vol. 218, no. 3, pp. 233–239, 2005.

[34] M. Roushan, P. Kaur, A. Karpusenko, P. J. Countryman, C. P. Ortiz, S. Fang Lim, H. Wang, and R. Riehn, “Probing transient protein-mediated DNA linkages using nanoconfinement,” *Biomicrofluidics*, vol. 8, no. 3, p. 034113, May 2014.

[35] S. E. Halford, A. J. Welsh, and M. D. Szczelkun, “Enzyme-mediated DNA looping.,” *Annu. Rev. Biophys. Biomol. Struct.*, vol. 33, no. 35, pp. 1–24, Jan. 2004.

[36] R. Schleif, “DNA looping.,” *Annu. Rev. Biochem.*, vol. 61, pp. 199–223, Jan. 1992.

[37] W. Su, S. Jackson, R. Tjian, and H. Echols, “DNA looping between sites for transcriptional activation: self-association of DNA-bound Sp1.,” *Genes Dev.*, vol. 5, no. 5, pp. 820–826, May 1991.

[38] Y. Jiang and P. E. Marszalek, “Atomic force microscopy captures MutS tetramers initiating DNA mismatch repair,” *Embo J*, vol. 30, no. 14, pp. 2881–2893, 2011.

[39] R. M. Stansel, T. de Lange, and J. D. Griffith, “T-loop assembly in vitro involves binding of TRF2 near the 3’ telomeric overhang.,” *EMBO J.*, vol. 20, no. 19, pp. 5532–40, Oct. 2001.

[40] S. Adhya, “Multipartite genetic control elements: communication by DNA loop.,” *Annu. Rev. Genet.*, vol. 23, no. 53, pp. 227–50, Jan. 1989.

[41] S. Courbet, S. Gay, N. Arnoult, G. Wronka, M. Anglana, O. Brison, and M. Debatisse, “Replication fork movement sets chromatin loop size and origin choice in mammalian cells.,” *Nature*, vol. 455, no. 7212, pp. 557–60, Sep. 2008.

[42] E. Lieberman-Aiden, N. L. van Berkum, L. Williams, M. Imakaev, T. Ragoczy, A. Telling, I. Amit, B. R. Lajoie, P. J. Sabo, M. O. Dorschner, R. Sandstrom, B. Bernstein, M. a Bender, M. Groudine, A. Gnirke, J. Stamatoyannopoulos, L. a Mirny, E. S. Lander, and J. Dekker, “Comprehensive mapping of long-range interactions reveals folding principles of the human genome.,” *Science (80-.).*, vol. 326, no. 5950, pp. 289–93, Oct. 2009.

[43] N. Naumova, M. Imakaev, G. Fudenberg, Y. Zhan, B. R. Lajoie, L. a Mirny, and J. Dekker, “Organization of the mitotic chromosome.,” *Science (80-.).*, vol. 342, no. 6161, pp. 948–53, Nov. 2013.

[44] L. Cui, I. Murchland, K. E. Shearwin, and I. B. Dodd, “Enhancer-like long-range transcriptional activation by λ CI-mediated DNA looping.,” *Proc. Natl. Acad. Sci. U. S. A.*, vol. 110, no. 8, pp. 2922–7, Mar. 2013.

[45] D. Lewis, P. Le, C. Zurla, L. Finzi, and S. Adhya, “Multilevel autoregulation of λ repressor protein CI by DNA looping in vitro.,” *Proc. Natl. Acad. Sci. U. S. A.*, vol. 108, no. 36, pp. 14807–12, Oct. 2011.

[46] J.-F. Allemand, S. Cocco, N. Douarche, and G. Lia, “Loops in DNA: an overview of experimental and theoretical approaches.,” *Eur. Phys. J. E*, vol. 19, no. 3, pp. 293–302, Mar. 2006.

[47] E. Alipour and J. F. Marko, “Self-organization of domain structures by DNA-loop-extruding enzymes.,” *Nucleic Acids Res.*, vol. 40, no. 22, pp. 11202–12, Dec. 2012.

[48] C. a Brackley, S. Taylor, A. Papantonis, P. R. Cook, and D. Marenduzzo, “Nonspecific bridging-induced attraction drives clustering of DNA-binding proteins

and genome organization.," *Proc. Natl. Acad. Sci. U. S. A.*, vol. 110, no. 38, pp. E3605–11, Sep. 2013.

[49] L. S. Shlyakhtenko, V. N. Potaman, R. R. Sinden, a a Gall, and Y. L. Lyubchenko, "Structure and dynamics of three-way DNA junctions: atomic force microscopy studies.," *Nucleic Acids Res.*, vol. 28, no. 18, pp. 3472–7, Sep. 2000.

[50] Z. Katiliene, E. Katilius, and N. W. Woodbury, "Single molecule detection of DNA looping by NgoMIV restriction endonuclease.," *Biophys. J.*, vol. 84, no. 6, pp. 4053–61, Jun. 2003.

[51] S. Chatterjee, Y. N. Zhou, S. Roy, and S. Adhya, "Interaction of Gal repressor with inducer and operator: induction of gal transcription from repressor-bound DNA.," *Proc. Natl. Acad. Sci. U. S. A.*, vol. 94, no. 7, pp. 2957–62, Apr. 1997.

[52] L. Finzi and J. Gelles, "Measurement of Lactose Repressor-Mediated Loop Formation and Breakdown in Single DNA-Molecules," *Science (80-.).*, vol. 267, no. 5196, pp. 378–380, 1995.

[53] C. Manzo, C. Zurla, D. D. Dunlap, and L. Finzi, "The effect of nonspecific binding of lambda repressor on DNA looping dynamics.," *Biophys. J.*, vol. 103, no. 8, pp. 1753–61, Oct. 2012.

[54] H. Wang, I. B. Dodd, D. D. Dunlap, K. E. Shearwin, and L. Finzi, "Single molecule analysis of DNA wrapping and looping by a circular 14mer wheel of the bacteriophage 186 CI repressor.," *Nucleic Acids Res.*, vol. 41, no. 11, pp. 5746–56, Jul. 2013.

[55] S. M. Hamdan, J. J. Loparo, M. Takahashi, C. C. Richardson, and A. M. van Oijen, "Dynamics of DNA replication loops reveal temporal control of lagging-strand synthesis.," *Nature*, vol. 457, no. 7227, pp. 336–9, Jan. 2009.

[56] M. Sun, T. Nishino, and J. F. Marko, "The SMC1-SMC3 cohesin heterodimer structures DNA through supercoiling-dependent loop formation.," *Nucleic Acids Res.*, vol. 41, no. 12, pp. 6149–60, Jul. 2013.

[57] Y.-F. Chen, J. N. Milstein, and J.-C. Meiners, "Protein-Mediated DNA Loop Formation and Breakdown in a Fluctuating Environment," *Phys. Rev. Lett.*, vol. 104, no. 25, p. 258103, Jun. 2010.

[58] Z. Hensel, X. Weng, A. C. Lagda, and J. Xiao, "Transcription-factor-mediated DNA looping probed by high-resolution, single-molecule imaging in live E. coli cells.," *PLoS Biol.*, vol. 11, no. 6, p. e1001591, Jan. 2013.

[59] Y. Doksani, J. Y. Wu, T. de Lange, and X. Zhuang, “Super-Resolution Fluorescence Imaging of Telomeres Reveals TRF2-Dependent T-loop Formation.,” *Cell*, vol. 155, no. 2, pp. 345–56, Oct. 2013.

[60] D. Skoko, M. Li, Y. Huang, M. Mizuuchi, M. Cai, C. M. Bradley, P. J. Pease, B. Xiao, J. F. Marko, R. Craigie, and K. Mizuuchi, “Barrier-to-autointegration factor (BAF) condenses DNA by looping.,” *Proc. Natl. Acad. Sci. U. S. A.*, vol. 106, no. 39, pp. 16610–5, Sep. 2009.

[61] J. O. Tegenfeldt, C. Prinz, H. Cao, S. Chou, W. W. Reisner, R. Riehn, Y. M. Wang, E. C. Cox, J. C. Sturm, P. Silberzan, and R. H. Austin, “The dynamics of genomic-length DNA molecules in 100-nm channels.,” *Proc. Natl. Acad. Sci. U. S. A.*, vol. 101, no. 30, pp. 10979–83, Jul. 2004.

[62] D. R. Tree, Y. Wang, and K. D. Dorfman, “Extension of DNA in a Nanochannel as a Rod-to-Coil Transition,” *Phys. Rev. Lett.*, vol. 110, no. 20, p. 208103, May 2013.

[63] D. E. Streng, S. F. Lim, J. Pan, A. Karpusenka, and R. Riehn, “Stretching chromatin through confinement,” *Lab Chip*, vol. 9, no. 19, pp. 2772–2774, 2009.

[64] C. Zhang, D. Guttula, F. Liu, P. P. Malar, S. Y. Ng, L. Dai, P. S. Doyle, J. A. van Kan, and J. R. C. van der Maarel, “Effect of H-NS on the elongation and compaction of single DNA molecules in a nanospace,” *Soft Matter*, pp. 9593–9601, 2013.

[65] K. Frykholm, M. Alizadehheidari, J. Fritzsche, J. Wigenius, M. Modesti, F. Persson, and F. Westerlund, “Probing Physical Properties of a DNA-Protein Complex Using Nanofluidic Channels.,” *Small*, vol. 10, no. 5, pp. 884–7, Mar. 2014.

[66] J. H. Carpenter, A. Karpusenko, J. Pan, S. F. Lim, and R. Riehn, “Density fluctuations dispersion relationship for a polymer confined to a nanotube,” *Appl Phys Lett*, vol. 98, no. 25, p. 253704, 2011.

[67] A. Karpusenko, J. H. Carpenter, C. Zhou, S. F. Lim, J. Pan, and R. Riehn, “Fluctuation modes of nanoconfined DNA.,” *J. Appl. Phys.*, vol. 111, no. 2, pp. 24701–247018, Jan. 2012.

[68] S. L. Levy, J. T. Mannion, J. Cheng, C. H. Reccius, and H. G. Craighead, “Entropic unfolding of DNA molecules in nanofluidic channels.,” *Nano Lett.*, vol. 8, no. 11, pp. 3839–44, Nov. 2008.

[69] R. Metzler, W. Reisner, R. Riehn, R. Austin, J. O. Tegenfeldt, and I. M. Sokolov, “Diffusion mechanisms of localised knots along a polymer,” *Europhys. Lett.*, vol. 76, no. 4, pp. 696–702, Nov. 2006.

[70] D. Shore, J. Langowski, and R. L. Baldwin, “DNA flexibility studied by covalent closure of short fragments into circles,” *Proc. Natl. Acad. Sci.*, vol. 78, no. 8, pp. 4833–4837, Jan. 1981.

[71] D. Shore and R. L. Baldwin, “Energetics of DNA twisting. I. Relation between twist and cyclization probability.,” *J. Mol. Biol.*, vol. 170, no. 4, pp. 957–81, Nov. 1983.

[72] J. Shimada and H. Yamakawa, “Ring-closure probabilities for twisted wormlike chains. Application to DNA,” *Macromolecules*, vol. 17, no. 4, pp. 689–698, Jul. 1984.

[73] W. H. Taylor and P. J. Hagerman, “Application of the method of phage T4 DNA ligase-catalyzed ring-closure to the study of DNA structure. II. NaCl-dependence of DNA flexibility and helical repeat.,” *J. Mol. Biol.*, vol. 212, no. 2, pp. 363–76, Mar. 1990.

[74] I. R. Lehman, “DNA ligase: structure, mechanism, and function.,” *Science (80-.).*, vol. 186, no. 4166, pp. 790–7, Nov. 1974.

[75] H. Kuhn and M. D. Frank-Kamenetskii, “Template-independent ligation of single-stranded DNA by T4 DNA ligase.,” *FEBS J.*, vol. 272, no. 23, pp. 5991–6000, Dec. 2005.

[76] S. V Nilsson and G. Magnusson, “volume 10 Number 51982 Nucleic A c i d s Research,” *Nucleic Acids Res.*, vol. 10, no. 5, 1982.

[77] D. F. Bogenhagen and K. G. Pinz, “The action of DNA ligase at abasic sites in DNA.,” *J. Biol. Chem.*, vol. 273, no. 14, pp. 7888–93, Apr. 1998.

[78] R. Rossi, A. Montecucco, G. Ciarrocchi, G. Biamonti, and G. Ciarochhi, “Functional characterization of the T4 DNA ligase: a new insight into the mechanism of action,” *Nucleic Acids Res.*, vol. 25, no. 11, pp. 2106–2113, Jun. 1997.

[79] A. V. Cherepanov and S. de Vries, “Dynamic mechanism of nick recognition by DNA ligase,” *Eur. J. Biochem.*, vol. 269, no. 24, pp. 5993–5999, Dec. 2002.

[80] T. E. Cloutier and J. Widom, “Spontaneous sharp bending of double-stranded DNA.,” *Mol. Cell*, vol. 14, no. 3, pp. 355–62, May 2004.

[81] Q. Du, C. Smith, N. Shiffeldrim, M. Vologodskaia, and A. Vologodskii, “Cyclization of short DNA fragments and bending fluctuations of the double helix.,” *Proc Natl Acad Sci USA*, vol. 102, no. 15, pp. 5397–402, Apr. 2005.

[82] C. Yuan, X. W. Lou, E. Rhoades, H. Chen, and L. A. Archer, “T4 DNA ligase is more than an effective trap of cyclized dsDNA.,” *Nucleic Acids Res.*, vol. 35, no. 16, pp. 5294–302, Jan. 2007.

[83] P. J. Hagerman and V. a Ramadevi, “Application of the method of phage T4 DNA ligase-catalyzed ring-closure to the study of DNA structure. I. Computational analysis.,” *J. Mol. Biol.*, vol. 212, no. 2, pp. 351–62, Mar. 1990.

[84] A. Rosa, N. B. Becker, and R. Everaers, “Looping probabilities in model interphase chromosomes.,” *Biophys. J.*, vol. 98, no. 11, pp. 2410–9, Jun. 2010.

[85] P. H. von Hippel and O. G. Berg, “Facilitated target location in biological systems,” *J Biol Chem*, vol. 264, no. 2, pp. 675–678, 1989.

[86] M. Reuter and D. T. F. Dryden, “The kinetics of YOYO-1 intercalation into single molecules of double-stranded DNA.,” *Biochem. Biophys. Res. Commun.*, vol. 403, no. 2, pp. 225–9, Dec. 2010.

[87] T. E. Cloutier and J. Widom, “Spontaneous sharp bending of double-stranded DNA.,” *Mol. Cell*, vol. 14, no. 3, pp. 355–62, May 2004.

[88] T. E. Cloutier and J. Widom, “DNA twisting flexibility and the formation of sharply looped protein-DNA complexes.,” *Proc. Natl. Acad. Sci. U. S. A.*, vol. 102, no. 10, pp. 3645–50, Mar. 2005.

[89] R. Riehn, W. Reisner, J. O. Tegenfeldt, Y. M. Wang, C.-K. Tung, S. F. Lim, E. C. Cox, J. Sturm, and R. H. Austin, “Nanochannels for Genomic DNA Analysis: The Long and Short of It,” in *Integrated Biochips for DNA Analysis*, 1st ed., R. H. Liu and A. P. Lee, Eds. Austin, Texas: Landes Bioscience, 2007, pp. 151–186.

[90] R. Riehn, M. C. Lu, Y. M. Wang, S. F. Lim, E. C. Cox, and R. H. Austin, “Restriction mapping in nanofluidic devices,” *Proc Natl Acad Sci U S A*, vol. 102, no. 29, pp. 10012–10016, 2005.

[91] P. Kaur, Qiang-Fu, A. Fuhrmann, R. Ros, L. O. Kutner, L. A. Schneeweis, R. Navoa, K. Steger, L. Xie, C. Yonan, R. Abraham, M. J. Grace, and S. Lindsay, “Antibody-unfolding and metastable-state binding in force spectroscopy and recognition imaging.,” *Biophys. J.*, vol. 100, no. 1, pp. 243–50, Jan. 2011.

[92] D. R. Tree, Y. Wang, and K. D. Dorfman, “Extension of DNA in a Nanochannel as a Rod-to-Coil Transition,” *Phys. Rev. Lett.*, vol. 110, no. 20, p. 208103, May 2013.

[93] L. Dai, S. Y. Ng, P. S. Doyle, and J. R. C. van der Maarel, "Conformation Model of Back-Folding and Looping of a Single DNA Molecule Confined Inside a Nanochannel," *ACS Macro Lett.*, vol. 1, no. 8, pp. 1046–1050, Aug. 2012.

[94] F. Persson, P. Utko, W. Reisner, N. B. Larsen, and A. Kristensen, "Confinement spectroscopy: probing single DNA molecules with tapered nanochannels.," *Nano Lett.*, vol. 9, no. 4, pp. 1382–5, Apr. 2009.

[95] P. G. De Gennes, *Scaling Concepts in Polymer Physics*. Ithaca, NY: Cornell University Press, 1979.

[96] D. W. Schaefer, J. F. Joanny, and P. Pincus, "Dynamics of Semiflexible Polymers in Solution," *Macromolecules*, vol. 13, no. 5, pp. 1280–1289, 1980.

[97] Y. Wang, D. R. Tree, and K. D. Dorfman, "Simulation of DNA Extension in Nanochannels.," *Macromolecules*, vol. 44, no. 16, pp. 6594–6604, Aug. 2011.

[98] F. Persson, F. Westerlund, J. O. Tegenfeldt, and A. Kristensen, "Local conformation of confined DNA studied using emission polarization anisotropy.," *Small*, vol. 5, no. 2, pp. 190–3, Feb. 2009.

[99] K. Frykholm, M. Alizadehheidari, J. Fritzsche, J. Wigenius, M. Modesti, F. Persson, and F. Westerlund, "Probing Physical Properties of a DNA-Protein Complex Using Nanofluidic Channels.," *Small*, vol. 10, no. 5, pp. 1–4, Jan. 2014.

[100] C. Zhang, P. G. Shao, J. A. van Kan, and J. R. C. van der Maarel, "Macromolecular crowding induced elongation and compaction of single DNA molecules confined in a nanochannel.," *Proc. Natl. Acad. Sci. U. S. A.*, vol. 106, no. 39, pp. 16651–6, Sep. 2009.

[101] J. Jones, J. van der Maarel, and P. Doyle, "Effect of Nanochannel Geometry on DNA Structure in the Presence of Macromolecular Crowding Agent," *Nano Lett.*, vol. 11, pp. 5047–5053, 2011.

[102] S. Jun, D. Thirumalai, and B.-Y. Ha, "Compression and Stretching of a Self-Avoiding Chain in Cylindrical Nanopores," *Phys Rev Lett*, vol. 101, no. 13, pp. 138101/1–4, Sep. 2008.

[103] P. Cifra, "Weak-to-strong confinement transition of semi-flexible macromolecules in slit and in channel.," *J. Chem. Phys.*, vol. 136, no. 2, p. 024902, Jan. 2012.

[104] P. Cifra and T. Bleha, "Detection of chain backfolding in simulation of DNA in nanofluidic channels," *Soft Matter*, vol. 8, no. 34, p. 9022, 2012.

[105] D. Račko and P. Cifra, “Segregation of semiflexible macromolecules in nanochannel.,” *J. Chem. Phys.*, vol. 138, no. 18, p. 184904, May 2013.

[106] Y.-L. Chen, “Electro-entropic excluded volume effects on DNA looping and relaxation in nanochannels.,” *Biomicrofluidics*, vol. 7, no. 5, p. 54119, Jan. 2013.

[107] B. Akerman and E. Tuite, “Single- and double-strand photocleavage of DNA by YO, YOYO and TOTO.,” *Nucleic Acids Res.*, vol. 24, no. 6, pp. 1080–90, Mar. 1996.

[108] S. Gurrieri, K. S. Wells, I. D. Johnson, and C. Bustamante, “Direct visualization of individual DNA molecules by fluorescence microscopy: characterization of the factors affecting signal/background and optimization of imaging conditions using YOYO.,” *Anal. Biochem.*, vol. 249, no. 1, pp. 44–53, Jun. 1997.

[109] C. H. Reccius, S. M. Stavis, J. T. Mannion, L. P. Walker, and H. G. Craighead, “Conformation, length, and speed measurements of electrodynamically stretched DNA in nanochannels,” *Biophys. J.*, vol. 95, no. 1, pp. 273–286, 2008.

[110] M. Roushan, Z. Azad, S. F. Lim, H. Wang, and R. Riehn, “Interference of ATP with the fluorescent probes YOYO-1 and YOYO-3 modifies the mechanical properties of intercalator-stained DNA confined in nanochannels,” *Microchim. Acta*, vol. 182, no. 7–8, pp. 1561–1565, 2015.

[111] D. Wirtz, “Direct measurement of the transport properties of a single DNA molecule.,” *Phys. Rev. Lett.*, vol. 75, no. 12, pp. 2436–2439, Sep. 1995.

[112] O. Bakajin, T. A. J. Duke, C. Chou, S. Chan, R. Austin, and E. Cox, “Electrohydrodynamic Stretching of DNA in Confined Environments,” *Phys. Rev. Lett.*, vol. 80, no. 12, pp. 2737–2740, Mar. 1998.

[113] T. T. Perkins, “Single Polymer Dynamics in an Elongational Flow,” *Science (80-.).*, vol. 276, no. 5321, pp. 2016–2021, Jun. 1997.

[114] B. Maier and J. Rädler, “Conformation and Self-Diffusion of Single DNA Molecules Confined to Two Dimensions,” *Phys. Rev. Lett.*, vol. 82, no. 9, pp. 1911–1914, Mar. 1999.

[115] S. Turner, M. Cabodi, and H. Craighead, “Confinement-Induced Entropic Recoil of Single DNA Molecules in a Nanofluidic Structure,” *Phys. Rev. Lett.*, vol. 88, no. 12, p. 128103, Mar. 2002.

[116] A. Glazer and H. Rye, “Stable dye-DNA intercalation complexes as reagents for high-sensitivity fluorescence detection,” *Nature*, vol. 359, no. 6398, pp. 859 – 861, 1992.

[117] S. B. Smith, L. Finzi, and C. Bustamante, “Direct Mechanical Measurements of the Elasticity of Single DNA-Molecules by Using Magnetic Beads,” *Science (80-.).*, vol. 258, no. 5085, pp. 1122–1126, 1992.

[118] A. Sischka, K. Toensing, R. Eckel, S. D. Wilking, N. Sewald, R. Ros, and D. Anselmetti, “Molecular mechanisms and kinetics between DNA and DNA binding ligands.,” *Biophys. J.*, vol. 88, no. 1, pp. 404–11, Jan. 2005.

[119] C. U. Murade, V. Subramaniam, C. Otto, and M. L. Bennink, “Interaction of oxazole yellow dyes with DNA studied with hybrid optical tweezers and fluorescence microscopy.,” *Biophys. J.*, vol. 97, no. 3, pp. 835–43, Aug. 2009.

[120] P. Doyle, B. Ladoux, and J.-L. Viovy, “Dynamics of a Tethered Polymer in Shear Flow,” *Phys. Rev. Lett.*, vol. 84, no. 20, pp. 4769–4772, May 2000.

[121] H. P. Spielmann, D. E. Wemmer, and J. P. Jacobsen, “Solution structure of a DNA complex with the fluorescent bis-intercalator TOTO determined by NMR spectroscopy.,” *Biochemistry*, vol. 34, no. 27, pp. 8542–53, Jul. 1995.

[122] F. Johansen and J. P. Jacobsen, “1H NMR studies of the bis-intercalation of a homodimeric oxazole yellow dye in DNA oligonucleotides.,” *J. Biomol. Struct. Dyn.*, vol. 16, no. 2, pp. 205–22, Oct. 1998.

[123] B. Kundukad, J. Yan, and P. S. Doyle, “Effect of YOYO-1 on the mechanical properties of DNA.,” *Soft Matter*, pp. 9721–9728, 2014.

[124] J. Kapuscinski, “DAPI: a DNA-specific fluorescent probe.,” *Biotech. Histochem.*, vol. 70, no. 5, pp. 220–33, Sep. 1995.

[125] X. Meng, W. Cai, and D. C. Schwartz, “Inhibition of restriction endonuclease activity by DNA binding fluorochromes.,” *J. Biomol. Struct. Dyn.*, vol. 13, no. 6, pp. 945–51, Jun. 1996.

[126] Y. Matsuzawa and K. Yoshikawa, “Change of the Higher Order Structure in a Giant DNA Induced by 4′, 6-Diamidino-2-phenylindole as a Minor Groove Binder and Ethidium Bromide as an Intercalator,” *Nucleosides and Nucleotides*, vol. 13, no. 6–7, pp. 1415–1423, Jul. 1994.

[127] A. Karpusenko, J. H. Carpenter, C. Zhou, S. F. Lim, J. Pan, and R. Riehn, “Fluctuation modes of nanoconfined DNA.,” *J. Appl. Phys.*, vol. 111, no. 2, pp. 24701–247018, Jan. 2012.

[128] M. Roushan, P. Kaur, A. Karpusenko, P. J. Countryman, C. P. Ortiz, S. Fang Lim, H. Wang, and R. Riehn, "Probing transient protein-mediated DNA linkages using nanoconfinement," *Biomicrofluidics*, vol. 8, no. 3, p. 034113, May 2014.

[129] C. Carlsson, M. Jonsson, and B. Akerman, "Double bands in DNA gel electrophoresis caused by bis-intercalating dyes.," *Nucleic Acids Res.*, vol. 23, no. 13, pp. 2413–20, Jul. 1995.

[130] J. F. Allemand, D. Bensimon, L. Jullien, a Bensimon, and V. Croquette, "pH-dependent specific binding and combing of DNA.," *Biophys. J.*, vol. 73, no. 4, pp. 2064–70, Oct. 1997.

[131] M. Reuter and D. T. F. Dryden, "The kinetics of YOYO-1 intercalation into single molecules of double-stranded DNA.," *Biochem. Biophys. Res. Commun.*, vol. 403, no. 2, pp. 225–9, Dec. 2010.

[132] R. Riehn, M. Lu, Y. M. Wang, S. F. Lim, E. C. Cox, and R. H. Austin, "Restriction mapping in nanofluidic devices," *Proc Natl Acad Sci U S A*, vol. 102, no. 29, pp. 10012–10016, 2005.

[133] A. V. Cherepanov and S. De Vries, "Kinetics and thermodynamics of nick sealing by T4 DNA ligase," *Eur. J. Biochem.*, vol. 270, no. 21, pp. 4315–4325, Oct. 2003.

[134] S. Das, P. Dubsky, A. Van Den Berg, and J. C. T. Eijkel, "Concentration polarization in translocation of dna through nanopores and nanochannels," *Phys. Rev. Lett.*, vol. 108, no. 13, pp. 1–5, 2012.

[135] Z. Azad, M. Roushan, and R. Riehn, "DNA Brushing Shoulders: Targeted Looping and Scanning of Large DNA Strands," *Nano Lett.*, p. 150713103730004, 2015.

[136] J. Clemmens, H. Hess, R. Doot, C. M. Matzke, G. D. Bachand, and V. Vogel, "Motor-protein 'roundabouts': microtubules moving on kinesin-coated tracks through engineered networks.," *Lab Chip*, vol. 4, no. D, pp. 83–86, 2004.

[137] S. J. Kron and J. a Spudich, "Fluorescent actin filaments move on myosin fixed to a glass surface.," *Proc. Natl. Acad. Sci. U. S. A.*, vol. 83, no. 17, pp. 6272–6276, 1986.

[138] M. D. Frank-kamenetskii, *Biophysics of the DNA molecule*, vol. 1573, no. 97. 1997.

[139] K. Royer, M. Lukosi, and B. K. Royer, "YOYO-1 Green Fluorescent Dye : The Advanced Dye of the Future," no. 555.